Multi-century records of hydroclimate dynamics and steelhead trout abundance from tree rings in northern British Columbia, Canada

by

Cedar Welsh
B.Sc., Trent University, 2004
M.Sc., University of Northern British Columbia, 2007

A Dissertation Submitted in Partial Fulfillment
of the Requirements for the Degree of

DOCTOR OF PHILOSOPHY

in the Department of Geography

University of Victoria

Supervisory Committee

Multi-century records of hydroclimate dynamics and steelhead trout abundance from tree rings in northern British Columbia, Canada

by

Cedar Welsh
B.Sc., Trent University, 2004
M.Sc., University of Northern British Columbia, 2007

Supervisory Committee

Dr. Dan J. Smith (Department of Geography)
Supervisor

Dr. Tom W.D. Edwards (Department of Geography)
Departmental Member

Dr. David Wilford (Ministry of Forests, Natural Resource Operations)
Outside Member

Abstract

Supervisory Committee

Dr. Dan J. Smith (Department of Geography)
Supervisor

Dr. Tom W.D. Edwards (Department of Geography)
Departmental Member

Dr. David Wilford (Ministry of Forests and Natural Resource Operations)
Outside Member

The impacts of climate variability and change on streamflow are of increasing concern, particularly as human demands on water supplies compete with the needs of natural ecosystems. The consequences on the hydrological cycle are predicted to be most severe for mid- to high-latitude regions. Of particular concern is reduced mountain snow accumulation and related reductions in the snow- and glacier-derived water supply. In northern British Columbia (BC), recent snowpack declines have caused a unique water management challenge. Diminishing water security in a region considered water-abundant has intensified over the last decade. Characterizing the climate controls on hydrologic variability is a priority for developing baseline information required for water supply forecasting. This research focuses on developing multi-century, annually-resolved records of snow water equivalent (SWE) and streamflow to provide a better understanding of long-term hydroclimate variability for the design and implementation of management strategies that balance riverine ecosystem services, such as recreation and fish habitat, with increasing economic and social demands.

Climate sensitive tree-ring chronologies provide the opportunity to extend instrumental records of hydroclimate by capitalizing on the influence of climate on both

annual radial growth and seasonal runoff. Traditional dendrohydrology relies on moisture-limited tree species from dry, continental settings. This dissertation presents a new method by focusing on mid- to high-elevation conifers sensitive to snowpack variability. Ring-width and maximum latewood density records from mountain hemlock (*Tsuga mertensiana* (Bong.) Carriere), white spruce (*P. glauca* (Moench) Voss), and subalpine fir (*Abies lasiocarpa* (Hook.) Nutt.) stands were collected at sites in northern BC. Dendrochronological techniques were used to develop a: 1) 223-year record of April 1 SWE for the Stikine River basin; 2) 417-, 716-, and 343-year record of summer streamflow for the Skeena, Nass and Stikine rivers, respectively; and, 3) a 193-year reconstruction of summer-run Skeena River steelhead abundance based on the influence of ocean-atmospheric forcings on both radial tree growth and steelhead escapement. The April 1 SWE record suggests that there has been considerable variability in snowpack levels in the Stikine basin and a distinct in-phase relationship with seasonalized Pacific Decadal Oscillation (PDO) indices, not seen in basins to the south. The summer streamflow records also support a north-south "see-saw" effect, suggesting an association between moisture transport and atmospheric-ocean circulation in the region. In addition to the snow-sensitive tree-ring data, the streamflow models incorporated paleo-hemispheric records to improve predictive skill. Finally, the steelhead model described alternating intervals of persistently above-average and below-average abundance that corresponded to oceanic PDO-like influences and describe links to "warm-warm" ENSO-PDO years associated with in-river low flow periods.

The reconstructions suggest that: 1) recent snowpack and streamflow declines are a rare event over a multi-century context; and, 2) existing instrumental records do not

adequately represent the historic range of basin-specific hydroclimate variability necessary for new planning horizons. Mid- to high-elevation, snow-sensitive conifers have strong potential as paleohydrological proxies and for expanding the application of dendrohydrology to non-arid settings. Current conditions in northern BC, compounded by land use changes and climate change, are predicted to become more severe in the future. It is important that planning regimes incorporate long-term hydroclimate data to better understand and quantify how water supply and ecosystems will respond to future changes.

Table of Contents

List of Tables

List of Figures

Acknowledgements

I would like to thank my supervisory committee for their support and transfer of knowledge throughout this incredible experience. The mentorship and encouragement over the past several years has exceeded my expectations and has been invaluable to my growth as a scientist. I would especially like to thank my supervisor, Dan Smith. Dan, your advice and confidence in me during this process were very important to the completion of this work. Thank you to Trevor Porter for graciously agreeing to act as my external examiner. To Dave Meko, thank you for sponsoring my visit to the LTRR and sharing your knowledge of dendrohydrology.

A big thank you goes to Marie-Christine Claveau, Lauren Fraychineaud, Jill Harvey, Suzi Hopkinson, Holly Hovland, Ashely Long, Todd Sherstone, Debbie Schwartz and Doug Thompson: I will never forget all the adventures working in the most beautiful place in the world! I also need to acknowledge my Victoria family who cared for me while I was away from home. To Maureen Scott, Colin Hagen, Sandy Allen, and Doug McMillan, thank you for all the family dinners and a place to stay. Also, to the UVTRL crew for accommodating me when I "showed up" in the lab, particularly to Bryan Mood who became a familiar face for me.

Thank you to my family and friends for the encouragement and patience, especially Todd, without whom the completion of this work would not have been possible.

Dedication

To Solo and Lulu

Chapter 1: Introduction

1.1 Background

The impacts of climate variability and change on streamflow are of increasing concern, particularly as human demands on water supplies compete with the needs of natural ecosystems (Moore and McKendry, 1996). Declining mountain snow accumulation and concomitant reductions in snow- and glacier-derived water supply are among the primary consequences expected from climate warming. Understanding the natural range of long-term hydroclimate variability and extreme hydrological events is critical for the design and implementation of effective management strategies (Fleming et al., 2016).

Seasonal runoff in northern BC is either snow-dominated (i.e., nival regime) or snow-influenced (i.e., hybrid nival-pluvial or nival-glacial regime) (Eaton and Moore, 2010). These regimes typically exhibit peak flows in the spring freshet (as a result of melt-season temperatures) and low flows in the late summer extending through the winter during the snow accumulation period (Easton and Moore, 2010). A lack of adequate snow accumulation or anomalously early melt can contribute to summer drought conditions (Bonsal et al., 2011). Fluctuations in large-scale ocean and atmospheric climate oscillations have considerable influence on the climate variables driving streamflow in western Canada (Moore, 1996; Moore and McKendry, 1996; Stewart et al., 2004; Thorne and Woo, 2011). For example, the influence of the El Niño-Southern Oscillation (ENSO) phenomenon and variations in the intensity of the Pacific North America (PNA) circulation pattern have been linked to interannual variations in temperature and precipitation patterns during the winter months (Moore and McKendry,

1996). Minor shifts in the spatial and temporal patterns of these climate variables can have major consequences for water availability (O'Neil et al., 2017). Studies have also demonstrated that the Pacific Decadal Oscillation (PDO) has important implications for water resources in western North America (Mantua et al., 1997; Whitfield et al., 2010). The PDO is a driver of surface climate variability in BC and has been a major research focus for the past two decades (e.g., Manuta et al., 1997; McCabe et al., 2004; Whitfield et al., 2010). As the name implies, the PDO is dominated by oscillations – more specifically, "cool" and "warm" regime shifts – that happen every 20 to 40 years (Whitfield et al., 2010). The last clearly detected shift in the PDO occurred in the mid-1970s, when the North Pacific Ocean region abruptly shifted from a cool to a warm phase; a shift accompanied by above-average winter temperatures and variable precipitation patterns in BC (Mantua et al., 1997; Rodenhuis et al., 2009).

Information on how climate warming may interact with ocean-atmospheric climate oscillations and impact hydrological responses will be important for forecast planning. There is evidence to suggest that global anthropogenically-driven climate changes may be influencing regional climate more than large-scale climate processes (e.g., ENSO and PDO). For instance, there has been an observed shift in the timing of spring high flows (freshets) towards an earlier onset of spring melt at the expense of summer runoff in BC (Zhang et al., 2001, Déry et al., 2009). Concurrent with these timing trends, average annual temperatures over the northwestern part of North America have increased by 1-2°C since the 1940s (Dettinger and Cayan, 1995). Evidence also indicates a decline in winter snow accumulation, and a trend towards warmer and drier summers (Barnett et al., 2005). In recent years, these conditions have prompted the implementation of provincial

water-use restrictions (BC Ministry of Environment and Climate Change, 2018), contributed to unprecedented wildfire seasons (BC Ministry of Forests, Lands, and Natural Resource Operations, 2018), and have seriously impacted spawning habitats imperiling the survival of wild Pacific salmon and steelhead trout in BC (Pacific Fisheries Resource Conservation Council, 2016). Future consequences of hydrological change are predicted to be most severe for mid- to high-latitude regions under projected climate change (Zhang et al., 2001).

Despite the importance of mountain regions in BC to the hydrologic cycle and regional water supplies, there is a lack of long-term hydroclimate data (Bales et al., 2006). Hydroclimate records seldom exceed 100 years in Canada and most are considerably shorter, especially in remote areas (Beriault and Sauchyn, 2006). Detection of recent environmental change requires these long-term records because natural climatic patterns, such as the PDO, persist over multiple decades and can obscure climate change effects (Moore et al., 2007). Recently acquired paleoclimatic data has played a major role in convincing hydrologists and water resources planners that the length of climatic variation provided by the short instrumental record may not be sufficient to capture the long-term natural range of hydroclimate variability that is essential for the assessment of changing freshwater resources and management planning (Meko and Woodhouse, 2011). Moreover, long hydroclimate records are required to derive reliable trends of the past and hence, plausible projections of the future (Salzmann et al., 2014).

1.2 Dendrohydrology

Climate sensitive tree-ring chronologies provide the opportunity to extend instrumental records of hydroclimate variability by capitalizing on the influence of climate on both annual radial growth and the seasonal factors that drive streamflow (Loaiciga et al., 1993; Gedalof et al., 2004; Meko and Woodhouse, 2011). Dendrohydrologic modeling has largely been accomplished in dry, continental settings where the annual radial growth is limited by available soil moisture (Meko and Woodhouse, 2011). Where reconstructions of hydroclimate from tree rings have been successful, they have played a prominent role in describing how precipitation, snowpack, streamflow runoff, and drought have varied in the past (e.g., Axelson et al., 2009; Margolis et al., 2011; Meko et al., 2012). Both within and outside of Canada, dendrohydrology has rarely been applied in "non-traditional" environments (i.e., non-arid or water-abundant environments). A few recent studies have demonstrated that mid- to high-elevation conifers sensitive to snowpack variability in southern BC can form the basis for paleohydrological models of snow and snow-influenced processes (e.g., Hart et al., 2010; Coulthard et al., 2016), but few attempts to model hydroclimatic outcomes from tree-ring chronologies are known for northern BC. Increasing water management challenges and concerns about the potential for extreme hydrologic events in northern BC invites the application of dendrohydrology in this region.

Hydroclimate information has most often been gleaned from interannual variations in ring-width growth, but there are other sources of tree ring measurements, such as wood density, that are rapidly gaining interest in dendrohydrological applications (e.g., Starheim et al., 2013a). Ring-width growth is dependent upon seasonally variable, periclinal cell division with enlargement occurring in the cambial region, an indicator of

early-season climate variability (Fritts, 1976); whereas ring density is primarily determined by cell-wall thickness, an anatomical alteration that begins in the late-summer once cell division and enlargement cease. Ring density variations are, therefore, better correlated to end-of-growing season climates (Polge, 1966; Pitman and Smith, 2013). The identification of distinct early and late season climate signals demonstrates the value of employing multi-proxy tree-ring parameters to provide complementary climate information, and in some situations, used to collectively to improve the reliability of the hydroclimate record.

1.3 Tree-rings and Steelhead Trout

Widespread changes in Pacific salmonid abundance are known to be closely tied to low-frequency climate shifts associated with the Aleutian Low (AL) pressure centre, and sea surface temperatures (SSTs) (Beamish and Bouillon, 1993; Beamish et al., 1997; Mantua et al., 1997; Starheim et al., 2013b; Mood et al., *unpublished*). The PDO is the leading principal component of monthly SST anomalies in the North Pacific, poleward of 20°N (Mantua et al., 1997), and tends to vary positively with the strength of the AL. Climate sensitive tree-rings provide an opportunity to extend these abundance records to multi-century timescales by capitalizing on the influence of large-scale ocean-atmospheric forcings on the radial growth of trees and escapement estimates. Recent paleoecological studies have demonstrated the utility of tree-ring models of Pacific salmonid abundance to examine long-term trends in population levels (e.g., Drake and Naiman, 2007; Starheim et al., 2013b; Mood et al., *unpublished*). These studies uncovered a number of previously unrecorded population collapses and characterized the long-term influence of large-scale climate and ocean oscillations on population trends.

Steelhead trout (*Oncorhynchus mykiss*), the anadromous form of rainbow trout, are found in all major coastal river systems in BC. Steelhead abundance is of increasing concern to fisheries managers in BC, as the status of many populations require increased emphasis on conservation (Slaney et al., 1996). Unfortunately, the short duration of both climate and steelhead abundance records largely restricts our understanding to the past century. With persistent pressure on steelhead by humans, the increasing threat of climate change, and continued calls for recovery, monitoring population abundance and survival trends over space and time is essential for identifying the factors affecting population dynamics to guide appropriate management and conservation actions (Burke et al., 2013).

1.4 Study Area

The Skeena, Nass and Stikine river basins drain a large area of northern BC (total area of ~230,239 km^2). The rivers share the same headwater location, originating in the semi-arid Spatsizi Plateau of northern interior BC. The rivers drain a large number of glacierized, high-elevation watersheds in the BC Coast Ranges and exit into the Pacific Ocean.

Climates vary with respect to relative proximity to the Pacific Ocean and the Coast Mountain ranges. The western flank of the study area is typified by abundant precipitation (average 2,310 mm per year), cool summers and mild winters. Precipitation reaches a maximum in the fall and early winter when it is associated with intense cyclonic storms from the North Pacific that can cause severe and sudden flooding, particularly in the form of rain-on-snow events. The degree and extent of the moderating coastal influence diminishes quickly with elevation and in an easterly direction. The interior portion of the study area has a cooler and drier boreal climate. This region

receives annual precipitation totals ranging from ~600 to 400 mm, with variable amounts of snow, depending upon elevation, that range from approximately 60% to 40% of the annual precipitation total.

1.5 Dissertation Objectives

Winter snowpack is an important control of streamflow over the water year in northern BC (e.g., Watson and Luckman, 2002), and is sensitive to fluctuations in the ocean and atmosphere over the North Pacific Ocean. There is considerable evidence to suggest that the radial growth of some mid- to high-elevation conifers is sensitive to annual snowpack variability, and can form the basis for developing tree-ring reconstructions of basin-scale snowpack and streamflow. These long-term records will complement and expand on the existing understanding of the region's hydroclimate dynamics. For regional water managers tasked with planning for the future, tree-ring reconstructions of magnitude, severity and periodicity of long-term hydroclimate variability provide a solid basis for planning (Woodhouse and Lukas, 2006).

Mid- to high-elevation conifers sensitive to annual variations in snowpack depth have rarely been used in dendrohydrology. Mountain hemlock (*Tsuga mertensiana* (Bong.) Carrière) and subalpine fir (*Abies lasiocarpa* (Hook.) Nutt.) trees exhibit a form of snowpack-related, energy-limitation by which the length of the growing season (or photosynthesic season) is controlled by the duration of the seasonal snowpack. Smaller-than-normal tree rings characterize deep winter snowpack seasons when late-lying snowpacks limit radial growth (Peterson and Peterson, 1994; Larocque and Smith, 1999; Gedalof and Smith, 2001; Starheim et al., 2013a). This energy-limitation is distinct from moisture-limitation by snow. Moisture-limited conifers respond to snowmelt by way of

water recharging soil moisture; low soil moisture in the root zone, as well as high evaporative demand of the atmosphere. These conditions create a low internal water potential and result in reduced cambial growth (i.e., smaller-than-normal rings) (Fritts 1976). Although white spruce (*Picea glauca* (Moench) Voss) is a well-known moisture-limited species it has not been previously examined as a proxy for snowpack variation. A comprehensive investigation into the relationship between growth chronologies from moisture- and energy-limited tree species and hydroclimate records may provide new and more robust reconstructions of snowpack and streamflow in northern BC.

This research was designed to fill critical knowledge gaps by providing a comprehensive analysis of the following objectives:

1. Confirm that the radial growth of white spruce can serve as a proxy for snowpack variability.
2. Develop a multi-century record of snow water equivalent (SWE) for the Stikine River basin in northern BC.
3. Develop reconstructions of summer streamflow for three major river basins in northern BC (Skeena, Nass, and Stikine rivers).
4. Conduct an interbasin comparison of streamflow variability and relate basin-scale patterns to North Pacific climate variability.
5. Link large-scale ocean and atmospheric forcings to annual radial growth and steelhead escapement estimates to generate a long-term history of abundance in the Skeena River.

1.6 Thesis Format

This thesis is divided into five chapters. This first chapter provides an introduction and context to the research. *Chapters 2, 3, and 4* present the main results of the dissertation research, and were composed as stand-alone manuscripts. *Chapter 2* focuses on April 1 snow-water-equivalent reconstructions using white spruce in the Stikine River basin and has been published in *Hydrological Processes* (Welsh et al., 2019). *Chapter 3* focuses on streamflow reconstructions for the Skeena, Nass, and Stikine rivers. *Chapter 4* capitalizes on the climate-growth relationships established *in Chapters 2 and 3*, and provides a reconstruction of steelhead trout abundance histories. The dissertation concludes with *Chapter 5*, where the findings of *Chapters 2, 3,* and *4* are synthesized, and are used to recommend future directions for both research and water resource management.

Chapter 2: Tree-ring records unveil long-term influence of the Pacific Decadal Oscillation on snowpack dynamics in the Stikine River basin, northern British Columbia

Article information:

This chapter consists of a manuscript published in January, 2019, in the journal *Hydrological Processes*. The text and figures are presented as prepared for the published paper, but have been renumbered and reformatted for consistency within the thesis. Citation style has also been reformatted for consistency.

Authors' names and affiliations:

Cedar Welsh[a*], Dan J. Smith[a] and Bethany Coulthard[b]

[a] University of Victoria Tree-Ring Laboratory, Department of Geography, University of Victoria, 3800 Finnerty Road, Victoria, British Columbia, V8P 5C2, Canada

[b] University of Arizona, Laboratory of Tree-Ring Research, 1215 E. Lowell Street, Tucson, Arizona, 85721-0045, USA

*Corresponding author: welsh@uvic.ca

Author and coauthors' contributions

Welsh developed the study and hypothesis, conducted laboratory work and statistical testing, wrote the manuscript, and produced all of the tables and figures. Smith and Coulthard reviewed and edited the manuscript.

2.1 Abstract

Long hydroclimate records are essential elements for the assessment and management of changing freshwater resources. These records are especially important in transboundary watersheds where international cooperation is required in the joint planning and management process of shared basins. Dendrochronological techniques were used to develop a multi-century record of April 1 snow water equivalent (SWE) for the Stikine River basin in northern British Columbia, Canada, from moisture-sensitive white spruce (*Picea glauca*) tree rings. Explaining 43% of the instrumental SWE variability, to our knowledge this research represents the first attempt to develop long-term snowpack reconstructions in northern British Columbia. The results indicated that 15 extreme low April 1 SWE events occurred from 1789 to the beginning of the instrumental record in 1974. The reconstruction record also shows that the occurrence of hydrologic extremes in the Stikine basin is characterized by persistent below-average periods in SWE consistent with phase shifts of the Pacific Decadal Oscillation (PDO). Spectral analyses indicate a very distinct in-phase (positive) relationship between the multidecadal frequencies of variability (~40 years) extracted from the SWE tree-ring reconstruction and other reconstructed winter and spring PDO indices. Comparison of the reconstructed SWE record with other tree ring-derived PDO proxy records show coherence at multidecadal frequencies of variability. The research has significant implications for regional watershed management by highlighting the hydrological response of the Stikine River basin to prior climate changes.

2.2 Introduction

The impacts of climate variability and change on streamflow are of increasing concern, particularly as human demands on water supplies compete with the needs of natural ecosystems (Moore and McKendry, 1996). Fluctuations in large-scale ocean and atmospheric climate oscillations have considerable influence on the climate variables driving streamflow, including winter snow accumulation and melt-season temperatures (Moore, 1996; Moore and McKendry, 1996; Stewart et al., 2004; Thorne and Woo, 2011). Of particular concern is the loss of mountain snow accumulation and related reductions in the snow- and glacier-derived water supply, which are among the primary consequences expected from climate warming (Stewart et al., 2005). Knowledge about the possible range of natural hydroclimate variability at a variety of time scales is critical for the design and implementation of management strategies that balance riverine ecosystem services, such as recreation and fish habitat, with increasing economic and social demands (Fleming et al., 2016).

Average annual temperatures over the northwestern part of North America have increased by 1-2°C since the 1940s, most notably during the winter and spring seasons. Although there is uncertainty about the magnitude of future increases, most assessments indicate that future warming is "*likely*" and more frequent hot and fewer cold temperature extremes "*virtually certain*" (Stocker et al., 2013). There is also a theoretical expectation that climate warming will result in increased evapotranspiration and precipitation (in the form of rainfall), leading to the hypothesis that one of the major consequences will be an intensification of the hydrologic cycle (Arnell and Liu, 2001; Huntington, 2006). Moreover, there is evidence that the global anthropogenically-driven climate changes may be influencing regional climates more than irreducible internal climate processes

(eg., El Niño/Southern Oscillation; ENSO and Pacific Decadal Oscillation; PDO) (eg., Arendt et al., 2009).

Recent national and provincial assessments of climate change impacts and adaptation have identified shifts in the distribution of water resources in western Canada. In particular, nival-dominated basins in the mid- to high-latitudes that are the most reliable source of spring and summer runoff are losing the snowpack storage advantages that accompany cold winters (Barnett et al., 2005). Sensitivity analysis of mountain snowmelt hydrology demonstrates a shift towards an earlier freshet at the expense of summer runoff (Whitfield and Taylor, 1998; Nijssen et al., 2001; Déry et al., 2009). These changes in the seasonal hydrograph are particularly concerning for northern British Columbia (BC) where climate-driven hydrologic variability propagates downstream into coastal marine ecosystems to impact the spawning migration success of important Pacific salmon commercial and subsistence fisheries (O'Neel et al., 2015).

Long hydroclimate records are required for the assessment of changing freshwater resources. However, hydroclimate records seldom exceed 100 years in Canada and most are considerably shorter, especially in remote areas (Beriault and Sauchyn, 2006). In addition, detection of recent environmental change requires these long-term records because natural climatic patterns, such as the PDO, persist over multiple decades and can obscure climate change effects (Moore et al., 2007). Recently acquired paleoclimatic data has played a major role in convincing hydrologists and water resources planners that the length of climatic variation provided by the short instrumental record may not be sufficient to capture the long-term natural variability in hydroclimate that is essential for resource management planning (Meko and Woodhouse, 2011).

Tree rings provide annually or seasonally resolved data that is precisely dated, and it has played a prominent role in attempts to establish how hydroclimate has varied in the recent past (eg., Axelson et al., 2009; Margolis et al., 2011; Meko et al., 2012). The immediate aim of dendrohydrology is the temporal extension of the climate phenomena that drive river discharge beyond the instrumented gauge record (Meko and Woodhouse, 2011). While tree ring variables such as wood density and stable isotopes are increasingly applied in dendrohydrological applications (eg., Edwards et al., 2008; Starheim et al., 2013a), the biological response of trees to hydroclimate forcing is primarily recorded by variations in the widths of annual tree rings (Fritts, 1976; Loaiciga et al., 1993). While tree-rings have been extensively used to extend climate variables such as streamflow, temperature and precipitation, relatively few studies have reconstructed regional snowpack trends using tree-ring chronologies as predictors (e.g., Woodhouse, 2003; Larocque and Smith, 2005; Coulthard and Smith, 2016).

The Stikine River is the largest transboundary river found in northeast Pacific North America (Fleming et al., 2016). Following successive years of earlier snowmelt onset, 2016 marked a "*well below normal*" snowpack year (<60% of basin index) for the Stikine region (Snow Survey Bulletin, B.C. River Forecast Centre). Understanding the influence of the long-term climate shifts affecting variations in snowpack accumulation is a crucial first step towards predicting how watersheds in the Stikine region may respond to ongoing climate changes. Characterizing the climatic controls on hydrologic variability is therefore a priority for developing the baseline information required for water and ecosystem management in this transboundary area (Fleming et al., 2016).

The purpose of this research was to develop a multi-century record of snow water

equivalent (SWE) for the Stikine basin in northern BC, and to understand the influence of major teleconnection patterns on long-term snowpack variability in this region. A dendroclimatological approach was used to reconstruct long-term proxy records of SWE using moisture-sensitive white spruce (*P. glauca* (Moench) Voss) tree-ring width chronologies. The study confirms that the radial growth of white spruce growth can serve as a proxy for snowpack and represents the first attempt to develop long-term snowpack records reconstructions from tree-ring data in northern BC.

2.3 Study Area

The Stikine River basin is a large international watershed with an approximate area of 52,000 km^2 located in transboundary area of BC-Alaska (AK). The Stikine River is ~610 km long, with its headwaters located in the semi-arid Spatsizi Plateau of interior northern BC. Water flows westward from the BC interior through the coastal temperate rainforest to exit into the Pacific Ocean (Figure 2.1).

The climate, physiography and hydrology of the Stikine basin are distinguished by three physiographic subdivisions: the Boundary Ranges; the Stikine Plateau; and, the Skeena Mountains (Figure 2.1). Rivers originating within the coastal Boundary Ranges drain a large number of glaciated, high-elevation basins. Streams flowing from the interior portion of the watershed originate within the more subdued topography of the Stikine Plateau composed of wide, glacial drift-filled, valleys and rolling uplands. The Skeena Mountains are located within the south central section of the Stikine Basin and include a number of minor tributaries that drain westward into the upper Iskut River before flowing into the Stikine River.

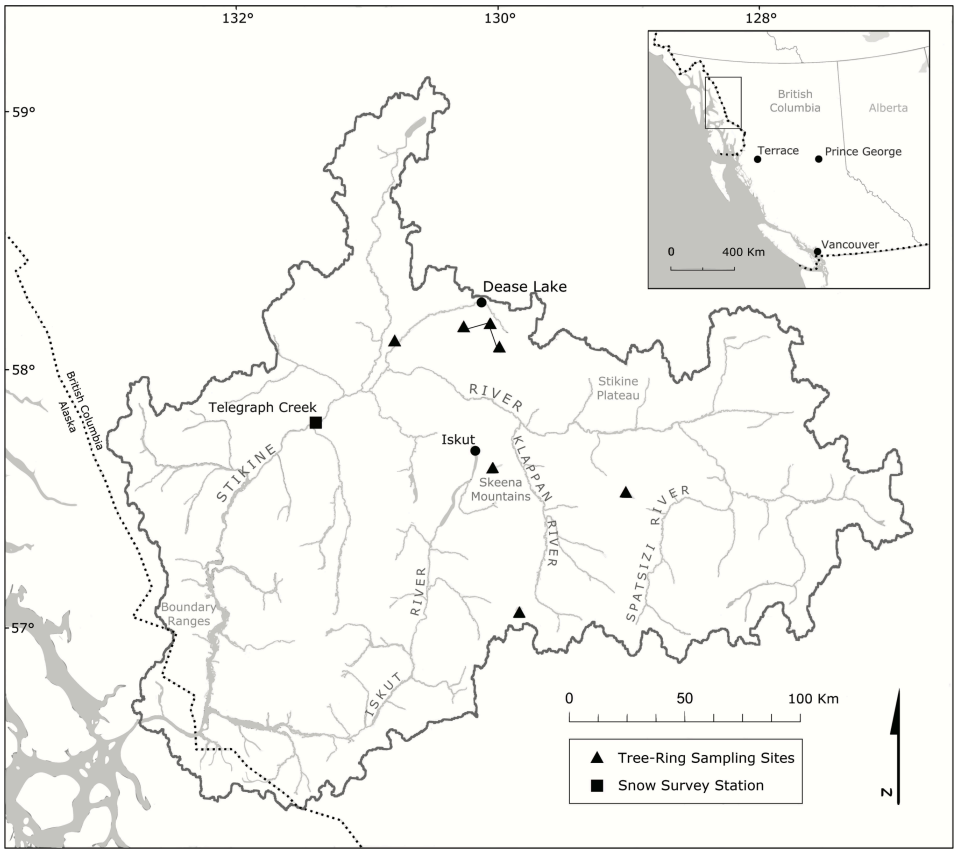

Figure 2.1: Map of the Stikine River basin showing hydroclimate and site locations.

Climate varies considerably in the Stikine basin. The climate in the coastal reaches of the drainage result in annual snow-dominated precipitation totals that average 2,400 mm and mean annual mean temperatures near -2.5°C (Environment Canada, 2015). Summers are typically cool with moderate rainfall, whereas winters are mild with precipitation totals reaching a maximum in the fall and early winter. Intense cyclonic storms originating in the northeast Pacific Ocean influence most coastal watersheds and can cause severe and sudden flooding, particularly in the form of rain-on-snow events. Annual precipitation totals rapidly diminish eastward in the interior Stikine Plateau, as the coastal mountains intercept snow and rain from onshore Pacific storms. The drier interior receives less than 600 mm of mean annual precipitation, and is influenced mainly

by a continental climatic regime characterized by long, cold winters and short, cool summers. Annual precipitation-as-snow varies year-to-year in the interior, ranging from approximately 42 to 60% of the annual total (data not shown), with snow accumulation least at lower elevations. Precipitation stored as snowpack is released during the spring freshet (Eaton and Moore, 2010). Snow survey sites indicate that annual SWE measurements are typically highest on or near April 1 in this region (BC River Forecast Centre).

Coastal regions in the study area are located within the Coastal Western Hemlock (CWH) biogeoclimatic zone (Pojar et al., 1987). Stands of mountain hemlock (*Tsuga mertensiana* (Bong.) Carriere) and subalpine fir (*Abies lasiocarpa* (Hook.) Nutt.) dominate high-elevation forests. The Interior Cedar-Hemlock (ICH) zone occupies low- and mid-elevations in the central portions of the Iskut and Stikine rivers. Mature climax forests of western redcedar (*Thuja plicata* (Donn) D. Don) and western hemlock (*Tsuga heterophylla* (Raf.) Sarg.) dominate the ICH landscape. The Boreal White and Black Spruce (BWBS) zone occupies Stikine Plateau valley bottoms up to 1100 m asl. Major coniferous species include white spruce, and lodgepole pine (*Pinus contorta* var. *latifolia* (Engelm.) S. Watson) black spruce (*Picea mariana* (Mill.) Britt.) and subalpine fir. The Spruce Willow-Birch (SWB) zone occurs on plateaus and steep mountain slopes lying above the BWBS, where the forests consist primarily of white spruce and subalpine fir (~900-1500 m asl) (Pojar et al., 1987). White spruce stands located in the BWBS and SWB biogeoclimatic zones were targeted for study.

2.4 Methods

2.4.1 Climate data

SWE data for the Stikine basin is sparse and of short duration, with only three manual snow survey stations located within the entire watershed: Kinaskan Lake (4D11P), Iskut (4D02), and Telegraph Creek (4D01). Data from the Telegraph Creek station was chosen for inclusion in the study as it provided the most complete April 1 SWE record that approximates the maximum seasonal snowpack (1974-2016; station code 4D01; latitude: 57.94° N, longitude: 131.15° W, elevation: 490 m asl). The snow survey records from Telegraph Creek were retrieved from the BC River Forecast Centre (http://bcrfc.env.gov.bc.ca/).

Mean monthly temperature and total monthly precipitation records were retrieved from the Adjusted Homogenized Canadian Climate Database. Climate records at the Dease Lake station (station code 1192341; latitude 58.42° N, longitude: -130.00; elevation: 807 m asl) were considered representative of climate variability in the immediate study area. Temperature records extend from 1947 to 2016, but precipitation records were shorter, extending from 1947 to 2007. Missing values within the climate records were few (<1%) and where present, were replaced with long-term averages calculated over the period of each instrumental record.

2.4.2 Tree-ring data

Tree-ring records were developed from white spruce increment core samples collected at five sites in 1983, 2011, 2014 and 2015 (Table 2.1; Figure 2.1). Sampling for ring-width chronologies involved extracting two 5-mm increment cores from 20 trees at each site. Sample preparation, crossdating and chronology construction followed standard

dendrochronological methods (Stokes and Smiley, 1968; Cook and Kairiūkštis, 1990). Annual ring-widths were measured to the nearest 0.001mm using a Velmex "TA" System in conjunction with J2X software (version 5.0). Calendar dates were assigned to the cores and verified with the COFECHA 3.0 crossdating program (Holmes, 1983; Grissino-Mayer, 2001). COFECHA uses segmented cross correlation techniques to detect measurement and visual crossdating errors. For this study, the time series were partitioned into 50-year segments with 25-year lags and significance determined at a 99% critical level at a correlation of 0.320.

The crossdated site series were standardized with the ARSTAN program (Cook and Holmes, 1984) to produce site-specific master chronologies. Standardization involved fitting an estimated growth function to the ring-width series and computing ring width indices by dividing width measurements by the expected value of the growth curve. For this study, long-term trends unrelated to climate were removed by fitting a cubic smoothing spline with a 50% frequency response cutoff at a wavelength of 67% of the series length to each series. Residual chronologies that contained no statistical persistence were developed by fitting a low-order autoregressive model to the tree-ring data (Box and Jenkins, 1976), with order identified by the Akaike Information Criterion (AIC) (Holmes, 1983). Series from individual cores were combined into single representative master chronologies at each site using a bi-weight robust mean (Mosteller and Tukey, 1977). Adequacy of the sample size is based on the somewhat arbitrary expressed population signal (EPS) statistic (Wigley et al., 1984). Chronologies were truncated where EPS values fell below the standard value of 0.85 with only one decade of this time permitted to drop to an EPS value of 0.80.

Table 2.1: Tree-ring sampling locations of white spruce sites.

Name	ID	Collection year	Easting UTM	Northing UTM	Elevation (m asl)
Tumeka Lake	TL	2014	0463783	6341715	1179
Telegraph Creek	TC	2014	0404699	6457089	720
Ealue Lake	EL	2014	0449555	6403935	930
Danihue Pass	DP	2015	0507624	6395571	1241
Gnat Pass	GP	1983[1]; 2011[2]; 2015	0450205	6456084	1240

[1] Crossdated tree-ring series from International Tree Ring Data Bank (ID: NOAA-tree-4426; Schweingruber, 1983)
[2] Raw cores from the University of Victoria Tree-Ring Laboratory (UVTRL) archives

2.4.3 Diagnostic tree ring-climate relationships

To test the basic assumption of a physiological link between April 1 SWE and white spruce radial tree growth, the residual tree-ring chronologies were compared to the monthly climate data using a Pearson's correlation. Correlation coefficients were evaluated for each month of a 17-month period beginning in April of the previous year and ending in August of the current year. Previous-year climate data was included because current-year growth is often influenced by previous-year growing conditions (i.e., Szeicz and MacDonald, 1996). Correlations were also checked to determine whether April 1 SWE survey data are controlled by the expected climate parameters (winter precipitation and temperatures) to determine whether the tree-ring width data can serve as a proxy for the climate conditions that drive April 1 SWE variability.

The strength of the linear associations between the residual site chronologies and April 1 SWE data were summarized by Pearson's correlation coefficients using the program Seascorr (Meko et al., 2011). To evaluate the temporal stability of the tree ring-SWE relationship over time, a difference-of-correlations test was applied with Seascorr to non-overlapping data subperiods (ie., "early" and "late" sub-periods) utilizing a Fisher's Z-transformation to facilitate significance-testing (Snedecor and Cochran, 1989).

Chronologies that were significantly linear and showed temporally stable relationships with the April 1 SWE data were retained in the pool of candidate model predictors.

2.4.4 Reconstruction model selection and analysis

Multiple linear regression was used to estimate April 1 SWE from the set of candidate tree-ring predictors. Residual chronologies were entered in years *t*, *t+1* and *t+2*, so that the tree-ring information in subsequent years could inform on SWE conditions in a given year (Cook and Kairiūkštis, 1990). A reconstruction model was constructed using a forward stepwise procedure with a cross-validation stopping rule (Wilks, 1995). Given the short 38-year calibration period, a leave-one-out (LOO) cross-validation procedure was employed to validate the model against instrumental data not used in the calibrations (Michaelsen, 1987).

The strength of the regression models for the calibration period was reported using an adjusted R^2, which provides a measure of the model explanatory power. The *F* ratio of the regression model was computed as a goodness-of-fit-test and the standard error (SE) as a measure of uncertainty in the predicted values over the calibration period. Regression residuals were tested for autocorrelation using the Durbin-Watson test and the mean variance inflation factor (VIF) was calculated to identify multicollinearity among predictors. For the verification period the reduction of error (RE) statistic was used to provide a measure of skill of the model. RE has a possible range of $-\infty$ to 1. An RE of 1 indicates perfect prediction for the validation period, and can be achieved only if the model residuals are zero. As a rule of thumb, a positive RE is accepted as evidence of some prediction skill (Fritts, 1976). The root-mean-square error (RMSE) of cross-validation residuals was used to measure of the uncertainty in the predicted values over

the validation period and was compared to the SE as a measure of uncertainty in the regression estimates. The best model calibrated over the full common data period was used to reconstruct historical April 1 SWE variability over the length of the shortest predictor dataset.

The statistical properties of the tree-ring derived reconstruction and instrumental April 1 SWE records were compared to determine whether there were any significant differences within the reconstructed record over the instrumental era, and also to assess the capacity of the model to approximate the statistical characteristics of the instrumental April 1 SWE data. The following statistics of April 1 SWE were addressed in a long-term context: mean, variance and lag-1 autocorrelation coefficient. Box plots were used to compare distributions of the instrumental and reconstructed SWE series over common periods of time, and of the long-term reconstruction. Extreme low SWE years were defined based on a bottom tenth percentile threshold of April 1 SWE levels, calculated over the full reconstruction record. The magnitude of these extreme low SWE years was quantified as departures from the mean of the April 1 SWE record calculated over the reconstructed and instrumental shared period. To examine the effects of low April 1 SWE periods in the Stikine Basin, deviations in monthly Stikine River runoff were compared with the April 1 SWE reconstruction and instrumental data. Seascorr analysis was used to identify the gauged months highly correlated with instrumental April 1 SWE. Each record was standardized into deviations from the record average over the common data period (1974-2011). Comparisons were made using a 3-year moving average in order to better visualize and assess persistent departures. The variability in the departures was graphically compared over the time series. Mean monthly runoff records (1954-2016;

station code 08CE001) were downloaded from the Water Survey of Canada website (https://wateroffice.ec.gc.ca/search/historical_e.html).

The April 1 SWE reconstruction and instrumental data were compared with instrumental records of the PDO over the common data period to investigate large-scale climatological influences on low and high SWE events. A test of proportions (Newcome, 1998) was applied to determine whether the proportion of years with below- or above-median SWE during PDO cool phases (ie., 1900-1924, 1947-1976, 1998-2001 and 2008-2011) equals the proportion of years with below- or above-median SWE during PDO warm phases (ie., 1925-1946, 1977-1997 and 2002-2005). Monthly mean atmospheric teleconnection index records for the PDO (1900-2016) were obtained from the Joint Institute for the Study of the Atmosphere and Ocean website (JISAO, 2016).

2.4.5 Spectral and wavelet analysis

A multi-taper method (MTM) spectral analysis (Mann and Lees, 1996) was performed on the April 1 SWE reconstruction to evaluate dominant frequencies of variability in the time series. MTM offers the appeal of being nonparametric and does not prescribe an *a priori* model for the process generating the time series. The MTM uses orthogonal windows (or tapers) to obtain independent estimates of the power spectrum and averages them to yield a more stable spectral estimate compared to other single-taper methods. It is particularly well suited for short and noisy time series, in that it has the ability to detect small amplitude oscillations without the necessity of filtering the signal and allows for an *F* test to be used to determine the significance level of the different frequency components. The MTM spectral analysis was implemented using the MTM-SSA Toolkit with robust background estimation (Ghil et al., 2002). Following the

suggestion of Mann and Park (1993), where climate records consist of a few hundred observations, three tapers and a bandwidth parameter p=2 were employed. As a complement to the MTM method, a wavelet analysis was used to highlight the evolution of significant frequencies of variability in the April 1 SWE reconstruction over time (Torrence and Compo, 1998; Grinsted et al., 2004). The transformation was computed using the Morlet wavelet with a wavelet power of significance tested at a 90% confidence level against a red-noise background. The wavelet transformations were implemented in R package biwavelet (Gouhier et al., 2016). Significant frequencies of variability detected using the MTM and wavelet analysis were extracted using information from the MTM decomposition via the SSA-MTM toolkit (Ghil et al., 2002). The extracted time series were compared with the PDO index.

A wavelet transform coherence analysis was performed between the April 1 SWE reconstruction and PDO index to identify any interrelationships. The analysis reveals local similarities of power between two time series, and closely resembles the behaviour of a traditional correlation coefficient in the time-frequency plane. The analysis also detects relative phase lags between the time series. The wavelet coherence analysis was implemented using the R package biwavelet (Gouhier et al., 2016). The statistical significance level of the wavelet coherence was estimated using Monte Carlo methods with a red-noise background resulting in significant periodicities of coherence delineated by significance contours. Paleoclimate indices derived from prior tree rings were used to evaluate long-term interrelationships and phase relationships over the shared common period of the records. A moving average filter of 10-yrs was applied to the full reconstruction to better examine longer-term low and high SWE intervals.

2.5 Results

2.5.1 Tree-ring chronologies and climate relationships

Five site-specific white spruce chronologies were developed from a total of 248 radial series from 127 trees, with chronology lengths ranging from 324 to 204 years (Table 2.2). Series intercorrelation values, a measure of the strength of the signal common to all sampled trees, range from 0.548 to 0.658 (Table 2). Mean sensitivity is a measure that describes the interannual changes in ring width (Fritts, 1976) and, in this instance, the values range from 0.160 to 0.204 (Table 2.2). These values are comparable to those established within other white spruce chronologies (ie., Cropper, 1982; Pisaric, 2001), and indicate a strong synchronicity exists within the chronologies developed for this study. To assess the temporal variability in the strength of the common signal in radial growth in the chronologies, running series of average correlations (RBAR) were calculated for each chronology. RBAR is the mean correlation coefficient for all possible pairings among tree-ring series in a chronology, computed for a specified common time interval (Cook and Kairiūkštis, 1990). For this study, a 50-year window with an overlap of 25 years between adjacent windows was employed. RBAR values ranged from r = 0.299 to 0.474. First-order autocorrelation was removed during detrending (r_1 values in Table 2). Chronologies were truncated according to the EPS calculation.

Table 2.2: Tree-ring chronology information.

ID	Period (AD years)	Series, trees	Series intercorrelation	Mean sensitivity	RBAR[a]	r_1[b]	Year[c] EPS 0.80
TC	1773-2014	39, 20	0.658	0.204	0.474	-0.006	1775
EL	1689-2013	40, 20	0.548	0.178	0.299	-0.003	1708
DP	1802-2015	39, 20	0.614	0.174	0.380	0.000	1808
GP	1757-2015	90, 47	0.558	0.160	0.301	0.001	1789
TL	1809-2013	40, 20	0.619	0.173	0.437	0.003	1819

[a] Mean correlation coefficient among the tree-ring series
[b] First order autocorrelation coefficient after autoregressive modeling
[c] Year chronologies were truncated based on the EPS calculation

The results of the correlation analyses with the temperature and precipitation data are shown in Figures 2.2A and 2.2B. Correlations between the monthly climate data and the set of tree-ring chronologies indicate that high-elevation white spruce growth is largely regulated by temperatures spanning the previous growing season, early-spring and summer. More specifically, radial tree growth at sites DP, GP, and TL was generally favoured by cooler springs and warm summer conditions, except when these occurred during the previous growing season. Strong positive correlations with winter precipitation were observed between the two lower-elevation sites (TC and EL). When the temperature signal was removed by partial correlation, the total January precipitation still had a high correlation for TC (0.431, $p < 0.01$) and EL (0.370, $p < 0.01$) chronologies. The TC and EL sites show differing temperature relationships: (1) TC was correlated with previous summer temperatures; and, (2) EL was correlated with growing year summer temperatures. These results show that the tree-ring width data from the study area contains strong hydroclimatological signals.

Correlation was used to summarize the relationships between April 1 SWE and monthly climate records. Seascorr analyses indicate a positive association between winter precipitation (r=0.52 in November-January; p=0.01) and a negative association between

winter temperatures (r=-0.43 in February; p=0.05) (see Supplemental Information 2.9, Figure S2.1). All the chronologies were positively correlated with April 1 SWE over the calibration period. A consistent weakening of the late period correlations was observed, although no significant difference was detected between the early and late periods (Table 2.3). Correlations between tree-ring widths and April 1 SWE were as high or higher than for the other climate variables (Figure 2.2C), suggesting that tree rings integrate a set of climate variables similar to the ones that influence April 1 SWE that includes a mix of both temperature and precipitation conditions.

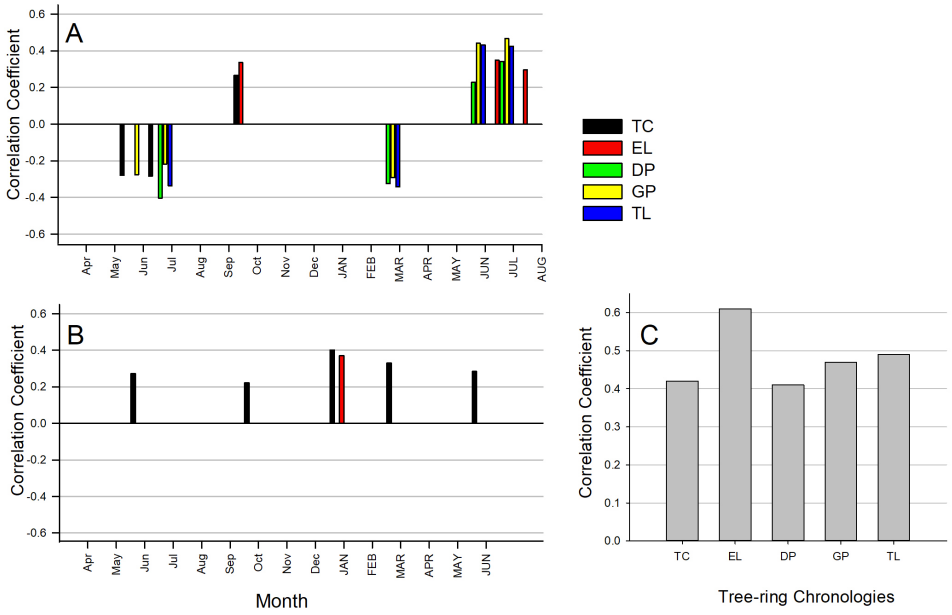

Figure 2.2: Significant Pearson's correlation coefficients ($p < 0.05$) between residual tree-ring chronologies and climate variables. A) mean monthly temperature, B) total monthly precipitation, C) April 1 SWE. Months in lower case are for year preceding growth. Correlations computed for full overlap of paired series, which varies by chronology (ie., time period vary; see Table 2.2).

Table 2.3: Temporal stability of correlations from early to late sub-periods.

Site ID	Correlation coefficient[a]		Effective sample size (N_1/N_2)[b]	Test statistic (ΔZ)[c]	P –value[d]
	Early period	Late period			
TC	0.620	0.330	19/19	0.379	0.284
EL	0.690	0.410	19/18	0.411	0.253
DP	0.610	0.220	20/19	0.473	0.174
GP	0.640	0.240	20/19	0.515	0.139
TL	0.600	0.380	19/18	0.287	0.424

[a] Pearson correlation of tree-ring index with April 1 SWE for the early period (1976-1994) and late period (1995- onward)
[b] Effective sample sizes for the correlations computed on the early (N_1) and late (N_2) periods
[c] ΔZ is the difference between the transformed correlations for the early and late periods
[d] p-value for difference of correlation test

2.5.2 April 1 SWE model estimation

April 1 SWE was reconstructed using white spruce residual chronologies to capture long-term snowpack variability in the Stikine Basin. Two predictor tree-ring chronologies selected for reconstruction, Gnat Pass and Ealue Lake at time t and $t + 2$, respectively. The model equation is:

$$SWE_t = -471.957 + 312.744\ (GP_t) + 307.256\ (EL_{t+2})$$

The reconstruction spans the interval from 1789-2011 and explains 43% of the variance in the April 1 SWE instrumental data. Regression and cross-validation statistics are summarized in Table 4. Analysis of the residual estimates using the Durbin-Watson (D-W) statistic showed no significant first-order autocorrelation. The VIF suggested no multicollinearity among the model predictors and the F-ratio indicates a statistically significant regression equation. The RE values of the cross-validation statistics indicate that the reconstruction has considerable predictive skill. The SE and RMSE are similar, suggesting only a 2.1 mm prediction error difference. The R^2 and r of the observed and LOO-estimates also attest to good model skill.

Table 2.4: Regression statistics of the tree-ring based April 1 SWE reconstruction. Cross-validation statistics in bold.

Calibration						Cross-validation			
R^2	Adjusted R^2	D-W[a]	VIF[b]	SE	*F* ratio	**RE**	**RMSE[c]**	r^d	R^2_v[e]
0.66	0.43	2.14	1.0	59.35	13.18	**0.34**	**61.44**	**0.59**	**0.34**

[a]Durban-Watson statistic
[b]Variance inflation factor
[c]Root mean square error
[d]Pearson correlation of observed and LOO-estimates
[e]R^2 of observed and LOO-estimates

The reconstructed and instrumental SWE survey data are compared over the calibration period in Figure 2.3. The reconstructed data capture the year-to-year variability of the instrumental April 1 SWE data with acceptable accuracy. The magnitudes of the lowest instrumental SWE years were accurately estimated: no major discrepancies between the instrumental and reconstructed records occur during those years. A visual inspection of the calibration time plot shows that the magnitudes of peak SWE years were slightly underestimated.

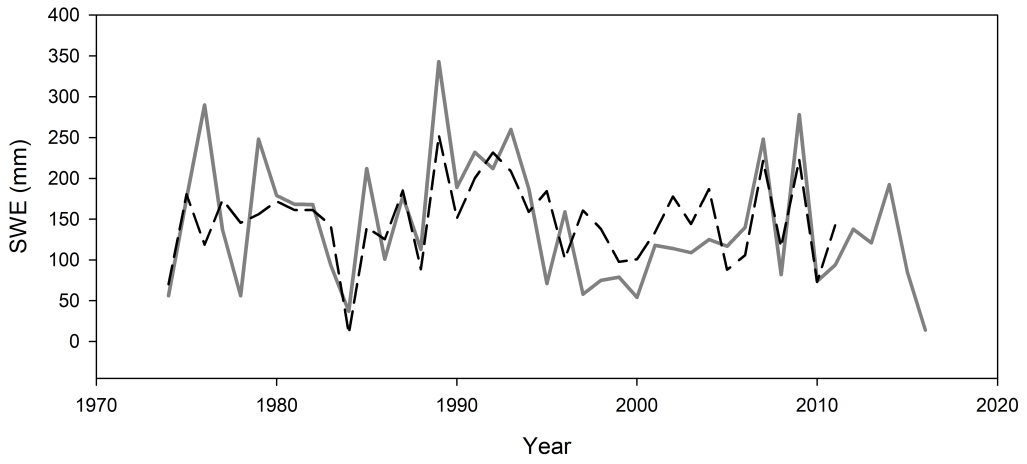

Figure 2.3: Time plot of April 1 SWE instrumental (solid line) and reconstructed (hashed line) for the calibration period (1974-2011).

Comparative statistics are listed in Table 2.5. The standard deviation is lower in the reconstruction than in the instrumental data for the same period (1974-2011), reflecting that not all variance of April 1 SWE is explained in the regression model. The mean SWE values are generally similar between the instrumental and reconstructed records, which is expected when linear least squares is used for reconstruction. Lag-1 autocorrelation is small for the reconstruction periods, and closely mirrors the instrumental autocorrelation (as was the intention in the reconstruction model development). Reconstruction bias towards higher median values, as well as the typical compression of variance by the reconstruction process is evident in box plots (Figure 2.4). Because the statistics of the reconstructions are biased relative to those of the instrumental time series, placement of the hydroclimate statistics of the short instrumental period in a long-term context is restricted to comparisons of reconstructed data.

Table 2.5: Descriptive statistics for the instrumental snow survey and reconstructed April 1 SWE records.

April 1 SWE data	Period (AD years)	Mean (mm)	SD[a]	r_1[b]
Instrumental (full period)	1974-2016	145.44	76.48	0.06
Instrumental (shared period)	1974-2011	148.53	76.56	0.04
Reconstruction (full period)	1789-2011	144.67	46.27	-0.11
Reconstruction (shared period)	1974-2011	148.17	50.10	-0.13

[a] Standard deviation
[b] First order autocorrelation

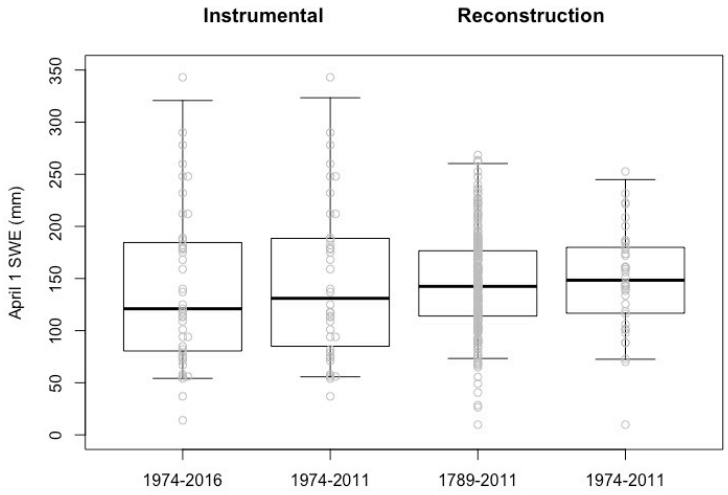

Figure 2.4: Box plots of April 1 SWE levels for instrumental (left two plots) and reconstruction (right two plots) periods with corresponding data (grey dots). Plots show median (bold horizontal line), 25th and 75th percentiles (boxes), and 5th and 95th percentiles (whiskers).

2.5.3 Analysis of the reconstruction

The full April 1 SWE reconstruction for the Stikine Basin is presented in Figure 2.5. The timing and magnitude of extreme low April 1 SWE years over the length of the reconstruction and instrumental period are shown in Figure 2.5A and listed in Table 2.6. A total of 18 extreme low SWE years occurred over the length of the reconstruction (1789-2011) based on the bottom tenth percentile threshold (SWE < 86.62 mm). Fifteen of these extreme low years occurred during the pre-instrumental period (prior to 1974). The most severe SWE mean departures in the reconstructed record occurred in 1984, 1810, 1815, 1887, and 1949. Three out of the four low April 1 SWE years observed during the instrumental record were captured in the reconstruction (Table 2.6). The year 2000 received low SWE levels but was not identified by the percentile cutoff in the reconstructed record (a difference met by only -14.34 mm). Conversely, the year 2010 was identified as a extreme low April 1 SWE year in the reconstructed record but not in

the instrumental record; a difference of only -18 mm was required to meet the threshold cutoff in the instrumental record. The year 2016 showed the lowest departures in the instrumental record, and 1984 was the second lowest.

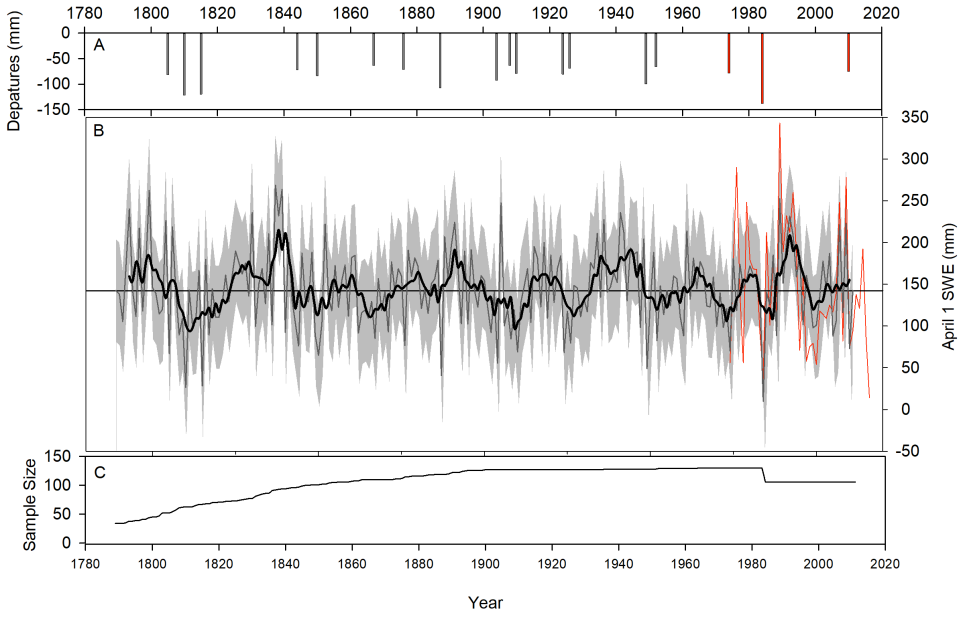

Figure 2.5: A) Extreme low April 1 SWE magnitudes (using the bottom tenth percentile threshold), plotted as departures from the reconstructed instrumental period mean (1974-2011). Red bars denote low SWE extremes in the instrumental period and grey bars denote low SWE extremes over the tree-ring reconstruction. B) The full April 1 SWE reconstruction (dark grey line; mm) for the period 1789-2011. The black line is a 5-year running mean of the reconstructed values, the red line is the instrumental SWE record (1974-2016), and the light grey bars are the ± 1 RMSE uncertainty estimates from the verification period. The horizontal line represents the calibration mean. C) Sample size of the reconstruction period.

Table 2.6: The timing and magnitude of the reconstructed and instrumental low April 1 SWE years, listed in order of severity. (A) Reconstructed bottom tenth percentile (SWE < 86.62 mm) April 1 SWE departures calculated from the 1974-2011 reconstructed mean. Low SWE events within the instrumental period are in bold font; (B) Instrumental bottom tenth percentile (SWE < 56 mm) April 1 SWE departures calculated from the 1974-2011 instrumental mean.

	Year	Departure (mm)
(A)	**1984**	**-138.40**
	1810	-121.70
	1815	-119.60
	1887	-107.60
	1949	-99.13
	1904	-92.63
	1850	-83.29
	1805	-81.38
	1924	-80.20
	1910	-79.22
	2010	**-75.18**
	1844	-72.02
	1876	-71.45
	1974	**-70.01**
	1926	-68.68
	1952	-65.78
	1908	-63.52
	1867	-63.08
(B)		
	2016	-128.12
	1984	-105.12
	2000	-88.12
	1974	-86.12

Correlation was used to summarize the relationships between April 1 SWE and monthly streamflow in the Stikine River. Seascorr analyses indicate a positive association between May-July streamflow (r=0.579). Figure 2.6 summarizes the 3-year moving average plot of departures in the instrumental and reconstructed April 1 SWE and May-July streamflow records. The plots showed a similar general trend of April 1 SWE and May-July streamflow variability. Considering the 3-year moving average, the negative departure duration averaged 4 years in both SWE records with a maximum duration of 9 years (1968-1976) in the reconstructed SWE record and 11 years in the instrumental

record (1996-2005). The negative departure duration averaged 6 years in the streamflow record with a maximum duration of 15 years (1966-1980); sharing a similar time period as the reconstructed SWE maximum departure period and largely occurring prior to the instrumental SWE record. There were a total of 34 deficit years in the SWE reconstruction and 33 in the gauged streamflow record (representing 60.7% and 58.9%, respectively of the total record). The extreme low SWE events identified in Table 2.6 correspond to deficit years in the May-July streamflow record.

Both the reconstructed and instrumental April 1 SWE records exhibited a significantly different proportion of below- and above-median values during cool relative to warm PDO phases. Interestingly, the proportion of below-median April 1 SWE values was highest during the PDO cool phase periods, whereas the proportion of above-median April 1 SWE values was highest during the PDO warm phase periods (Table 2.7). Winter and spring PDO indices were positively correlated to early-spring precipitation (see Supplemental Information 2.9, Figure S2.2), supporting the above findings.

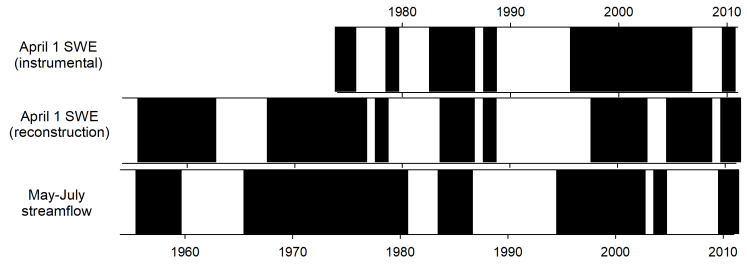

Figure 2.6: Negative departures indicated by a 3-year moving average for the April 1 SWE instrumental period (1974-2011) and over the shared common data period of the April 1 SWE reconstruction and May-July Stikine streamflow (1954-2011). Horizontal widths of vertical black bars indicate duration of negative departures.

Table 2.7: Test of proportions assessing the association of April 1 SWE with PDO warm/cool phases over the instrumental (1977-2016) and reconstructed (1990-2011) periods. Calculated using *R* function *prop.test*. Proportions of years in each SWE category in parentheses. The null hypothesis that the groups have the same true proportions was rejected for all tests, $p < 0.01$.

April 1 SWE category	#cool PDO years	#warm PDO years
Instrumental April 1 SWE		
Below median	9 (90.00%)	12 (42.86%)
Above median	1 (10.00%)	16 (57.14%)
Total	10 (100.00%)	28 (100.00%)
Reconstructed April 1 SWE		
Below median	40 (63.50%)	16 (34.04%)
Above median	23 (36.51%)	31 (65.96%)
Total	63 (100.00%)	47 (100.00%)

2.5.4 Spectral and wavelet analysis

The results of the MTM spectral analysis indicated a significant ($p \leq 0.05$) multidecadal component of variability (~40 yrs), as well as significant ($p \leq 0.05$) variability at interannual time scales (~2 to 3 yrs) in the SWE reconstruction (Figure 2.7). High frequency variability in the 2 to 3 year range is commonly associated with ENSO (Ribera and Mann, 2003). Frequencies within multidecadal bands (ie., 20-70 yr) have been associated with ocean-atmospheric forcings, such as the PDO, where shifts in oscillation patterns (ie., "warm" or "cool" phases) are marked by widespread shifts in climates in the Pacific Basin and North America (Minobe, 2000). The wavelet results generally mirror those of the MTM analysis, with significant multidecadal (~40 years) and 2- to 3- year variability over the majority of the time series (results not shown). The wavelet power spectrum also revealed a marked multidecadal band at ~20 years that persisted over the past century and a significant intermittent power concentration at quasidecadal timescales (ie., ~ 8-15 years) evident in the earlier (<1870 years) and later (>1975 years) part of the series. The results of both the MTM and wavelet spectral

analysis suggest that April 1 SWE may be influenced by interannual and multidecadal frequencies of variability associated with large-scale atmospheric teleconnections.

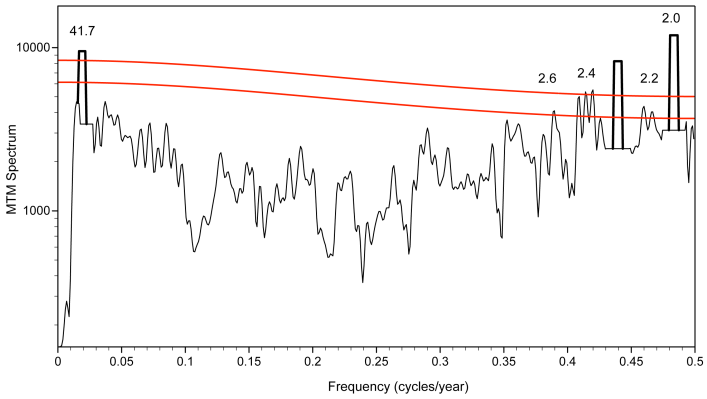

Figure 2.7: MTM spectral analysis of the April 1 SWE tree ring reconstruction for 1789-2011. Red curves represent the 95% and 99% confidence levels (from bottom to top). Significant ($p \leq 0.05$) power exists at the frequencies that are labeled. The black bars denote the harmonic features selected during the reshaping procedure. The reshaped MTM spectrum (solid black curve) denotes the remaining narrowband quasi-periodic components of the spectra and is based on $p = 2$ and $K = 3$, and a 90% F test significance criterion for reshaping.

2.5.5 Connections to the PDO

To examine possible large-scale drivers of April 1 SWE variability in the study region, the time series representing significant multidecadal frequencies of variability were extracted from the reconstructed SWE record using the information from the MTM decomposition. Correlation coefficients between instrumental PDO records and the extracted series were examined after correcting for first-order autocorrelation using the Cochrane-Orcutt transformation (Cochrane and Orcutt, 1949). The results suggest that spring PDO (March through May) conditions are significantly positively correlated (r = 0.302, p <0.01) with multidecadal variability in the April 1 SWE reconstruction. Winter (December to February) PDO conditions were not significantly correlated with the series

following the autocorrelation procedure. The long-term link between April 1 SWE levels and PDO was examined visually by plotting the multidecadal SWE variability against seasonal PDO indices (Figure 2.8A). The results indicate a very distinct in-phase (positive) relationship between reconstructed SWE levels and PDO in both winter and spring, which is consistent with findings in Table 2.7.

A wavelet coherence analysis was performed to examine covariance between SWE values reconstructed in this study and existing paleoreconstructions of the PDO (Biondi et al., 2001; D'Arrigo et al., 2001; Gedalof and Smith, 2001; MacDonald and Case, 2005; Figure 9). The contours (black lines) enclose regions where significant wavelet coherence was detected, based on a red-noise process as determined by a Monte Carlo experiment (Jevrejeva et al., 2003). An important feature of the wavelet analysis is the ability to investigate phase relationships between two time series during periods of coherence. Vectors (represented by arrows in Figure 2.9) pointing to the right indicate that the two signals are in-phase, whereas left aligned vectors indicates an anti-phase relationship. Arrows deviating from the horizontal indicate lead-lag relationships between the two series (Gobena and Gan, 2009). Because lead-lag relationships can be difficult to interpret (ie., a lead of 90° can also be interpreted as a lag of 270° or a lag of 90° relative to the anti-phase (Grinsted et al., 2004), for this study phase angle associations were noted strictly as either being in-phase/anti-phase locked, or as having a lead/lag relationship.

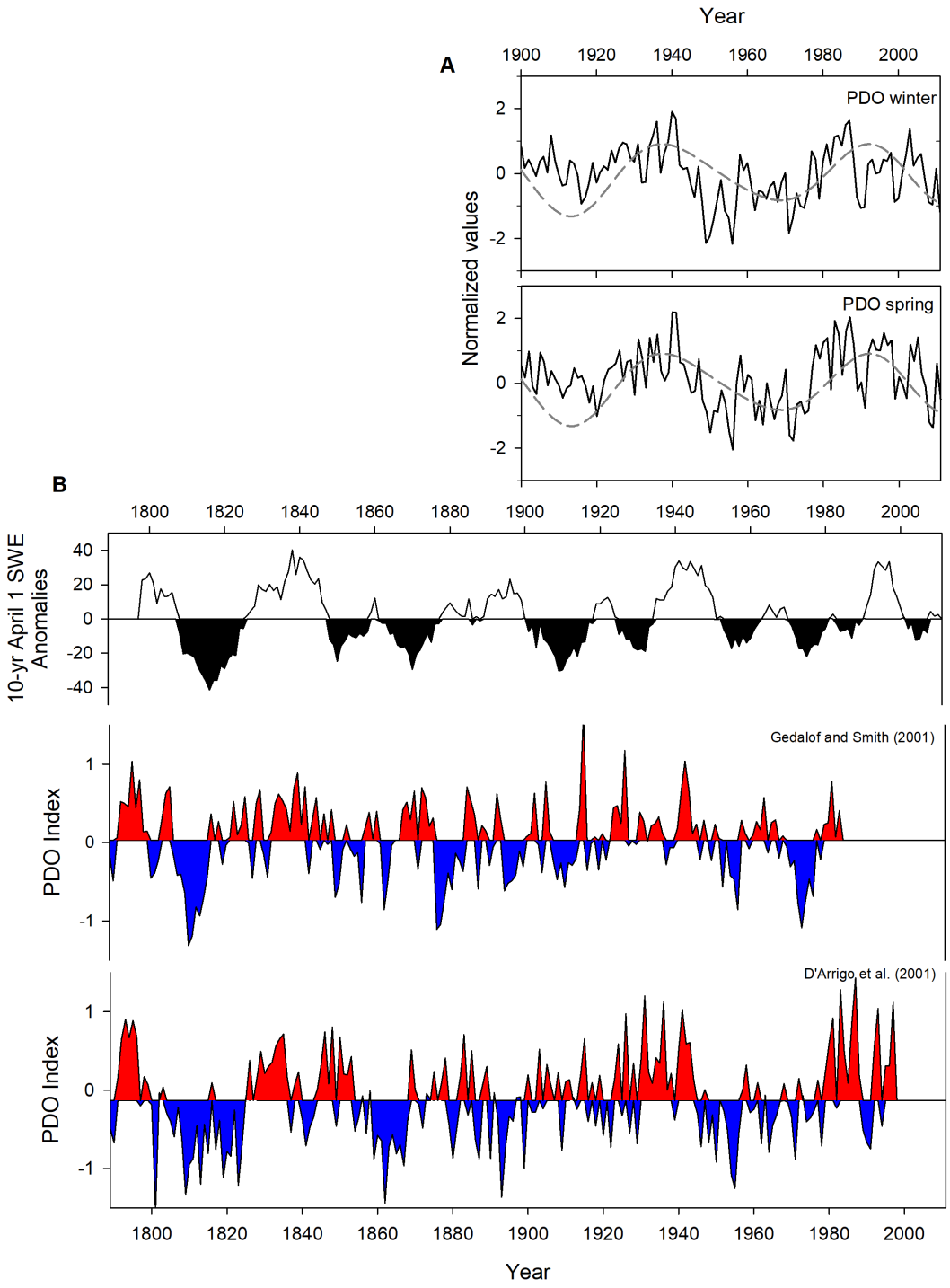

Figure 2.8: A) Plots showing the in-phase relationship between multidecadal variability extracted from the reconstructed SWE record (hashed line) and winter (r = 0.168) and spring (r= 0.302) PDO indices (black line). B) 10-year moving average of standardized (anomaly) values of the reconstructed SWE record (top) compared to the D'Arrigo et al. (2001) and Gedalof and Smith (2001) tree-ring based PDO reconstructions. The average value of each PDO dataset is depicted by the line separating the white/red (warm) and grey/blue (cool) PDO phases.

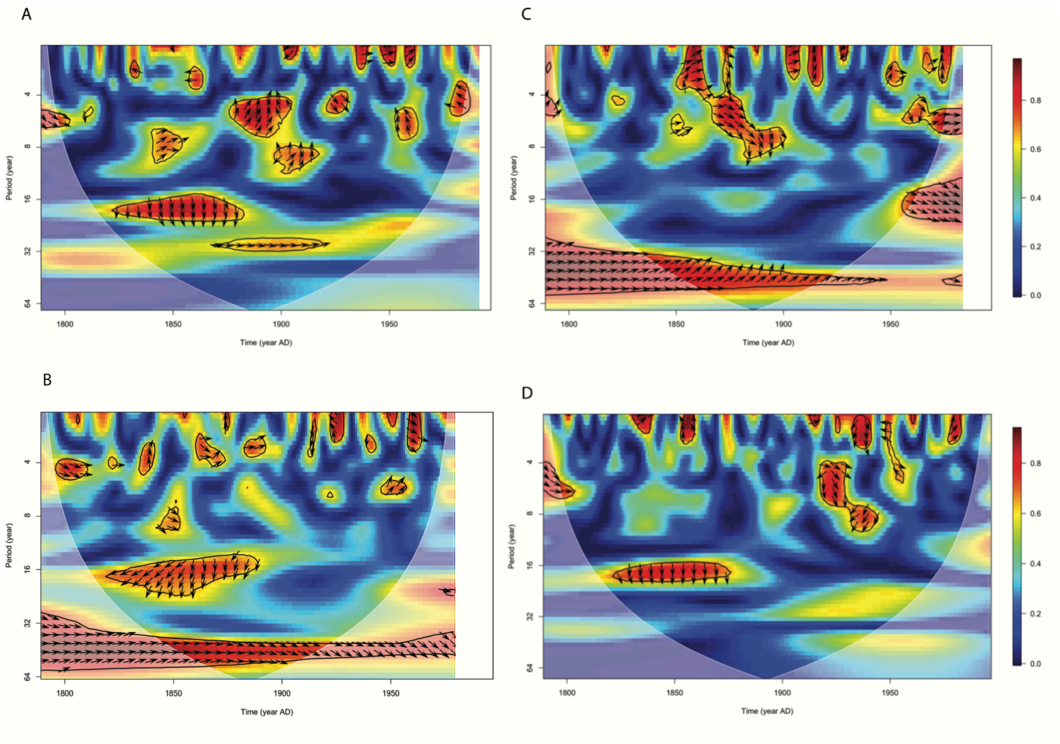

Figure 2.9: Wavelet choherence between the April 1 SWE reconstruction and selected proxy PDO indices: a) Biondi et al. (2001), b) D'Arrigo et al. (2001), c) Gedalof and Smith (2001) and, d) MacDonald and Case (2005) over the common period of each set. Black contours represent 90% confidence level based on a red-noise background spectrum with arrows representing phase relationships. The lighter shade was used to show the cone of influence where edge effects might be important. Legend indicates cross-wavelet power in colours.

The April 1 SWE reconstruction developed in this study shows persistent coherence with the multidecadal component of variability (~40 years) in the D'Arrigo et al., (2001) and Gedalof and Smith (2001) PDO proxy reconstructions (Figures 2.9B and 2.9C) over time. Results at this multidecadal time scale indicate a very distinct in-phase relationship, consistent with the results of the MTM-PDO correlations in Figure 2.8A. The results suggest that higher April 1 SWE was more common in warm PDO phases than in cool phases. In addition, variability at ~20 years shows significant coherence with the PDO proxy indicies of D'Arrigo et al. (2001) and Gedalof and Smith (2001) from the 1820s until the 1870s (Figures 2.9B and 2.9C), as well as the 1950s to present. It also appears

that there is a possible phase lead/lag relationship between the two signals of ~ 5 years. Similarily, the PDO proxy indicies of Biondi et al. (2001) and MacDonald and Case (2005) show significant coherencies at ~20 years during the same time period as D'Arrigo et al. (2001). Common coherence at high-frequencies (2-7 years) was also observed between the SWE-PDO proxy series since the 1900s, but phase relationships were not consistent and as a result, clear directional associations could not be determined.

The D'Arrigo et al. (2001) and Gedalof and Smith (2001) PDO proxy indicies were compared with the April 1 SWE reconstruction in a time plot (Figure 2.8B). To better visualize persistent periods of variability, the April 1 SWE reconstruction was examined through the application of a 10-year moving average filter and standardized. The three records exhibit similar periods of multidecadal variability over time. In addition, persistent low April 1 SWE intervals clearly correspond to the known cool PDO phase periods identified in the 20th century (ie., 1900-1924, 1947-1976, and possibly beginning in 1998). This suggests that April 1 SWE in Stikine basin has expereinced several persistent below-average periods between 1789-2011 that are consistent with long-term patterns of PDO variability. These results help to validate the reliability of the April 1 SWE reconstruction developed in this study, and demonstrate the utility of using climate-sensitive white spruce-derived tree-ring chronologies as a proxy for describing long-term SWE variability.

2.6 Discussion

2.6.1 Predictor selection and model estimation

A primary objective of the research was to develop a robust multi-century record of April 1 SWE variability in the Stikine basin based on white spruce tree-ring chronologies collected from mid- to high-elevation locations. The tree-ring model effectively reconstructs an April 1 SWE record from AD 1789 to 2011 that explains 43% of the variance in the instrumental record. Correlation analyses indicate that: (1) April 1 SWE data integrates both a late-winter temperature (negative) and winter precipitation (positive) signal; and, (2) the selected model predictors serve as proxies for the climate variables. The results are similar to those established in previous studies demonstrating that the radial growth of white spruce trees is significantly associated with annual hydroclimatic variation (ie., Larsen and MacDonald, 1995; Meko, 2006; Porter et al., 2013).

The candidate model predictors in this study show evidence of a common moisture signal but are manifest in three distinct ways: (1) a negative relationship between temperature during the early-spring of current-year growth (sites DP, GP, and TL); (2) a positive relationship with winter precipitation and a negative relationship with temperature during the previous-year growth (site TC); and (3) a positive relationship with winter precipitation and a positive relationship with temperature in the current growing year (site EL). The positive correlation between winter precipitation and white spruce growth highlight the importance of precipitation in determining radial growth at the lower elevation sites where snowpack is more limited (see Table 2.1 for site elevations). Corresponding relationships with temperature, however, suggest that the

physiological link should be interpreted as a record of moisture sensitivity (Szeicz and MacDonald, 1996). Moisture stress caused by high temperatures in the summer preceding ring growth could cause a decrease in photosynthesis and an increase in leaf senescence (Kozlowski et al., 1991; Szeicz and MacDonald, 1996) that would be reflected in decreased resources for early wood formation in the subsequent year. In contrast, a positive growth response to current-year temperatures, as seen in the EL chronology used as a model predictor, may reflect a response to increased availability of soil moisture to the shallow root systems late in the growing season (King, 2009). The negative response to temperatures observed in early-spring in the GP chronology (and others) is assumed related with late-lying snowpacks that limit water stress during the summer and may also help to protect the shallow root systems of white spruce to damaging cold temperatures during the transition from winter to spring (eg., King, 2009; McGuire et al., 2010; Szeicz and MacDonald, 1996). Entry of EL at a lag of two years suggests a significant delay in response to the inertia in the tree biology or the hydrology (e.g., moisture availability in one year still affecting tree vigor in following years). A similar lagged response of white spruce to precipitation in northern environments has previously been reported by Larsen and MacDonald (1995) and Meko (2006).

The cause of the reduction in sensitivity to variations in April 1 SWE during the Seascorr analyses is beyond the scope of this study. The results were deemed temporally stable between early (1976-1994) to late sub-periods (1995-onward) using the difference-of-correlations method. However, it is possible the white spruce chronologies are exhibiting some response to a change in soil moisture conditions. Nonlinear growth responses to soil moisture conditions have been reported in other studies. For instance,

Youngblut and Luckman (2013) propose that declining snowpacks in the southeastern portion of the Canadian Cordillera resulted in earlier snowmelt and less soil moisture availability during peak cambial activity in whitebark pine, and that this resulted in reduced radial growth. Other studies suggest that a delay in snowmelt and soil thawing may be causing a weakening of the climate-tree growth relationship. Vaganov et al. (1999) reported an increasing trend in winter precipitation in the Siberian subarctic, resulting in deeper snowpacks that were connected to a shift in the date of snowmelt and cambial initiation. The supposition is that delayed snowmelt shortens the optimal growing season, which indirectly controls the commencement of cambial activity, and results in decreased tree growth.

2.6.2 Reconstructed record and low April 1 SWE events

A total of 18 extreme low April 1 SWE years were identified from 1789 to 2011 (Figure 2.5A; Table 2.6). The lowest SWE levels were recorded during the instrumental SWE survey period (i.e., 1984). It is recognized that the reconstruction likely underestimates the magnitude of historical low SWE events due to expected variance compression and, as a result, comparisons with instrumental data should be interpreted with caution; however, it is plausible that 2016 levels may have surpassed the lowest April 1 SWE level recorded over the past 227 years. Snow survey reports suggest that snowpacks in 2016 were at levels <60% of the basin index, a level identified as "*well below normal*" in the Snow Survey Bulletin, B.C. River Forecast Centre. The transition from snow accumulation to snowmelt was also identified as two- to three-weeks earlier than the historical average (1981-2010).

Reconstruction of regional snowpack is necessary for the regional discrimination and representation of hydrologic variability within the Stikine Basin in a long-term perspective. Understanding snowpack variability is critical for assessing changing freshwater resources in the region. The temporal variation in the SWE reconstruction and May-July Stikine River departures were consistent (Figure 2.6). Given the examined relevance of April 1 SWE to the hydrology of the Stikine basin, an additional investigation of streamflow variability over an extended record is suggested.

2.6.3 Influences of PDO

Global climate variability at interannual to decadal time scales is linked to large-scale ocean and atmospheric teleconnection patterns such as those described by the ENSO and PDO (Moore, 1996; Fleming et al., 2007; Rodenhuis et al., 2009). These phenomena are major drivers of hydroclimate variability, and have been a major research focus for the past two decades (Mantua et al., 1997; McCabe et al., 2004; Whitfield et al., 2010). The PDO involves shifts between two dominant patterns of sea surface temperatures (SST) in the North Pacific Ocean (Mantua et al., 1997). Previous studies (to the south of our study area) characterized the warm (positive) phase of the PDO by below-normal SSTs in western Canada, unusually high winter temperatures, and negative precipitation anomalies in the mountains that reduce the seasonal snowpack (Moore et al., 2010). The PDO cool (negative) phase produces opposite SST and hydroclimate conditions. PDO oscillations typically persist for 20 to 30 years (Whitfield et al., 2010). Only two full PDO cycles appear to have occurred in the past century: warm PDO regimes prevailed in 1925-1946 and 1977-1997, while cool PDO regimes dominated in 1890-1924 and 1947-1976. PDO conditions, as described above, have been linked to

snowpack accumulation and streamflow timing and magnitude in catchments located throughout southern BC and US Pacific Northwest (Mantua et al., 1997; Wang et al., 2006; Fleming et al., 2007).

Our findings of lower-than-normal SWE during PDO cool phase is in contrast to prior findings (Cayan, 1996; Mote et al., 2003) to the south of the study area. The reconstruction highlights several persistent intervals of low SWE (Figure 2.8B). These intervals clearly correspond to the cool PDO phases identified in the 20th century and vice versa. Intervals of persistent low SWE pre-dating the instrumental PDO record occurred during the early 1800s and mid-to-late 1800s. These earlier intervals coincide broadly with cool PDO phases identified in other tree ring-based proxy records of that index (Figure 2.8B). Results of the wavelet also offer support that significant multidecadal variability in the long-term April 1 SWE reconstruction is consistent with PDO phase shifts. The physical link between PDO warm (cool) phases and increased (decreased) winter precipitation levels in the study region has been described in other studies. For instance, Mantua et al. (1997) demonstrate that wintertime precipitation (December through February) was positively correlated with PDO in the same season along the coast of the central Gulf of Alaska, and reported a tendency of coastal central AK to experience enhanced cyclonic activity by a deepening of the Aleutian Low that increased the flow of warm, moist air under positive PDO conditions in contrast to other areas in BC and Washington state. Warming (cooling) is known to increase (decrease) the moisture potential in the atmosphere and cause a poleward vapour transport to where storms are favoured (i.e., area of the Aleutian Low), leading to more (less) risk of heavy rain and snow events (Trenberth, 2011). The supplementary analyses (Figure S2.2) further support

this. Moore and McKendry (1996) were the first to identify a similar PDO-related north-south "see-saw" pattern in April 1 snowpack anomalies in BC. Moreover, Rodenhuis et al. (2009) found that during cool PDO phases April 1 SWE tended to be higher-than-average in the southern half of BC, but lower-than-average at the most northerly snow courses (which included stations from this study region).

Changes in synoptic-scale circulation involving the Aleutian Low has been observed to be associated with snowpack conditions across BC (Moore and McKendry, 1996). It has been suggested that SWE may be more responsive to the incoming Pacific storm events versus shifts in mean climate (Rodenhuis et al., 2009). The Aleutian Low is the dominant feature of the atmospheric pressure system in the northern North Pacific during the winter (Rodionov et al., 2007). The Aleutian Low influences the path and strength of winter cyclone activity along the coast of the Gulf of Alaska, and the PDO phase changes are closely associated with a strengthening or weakening of the Aleutian Low (Rodionov et al., 2005). Specifically, a strong PDO warm phase are associated with an anomalously strong Aleutian Low, which has a tendency to induce positive SSTs, surface air temperatures and precipitation anomalies in the Gulf of Alaska and negative anomalies in the central North Pacific and the reverse during a weak Aleutian Low (Trenberth and Hurrell, 1994; Mantua et al., 1997). Common coherence analysis with a suite of tree-ring proxy PDO records suggests an in-phase relationship at the multidecadal scales (ie., D'Arrigo et al., 2001; Gedalof and Smith, 2001; Figure 2.9B and C). Moreover, the variable presence or absence of PDO-SWE wavelet coherence (specifically, at ~20 years) suggests that snowpack teleconnections to the PDO strengthen and weaken over long timescales. A similar outcome was found using different methods

by Fleming and Sauchyn (2013) for PDO and streamflow relationships further inland in northwestern North America. This is an important result given the importance of the PDO as an organizing theme for understanding snowpack and water resource variability in the North American west.

The D'Arrigo et al. (2001) and Gedalof and Smith (2001) PDO proxies were developed from tree ring data collected at sites in coastal AK and in the Pacific Northwest. Two of the same temperature-sensitive ring-width chronologies (described in Wiles et al., 1998) were used in the Gedalof and Smith (2001) and D'Arrigio et al. (2001) PDO reconstructions, which could explain the shared coherency between these PDO reconstructions and the SWE reconstruction. This in-phase relationship was not observed with more distant PDO proxy reconstructions to the south of the study area (i.e., Biondi et al., 2001; MacDonald and Case, 2005; Figure 2.9A and D). It is important to emphasize that the SWE reconstruction developed in this study does not share any tree-ring predictors used to employ the PDO proxy reconstructions. Long tree-ring based reconstructions only reflect periodicities in climate variables present in the predictors, which may partially explain why the SWE reconstruction has a strong coherence with one PDO reconstruction and not with another at a particular frequency. Another explanation for the observed differences in cross-spectral properties between the proxies is that the individual cross-wavelet analyses were not run over the same time period. The in-phase behaviour observed with Gedalof and Smith (2001) and D'Arrigo et al. (2001) could suggest that the growth of the trees used in the reconstructions (PDO and April 1 SWE) are primarily "tuned" to synoptic–driven moisture variations associated with the Aleutian Low pressure system. This could further explain the observed difference in the

covariance between the April 1 SWE values and paleoreconstructions of the PDO, and not as an artifact of "tree-to-tree" correlation. Future analyses should consider comparisons with other ocean-atmospheric indices, such as the Pacific North American Index, which measures the overall strength of the Aleutian low.

This study contributes to growing evidence demonstrating a substantial change in synoptic-scale circulation associated with the multi-decadal pattern of the PDO, and teleconnections with SWE patterns in northern BC. The study shows that total springtime snowpack in the Stikine region has been influenced by, and is positively associated with, multidecadal PDO variability over the past two centuries. Connections between April 1 SWE and PDO are particularly concerning since the PDO is currently understood to be in its cool state, and suggests this association may continue to exacerbate the recent trend of diminishing snowpacks in the Stikine region. This finding offers further evidence that the PDO influences the hydrology of near coastal sections of northern BC and Alaska in a manner that is distinct from surrounding regions.

2.7 Conclusion

Long-term perspectives on hydroclimate variability are critical for water management and for the joint planning of climate adaptation in transboundary systems. Prospects of climate and global change leading to increases in extreme weather events have triggered critical reflection about prevailing water management paradigms. The "myth of abundance" (ie. stationary) of water supply has influenced water policy and management, and as a result has created a vulnerable system (Sauchyn et al., 2009). The April 1 SWE model presented in this study contributes to the growing number of successful dendrohydrological studies from "nontraditional" environments and

establishes the utility of using white spruce chronologies as a proxy for the climate variables that drive April 1 SWE variability. The reconstruction of April 1 SWE in this study indicates that there has been considerable variability in SWE levels over the past two centuries in the Stikine region, which is driven in part by multidecadal shifts in the PDO. The results of this study complement and expand on the existing understanding of the region's hydroclimate dynamics (Fleming et al., 2016). It demonstrates that the SWE values recorded in 2016 were likely among the lowest experienced within the past 200 years. This finding has important implications for water management strategies. Comparisons between the instrumental and reconstructed period could suggest that this "extreme" condition is a new phenomenon. Most importantly, any future anthropogenic climate and land-use change will likely exacerbate the severity of low snowpacks. Understanding the key controls of hydroclimate variability has important implications for successful water and ecosystem management, and modeling of future water use scenarios.

2.8 Acknowledgements

Thank you to Dave Meko (University of Arizona) and two anonymous reviewers for their insightful comments and suggestions. The research was supported by awards from the Natural Science and Engineering Research Council of Canada to Smith and Welsh, as well as the Pacific Institute for Climate Solutions and the Garfield Weston Foundation Award to Welsh. The authors would like to thank Jill Harvey, Todd Sherstone, and Doug Thompson for their assistance in the field, and James Telford for mapping support. BC Parks provided research access permits to provincial parks.

2.9 Supplemental Information

2.9.1 Relationship between seasonal climate and April 1 SWE

Figure S2.1 displays partial correlations between April 1 SWE and historical climate records from Dease Lake. These correlation tests were calculated using the program Seascorr, which summarizes the strength of monthly and seasonally aggregated climate data and assesses significance of correlation by a Monte Carlo method (Meko et al., 2011). I tested monthly and 3-month seasonal correlations between April 1 SWE data and the climate data over a 14-month period beginning in August of the previous year and ending in July of the current year. Partial correlations calculated by Seascorr were then used to identify any influence of seasonal precipitation on the SWE data independent of the temperature influence. The highest correlations indicate a positive association between winter precipitation (r=0.52 in November-January; p=0.01) and a negative association between winter temperatures (r=-0.43 in February; p=0.05). Partial correlations were adjusted for a weak negative inter-correlation during current year March between the precipitation and temperature data over the 3-month period. No other inter-correlations were observed.

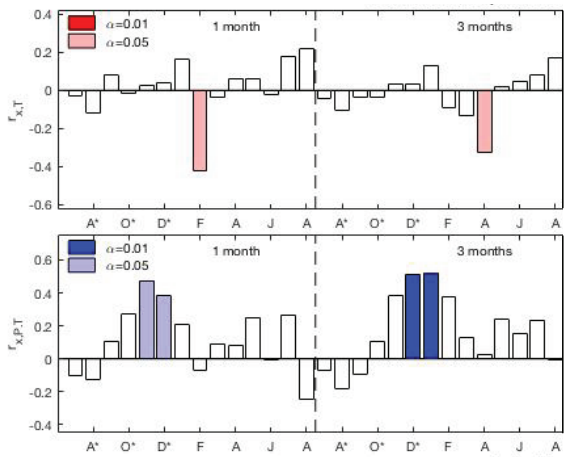

Figure S2.1: Correlations between April 1 SWE data with mean temperature (top; significant correlations in red) and partial correlations with total precipitation (bottom; significant correlations in blue), over 1- and 3-month sliding windows beginning in the previous July through current August and the common period 1950-2007. The temperature and precipitation records were retrieved from the Adjusted and Homogenised Canadian Climate Dataset.

2.9.2 Relationship between seasonal climate and PDO

Figure S2.2 displays partial correlations between winter and spring PDO indices and historical climate records from Dease Lake. These correlation tests were calculated using the program Seascorr, which summarizes the strength of monthly and seasonally aggregated climate and assesses significance of correlation by a Monte Carlo method (Meko et al., 2011). I tested monthly and 3-month seasonal correlations between winter and spring PDO indices and the climate data over a 14-month period beginning in July of the previous year and ending in August of the current year. Partial correlations indicate a positive correlation with March (0.240) and May (0.320) precipitation during winter PDO, and positive correlations with May (0.310) and June (0.300) during spring PDO. Partial correlations were adjusted for a weak negative inter-correlation during previous year September and current year March between the precipitation and temperature data. No other inter-correlations were observed.

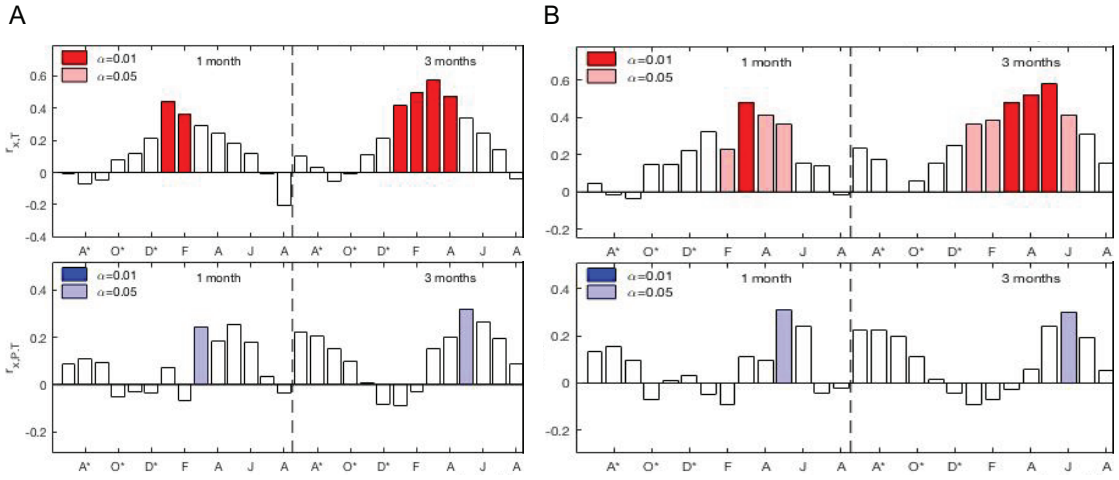

Figure S2.2: Correlations between A) winter PDO data and B) spring PDO with mean temperature (top; significant correlations in red) and partial correlations with total precipitation (bottom; significant correlations in blue), over 1- and 3-month sliding windows beginning in the previous July through current August and the common period 1950-2007. The temperature and precipitation records were retrieved from the Adjusted and Homogenised Canadian Climate Dataset.

Chapter 3: An interbasin comparison of tree-ring reconstructed streamflow in northern British Columbia

3.1 Abstract

Climate sensitive tree-ring chronologies provide an opportunity to extend streamflow records by capitalizing on the influence of climate on both annual radial growth and seasonal runoff. This study presents multi-century long reconstructions of July-August (summer) streamflow for the Skeena (1599-2016), Nass (1301-2016) and Stikine (1670-2012) rivers that serve important ecological and socio-economic values, and have experienced detrimental low flows in recent decades. Furthermore, the study establishes the use of conifers sensitive to snowpack variability in streamflow reconstructions for northern British Columbia (BC) and incorporates the use of regionally specific hemispheric records to improve reconstruction skill. By first demonstrating that tree-ring and hemispheric climate records capture much of the variance in summer streamflow records, and then placing the contemporary record of streamflow in a long-term context, managers now have more information to better plan for periods of low or high variability in flow. The results suggest that current drought conditions are a rare event over a multi-century context and that the instrumental record does not adequately represent the historic range of variability present in the reconstructions. Finally, this research identifies basin-specific variability in summer streamflow associated with moisture transport and atmospheric-ocean circulation. The results demonstrate a north-south "see-saw" pattern of streamflow variability. This study has attempted to refine and expand the existing understanding of temporal and spatial patterns of summer streamflow variability and its climate drivers in northern BC.

3.2 Introduction

Northern British Columbia (BC) has faced a unique water management challenge in the 21st century. Diminishing water security in a region considered water-abundant has intensified over the last decade. Changes to climate have affected the magnitude of winter snow accumulation and timing of melt, raising concerns about the potential for extreme hydrologic events (Sauchyn and Kulshreshtha, 2008). Many rivers in BC have experienced a prolonged summer drought in recent years, and the impact of worsening droughts on human water use, stream ecology and the survival of Pacific salmon is recognized by the provincial government as a critical environmental management challenge (BC Ministry of Environment and Climate Change, 2018). There is a growing need to better understand long-term regional streamflow variability and provide a more comprehensive characterization of past hydroclimate change for northern BC.

Seasonal runoff in northern BC is either snow-dominated (i.e., nival regime) or snow-influenced (i.e., hybrid nival-pluvial or nival-glacial regime) (Eaton and Moore, 2010). These regimes typically exhibit peak flows in the spring freshet (as a result of melt-season temperatures) and low flows in the late summer extending through the winter during the snow accumulation period (Eaton and Moore, 2010). A lack of adequate snow accumulation or anomalously early melt can contribute to summer drought conditions (Bonsal et al., 2011). Fluctuations in large-scale ocean and atmospheric climate oscillations have considerable influence on the climate variables driving streamflow in western Canada (Moore, 1996; Moore and McKendry, 1996; Stewart et al., 2004; Thorne and Woo, 2011). Many studies have demonstrated that the El Niño-Southern Oscillation (ENSO), Pacific Decadal Oscillation (PDO) and the Pacific North American (PNA) teleconnection pattern have important effects on the seasonal patterns of temperature and

precipitation (Mantua et al., 1997; Whitfield et al., 2010). Minor shifts in the spatial and temporal patterns of these climate variables can have major consequences for water availability at the watershed scale, including changes to the timing and magnitude of high and low streamflow (O'Neil et al., 2017).

Average annual temperatures over the northwestern part of North America have increased by 1-2°C since the 1940s, most notably during the winter and spring seasons. Of particular concern is the continued loss of mountain snow accumulation and related reductions in the snow- and glacier-derived water supply, which are among the primary consequences expected from climate warming (Stewart et al., 2005). Documented hydrologic trends have included a shift towards an earlier freshet at the expense of summer runoff (Whitfield and Taylor, 1998; Nijssen et al., 2001; Déry et al., 2009). These trends stress the importance of understanding the long-term variability of streamflow beyond the available instrumented gauged records, data that in most cases are sparse and of short duration.

Climate sensitive tree-ring chronologies provide the opportunity to extend instrumental records of streamflow by capitalizing on the influence of climate on both annual radial growth and seasonal runoff (Loaiciga et al., 1993; Gedalof et al., 2004; Meko and Woodhouse, 2011). Dendrohydrologic modeling has largely been accomplished in dry, continental settings where the annual radial growth is limited by available soil moisture (Meko and Woodhouse, 2011). Where reconstructions of hydroclimate from tree rings have been successful, they have played a prominent role in describing how water availability has varied in the past (e.g., Axelson et al., 2009; Margolis et al., 2011; Meko et al., 2012).

Prior attempts to reconstruct streamflow from tree-ring records in northern BC are not known, and the paucity of moisture-sensitive species makes it difficult to apply traditional methodologies. In this study, this predicament was resolved by focusing on mid- to high- elevation conifers sensitive to snowpack variability. This type of tree-ring data has rarely been used in dendrohydrology. Prehistoric reconstructions of hydroclimate variability in the study area were previously developed from snow depth-sensitive mountain hemlock (*Tsuga mertensiana* (Bong.) Carrière) (Starheim et al., 2013a) and white spruce (*Picea glauca* (Moench) Voss) (Welsh et al., 2019). These studies improved our understanding of long-term summer streamflow variability and large-scale teleconnection patterns in the lower Skeena River (Starheim et al., 2013a) and, in northern BC, the long-term influence of PDO on snowpack dynamics in the Stikine Basin (Welsh et al., 2019). Together, these studies allude to differences (both spatially and temporally) in synoptic-scale circulation associated with the multidecadal pattern of the PDO and teleconnections influencing winter precipitation delivery to snowmelt-dominated rivers (Welsh et al., 2019). Specifically, a possible long-term PDO-related north-south "see-saw" pattern in winter/spring precipitation anomalies was identified, a phenomena that was originally identified within gauged data (e.g., Moore and McKendry 1996; Mantua et al., 1997; Rodenhuis et al., 2009). Given the importance of the PDO as an organizing theme for understanding snowpack and water resource availability in western North America, this is a significant outcome of the prior research that requires further investigation.

For regional water managers tasked with planning for future droughts, tree-ring reconstructions of magnitude, severity and periodicity of long-term streamflow variability

provide a solid basis for planning (Woodhouse and Lukas, 2006). Long-term reconstructions can not only illuminate hydrologic extremes, but also reveal low-frequency variability of long-term, low and high flow periods. Finally, the annual resolution afforded by tree-ring reconstructions would allow water managers the opportunity to assess observed extremes in the context of the most accurate possible estimation of streamflow variability over multi-century scales (Woodhouse and Lukas, 2006). In addition, interbasin comparisons will enable identification of the common and disparate atmospheric, hydrologic and anthropogenic drivers of the variability in streamflow (Maxwell et al., 2017).

This study combines tree-ring records of ring-width and maximum latewood density records from snow depth-sensitive mountain hemlock (Peterson and Peterson, 1994; Larocque and Smith, 1999; Gedalof and Smith, 2001; Starheim et al., 2013a), white spruce (Welsh et al., 2019) and subalpine fir (*Abies lasiocarpa* (Hook.) Nutt.) (Wood and Smith, 2013) with palaeo-reconstructions of hemispheric teleconnections as predictors in a dendrohydrological model of summer streamflow. The major objectives of the research were to: (a) develop reconstructions of summer streamflow for three major river basins in northern BC (the Skeena River [LSR]; the Nass River [NSR]; and the Stikine River [STK], all sharing the same headwater region); (b) conduct an interbasin comparison of streamflow variability at three temporal scales: annual, decadal and multi-decadal; and, (c) relate streamflow patterns to the influence of North Pacific climate variability. A previous summer streamflow reconstruction of the Skeena River (Starheim et al., 2013a) was used to evaluate whether the incorporation of hemispheric teleconnection records and new tree-ring chronologies would improve this evolving

dendrohydrological modeling approach. Comparing the new Skeena River reconstruction and those from adjacent river basin reconstructions to potential climatological drivers offers a more comprehensive characterization of past hydroclimatological trends in northern BC.

3.3 Study Area

3.3.1 Hydroclimate setting

The Skeena, Nass and Stikine river basins drain a large area of northwest BC. The rivers share the same headwater location, originating in the semi-arid Spatsizi Plateau of northern interior BC. The rivers drain a large number of glacierized, high-elevation watersheds in the BC Coast Ranges and exit into the Pacific Ocean (Figure 3.1).

Climates vary with respect to relative proximity to the Pacific Ocean and the Coast Mountain ranges. The western flank of the study area is typified by abundant precipitation (average 2,310 mm per year) and cool summers and mild winters, where the daily average temperatures ranging from -0.2°C to 2.4°C in January to 13.3°C to 13.8°C in August (1981-2010 Climate Normals for Petersburg, AK, and Prince Rupert, BC, respectively; retrieved from National Weather Service, 2018 and Environment Canada, 2018 websites, respectively). Precipitation reaches a maximum in the fall and early winter when it is associated with intense cyclonic storms from the North Pacific that can cause severe and sudden flooding, particularly in the form of rain-on-snow events. The degree and extent of the moderating coastal influence diminishes quickly with elevation and in an easterly direction. The interior portion of the study area has a cooler and drier boreal climate, with daily average temperatures ranging from -16.1°C to -7.2 °C in January to 11.7°C to 14.6°C in August (1981-2010 Climate Normals for Dease Lake and

Smithers. BC; retrieved from Environment Canada, 2018 website). This region receives annual precipitation totals ranging from ~600 to 400 mm, with variable amounts of snow, depending upon elevation, that range from approximately 60% to 40% of the annual precipitation total (data not shown). Snow survey sites indicate that annual snow-water-equivalent (SWE) measurements are typically highest on or near April 1 in this region (BC River Forecast Centre).

More than 85-90% of the total annual discharge in the Skeena, Nass and Stikine rivers occurs during the May-October melt season (Figure 3.2). Precipitation stored as snowpack is released during the spring freshet, and stream flows typically reach maximum values in June. In contrast, winter season discharge (November-April) is characteristically low and puncuated by short duration extreme flow events resulting from rain or rain-on-snow events. The percentage of total annual flows contributed by July-August (summer) streamflow is 25-30%, with the Skeena River representing the smallest fraction.

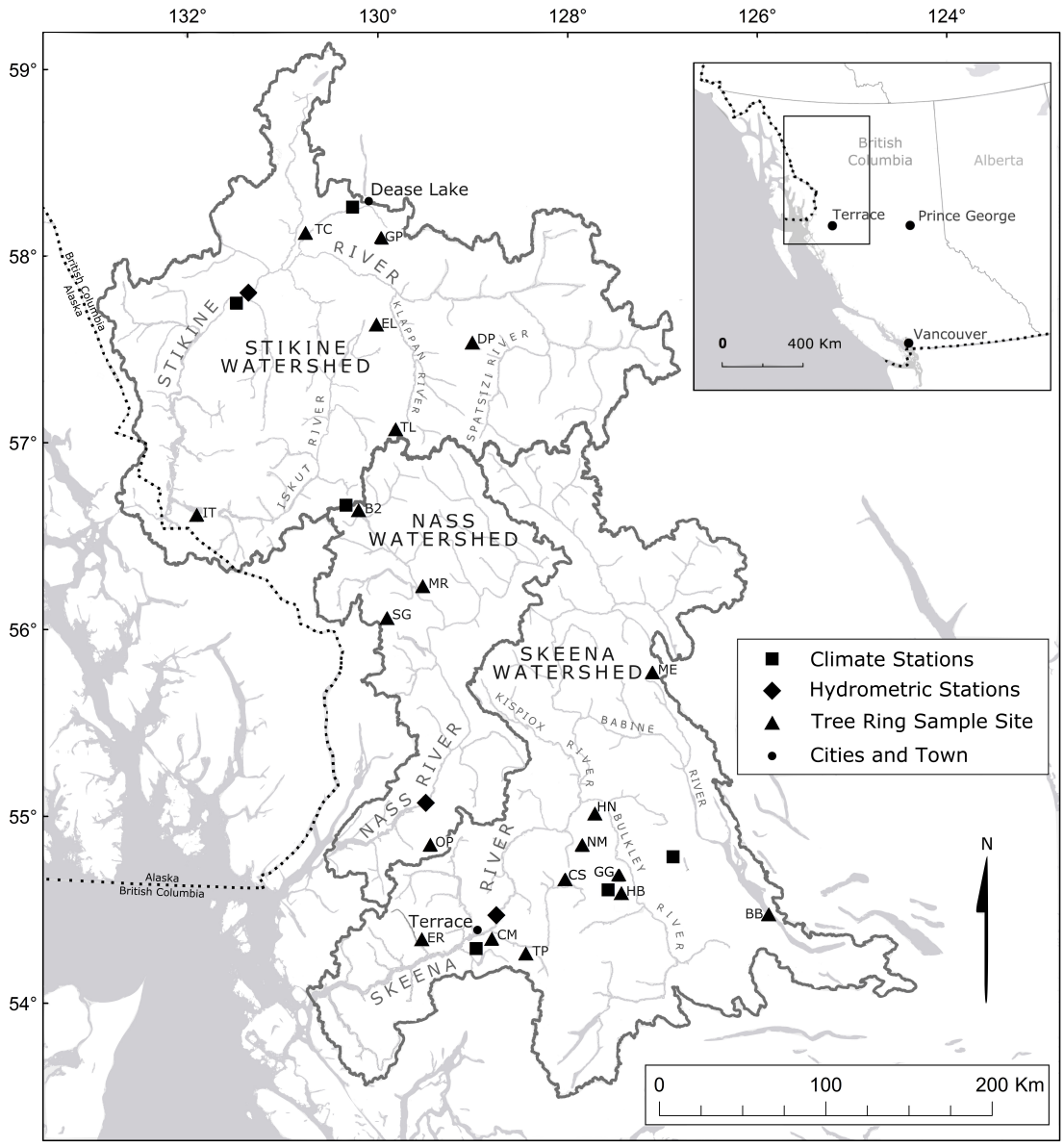

Figure 3.1: Map of the Stikine, Nass and Skeena river basins showing the position of hydroclimatic stations and the location of tree ring sample sites.

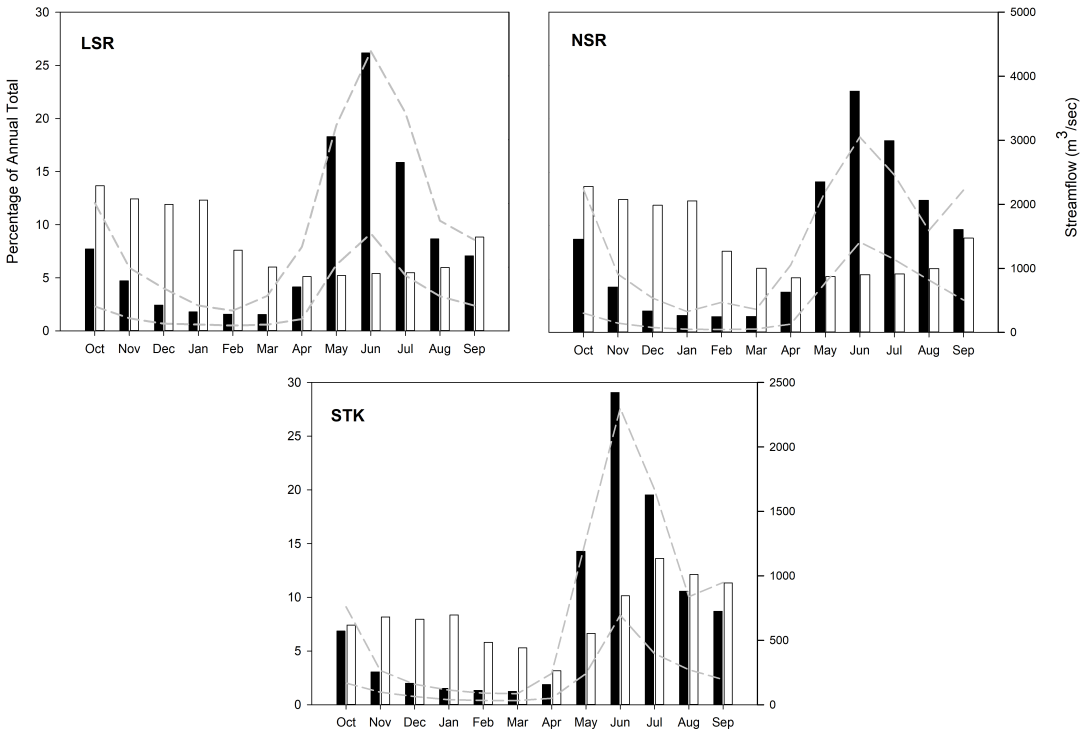

Figure 3.2: Gauged mean monthly discharge (black bars) and precipitation (white bars) represented as a percentage of the annual total over the length of the record used for the A) Skeena River; LSR, B) Nass River; NSR, and C) Stikine River; STK (Table 1). The hashed lines indicate the lowest and highest recorded monthly discharge in any year for the period of the record. Dease Lake total precipitation was used for STK; and a regionalized total precipitation of Terrace and Smithers was used for both LSR and NSR.

3.3.2 Forest stands

Coastal regions in the study area are located within the Coastal Western Hemlock (CWH) biogeoclimatic zone (Pojar et al., 1987). Western hemlock (*Tsuga heterophyll* (Raf.) Sarg.) is the most common tree species in the CWH, followed by western redcedar (*Thuja plicata* (Donn) D. Don), Sitka spruce (*Picea sitchensis* (Bong.) Carrière) and variable amounts of yellow-cedar (*Chamaecyparis nootkatensis* (D. Don) Spach) in coastal locations. Stands of mountain hemlock (*Tsuga mertensiana* (Bong.) Carrière) and subalpine fir (*Abies lasiocarpa* (Hook.) Nutt.) dominate high-elevation forests.

The Interior Cedar-Hemlock (ICH) zone occupies low and mid-elevations in the central to upper Skeena and Nass River drainages, and central portions of the Iskut and Stikine River watersheds. Mature climax forests of western redcedar and western hemlock dominate the ICH landscape. The Engelmann Spruce – Subalpine Fir zone (ESSF) lies above the ICH in the study area, where stands of Engelmann spruce (*Picea engelmannii* Parry ex Engelm.), amabilis fir (*Abies amabilis* Douglas ex J. Forbes) and subalpine fir trees dominate low and mid-elevations forests. Stands of mountain hemlock and subalpine fir characterize higher elevations in the ESSF. The Sub-Boreal Spruce (SBS) zone is situated east of the Skeena basin at elevations above the ICH and below the ESSF zones. The SBS represents an interior transition forest primarily composed of hybrid spruce (Roche spruce; *Picea sitchensis x glauca* or *Picea sitchensis x engelmannii*), subalpine fir and lodgepole pine (*Pinus contorta* var. *latifolia* (Engelm.) S. Watson). Douglas-fir (*Pseudotsuga* menziesii (Mirb.) Franco) is abundant on warm, dry and rich sites in the south-central portion of the SBS.

The Boreal White and Black Spruce (BWBS) zone occupies the Stikine Plateau up to 1100 m asl. Major coniferous species in this region include white spruce (*Picea glauca* (Moench) Voss), lodgepole pine, black spruce (*Picea mariana* (Mill.) Britt.) and subalpine fir. The Spruce Willow-Birch (SWB) zone occurs on the plateau surface and on steep mountain slopes lying above the BWBS, where the forests consist primarily of white spruce and subalpine fir (~900-1500 m asl) (Pojar et al., 1987).

3.4 Data and Methods

Several hydroclimate datasets were examined to reconstruct summer streamflow including hydrometric, April 1 SWE and regional climate records, as well as instrumental and proxy-based atmospheric teleconnection and sea surface temperature (SST) indices. Annual tree-ring width and maximum latewood density chronologies derived from multiple tree species that are potentially sensitive to variations in annual snowpack and streamflow were developed for this study. Tree-ring chronologies previously developed by Wood and Smith (2015), Welsh et al. (2019), and others were also incorporated in the study (Table 1). Several steps were undertaken to ensure the strongest datasets were analyzed.

3.4.1 Tree-ring width data

Tree-ring records were developed from mountain hemlock, white spruce, subalpine fir and Douglas-fir increment core samples collected at 20 sites (Table 3.1; Figure 3.1). Sampling involved extracting two 5-mm increment cores from 20 trees at each site whenever possible. Sample preparation, crossdating and chronology construction followed standard dendrochronological methods (Stokes and Smiley, 1968; Cook and Kairiūkštis, 1990). Annual tree ring-widths were measured to the nearest 0.001mm using a Velmex "TA" System in conjunction with J2X software (version 5.0). Calendar dates were assigned to the ring-width series and verified with the COFECHA 3.0 crossdating program (Holmes, 1983; Grissino-Mayer, 2001). COFECHA uses segmented cross correlation techniques to detect measurement and crossdating errors. For this study, the time series were partitioned into 50-year segments with 25-year lags, with the significance determined at a 99% critical level at a correlation of 0.320.

Each crossdated series was standardized using ARSTAN (Cook and Holmes, 1984) to produce site-specific master chronologies. Standardization involved fitting an estimated growth function to the ring-width series and computing ring width indices by dividing width measurements by the expected value of the growth curve. For this study, long-term trends unrelated to climate were removed by fitting a cubic smoothing spline with a 50% frequency response cutoff at a wavelength of 67% of the series length to each series. Series from individual cores were combined into single representative master chronologies at each site using a bi-weight robust mean (Mosteller and Tukey, 1977).

Table 3.1: Tree-ring sampling locations.

Name	ID	Species[a]	Data[b]	Collection year	Zone	Easting UTM	Northing UTM	Elevation (m asl)
Tumeka Lake	TL	Sw	TRW	2014	09V	0463783	6341715	1179
Telegraph Creek	TC	Sw	TRW; MXD	2014	09V	0404699	6457089	720
Ealue Lake	EL	Sw	TRW; MXD	2014	09V	0449555	6403935	930
Danihue Pass	DP	Sw	TRW	2015	09V	0507624	6395571	1241
Gnat Pass	GP	Sw	TRW	1983[c]; 2011[d]; 2015	09V	0450205	6456084	1240
Bell 2	B2	Hm	TRW; MXD	2011[d]; 2014	09V	0443525	6292381	1143
Mount Richie	MR	Hm	TRW	2014	09V	0484022	6248506	1088
Iskut	IT	Hm	TRW	2016	09V	0346393	6285490	842
Surprise Glacier	SG	Hm	TRW	2005[d]	09V	0463396	6228516	808
Copper Mountain	CM	Hm	TRW	2005[e]	09U	0534539	6039285	887
Cablespur	CS	Hm	TRW	2005[e]	09U	0577078	6076905	1090
Extew River	ER	Hm	TRW	2005[e]	09U	0492441	6037306	875
Hankin Mountain	HN	Hm	TRW	2015	09U	0593293	6116862	1053
Motase Lake	ME	Hm	TRW	2015	09U	0624300	6202858	1432
Trapper Mountain	TP	Hm	TRW	2015	09U	0555377	6031437	1256
Glacier Gulch	GG	Hm	TRW	2002[f]	09U	0610309	6075745	1400
Oscar Peak	OP	Hm	TRW	2016	09U	0495162	6093986	1306
Hudson Bay	HB	Bl	TRW	2003[d]	09U	0611306	6070014	1465
Nipple Mountain	NM	Bl	TRW	2012[d]	09U	0586472	6041601	814
Babine Lake	BB	Fd	TRW	2006[g]	10U	0345120	6041601	980

[a] White spruce (Sw); Mountain hemlock (Hm); Subalpine fir (Bl); Douglas-fir (Fd)
[b] Ring-width (TRW); maximum latewood density (MXD)
[c] Crossdated tree-ring series from International Tree Ring Data Bank (ID: NOAA-tree-4426; Schweingruber, 1983)
[d] Crossdated tree-ring series from the University of Victoria Tree-Ring Laboratory (UVTRL) archives
[e] Crossdated tree-ring series from Starheim et al. (2013a)
[f] Crossdated tree-ring series from International Tree Ring Data Bank (ID: ITRDB cana390, Aravena et al. 2002)
[g] Crossdated tree-ring series from Wood and Smith (2015)

Residual chronologies with no statistical persistence were constructed by fitting low-order autoregressive models to the tree-ring data (Box and Jenkins, 1976), with order identified by the Akaike Information Criterion (AIC) (Holmes, 1983). Adequacy of sample size is based on the expressed population signal (EPS) statistic (Wigley et al., 1984). Chronologies were truncated where EPS values fell below the standard value of 0.85, with only one decade of this time permitted to drop to an EPS value of 0.80.

3.4.2 Tree-ring density data

Maximum latewood density records were developed from 12-mm core samples collected at one mountain hemlock and two white spruce sites. Each 12 mm core was prepared for densitometric analysis by first gluing it flush to the surface of a 2.5 cm-wide fibreboard block. A 2-mm thick wood lath was cut (pith to bark) with a Waltech high precision twin-bladed saw to reveal the radial surface of the core (Haygreen and Bowyer, 1996). Resins were extracted from the laths using an acetone Soxhlet apparatus (Jensen, 2007). Each sample was then x-rayed using the University of Victoria Tree-Ring Laboratory (UVTRL) ITRAX MultiScanner densitometer (Cox Analytical Systems, see http://www.coxsys.se). Measurements were made at 0.05-mm increments for 125 µs, with the densitometer maintained at 30 kV and 40 mA. The digital x-ray images were analyzed using ITRAX Windendro® version (2008) to provide ring width and maximum density values.

The maximum latewood density series were crossdated by identifying characteristic annual ring patterns using the corresponding ring-width measurements. Series crossdating was verified using COFECHA 3.0 (Holmes, 1983; Grissino-Mayer, 2001) and annually resolved maximum latewood density chronologies were produced. The crossdated site

series were standardized with ARSTAN (Cook and Holmes, 1984) to produce species-specific master chronologies. A cubic smoothing spline with a 50% frequency response cutoff at a wavelength of 67% of the series length was applied to each series to remove non-climatic impacts. To eliminate autocorrelation issues, only residual chronologies estimate by autoregressive modeling (as described above) were used in subsequent analysis. Adequacy of sample size was determined by the EPS statistic.

3.4.3 Hydroclimate data

Mean monthly discharge records for the Skeena, Nass and Stikine rivers were downloaded from the Water Survey of Canada website (Table 3.2; https://wateroffice.ec.gc.ca/search/historical_e.html). Hydrometric stations were selected based on several criteria that included the requirement that ≥60 years of continuous natural flow data were available and that there was a uniform absence of year-to-year statistical persistence during summer flows (Table 3.3). The streamflow data (m^3) were seasonalized (summed) over July-August for each hydrometric station and *z*-scores calculated over the full data period. Shapiro-Wilks goodness-of-fit statistics and Lung-Box tests were used to evaluate the data for non-normality and autocorrelation persistence, respectively.

Table 3.2: Study basin information.

Gauge	Station ID	Code[a]	Basin	Drainage area (km^2)	Mean annual flow (m^3/s)	Length of record (yrs)
Skeena River	08EF001	LSR	Skeena	54,000	908.06	1940-2016
Nass River	08DB001	NSR	Nass	20,839	765.67	1956-2016
Stikine River	08CE001	STK	Stikine	52,000	406.49	1954-2016

[a] Gauge codes correspond to Figure 1

Table 3.3: Summer discharge statistics.

Station Code	CV[a]	Shapiro-Wilk test[b]	*p*-value[c]	Ljung-Box Statistic[d]	*p*-value[e]	% Missing value
LSR	0.27	0.96	0.06	2.55	0.86	0.00
NSR	0.15	0.97	0.22	7.08	0.31	0.00
STK	0.25	0.98	0.28	3.25	0.78	0.99

[a] Coefficient of variation for summer discharge.
[b] Normality determined by the Shapiro-Wilk test (Shapiro and Wilk, 1965).
[c] *p*-value associated with Shapiro-Wilk test; null hypothesis rejected.
[d] Test of randomness for lags 1 through 6; significance based on the asymptotic chi-square approximation (Ljung and Box, 1978).
[e] *p*-value associated with Ljung-Box test; null hypothesis rejected.

Mean monthly temperature and total monthly precipitation records were retrieved from the Adjusted and Homogenized Canadian Climate Database for Terrace (1915-2016; station code 1068134; latitude 54.47°N, longitude: 128.58°W; elevation: 217 m asl), Smithers (1923-2016; station code 1077500; latitude 54.82° N, longitude: 127.18°W; elevation: 522 m asl) and Dease Lake (station code 1192341; latitude 58.42° N, longitude: 130.00°W; elevation: 807 m asl) weather stations (https://www.ec.gc.ca/dccha-ahccd). While temperature records for the Dease Lake station extend from 1947 to 2016, precipitation records extend only from 1947 to 2007. Following verification by correlation analysis to ensure general statistical agreement between the station data, the temperature and precipitation series were regionalized by averaging accordingly. Missing values within the climate records were few (<1%) and where present were replaced with long-term averages calculated over the period of each instrumental record.

April 1 SWE data are sparse and of short duration in the study area. For this study, instrumental SWE data were retrieved from the BC River Forecast Centre (http://bcrfc.env.gov.bc.ca). April 1 SWE approximates the maximum seasonal snowpack in the study area. Data from three snow survey stations were selected based on the

duration of their record and preliminary correlation analysis (data not shown) with corresponding streamflow data: Telegraph Creek (1974-2016; station code: 4D01; elevation: 490 m asl), Ningunsaw (1974-2016; station code: 4B10; elevation: 647 m asl), Mount Cronin (1969-2016; station code: 4B08; elevation: 1491 m asl).

Monthly mean atmospheric teleconnection index (ATI) records for the Pacific Decadal Oscillation (PDO) (1900-2016) and the Pacific North America (PNA) (1950-2016) pattern were obtained from the Joint Institute for the Study of the Atmosphere and Ocean website (JISAO, 2016). Monthly Extended Reconstructed SST (ERSST version 4) in the Niño 3.4 region (1950-2016) were used to measure the variability linked to the El Niño-Southern Oscillation (ENSO) and were retrieved from the National Centre for Atmospheric Research (NOAA, 2016) database.

3.4.4 Hydroclimate relationships and diagnostic tree-ring correlation analysis

To identify the climate variables controlling summer streamflow in the study area, and to justify a largely snow-based reconstruction model of the rivers, correlations between gauged streamflow data and various monthly and seasonal climate records were examined. A Pearson correlation coefficient was used to summarize the strength of linear associations between summer streamflow and April 1 SWE using the program Seascorr (Meko et al., 2011). The nearest April 1 SWE station to each streamflow gauge was used in the correlation analysis. Correlations of the gauged streamflow data with regionalized temperature and precipitation were tested over 1-, 3-, 6- and 12-month intervals, with intervals ending in each month of a 14-month period beginning in July of the previous year and ending in August of the current year. To evaluate the temporal stability of the relationship over time, a difference-of-correlations test was applied with Seascorr to non-

overlapping data subperiods (i.e., "early" and "late" sub-periods) utilizing a Fisher's Z-transformation to facilitate significance-testing (Snedecor and Cochran, 1989).

The relationship between summer streamflow and selected ATIs (i.e., PDO and PNA) and SSTs (i.e., Niño 3.4) were also examined using the program Seascorr. Climate indices that were significantly linear, and showed temporally stable relationships with the streamflow data, were considered sufficiently robust for consideration as possible reconstruction predictors.

To test the basic assumption of a physiological link between the hydroclimate data and radial tree growth, the residual tree-ring chronologies were compared to the April 1 SWE and streamflow records using a Pearson's correlation. In order to determine whether the tree-ring width data could serve as a proxy for the climate conditions that drive summer streamflow variability, correlation analyses was used to identify whether streamflow was controlled by the same climate parameters responsible for radial growth. The temporal stability of the tree ring relationships over time was examined as described above. Chronologies that were significantly linear and showed temporally stable relationships with the April 1 SWE and streamflow data were retained in the pool of candidate model predictors for the corresponding basin.

3.4.5 Use of proxy-based Pacific Ocean climate indices

Previous dendrohydrological studies have shown an increased level of accuracy in reconstruction models when climate indices are introduced to augment the predictor pool (Anderson et al., 2012; Coulthard et al., 2016). In this instance several long-term, proxy climate indices were included in the predictor pool: a prior winter (November-January) Niño3.4 index (Li et al., 2013), a proxy PNA reconstruction (Starheim et al., 2013a), and

a mean spring PDO (March- May) proxy (Gedalof and Smith, 2001). It is important to emphasize that the streamflow reconstructions developed in this study do not share any tree-ring predictors with those used to construct these proxy records.

The canonical ENSO variability proxy was retrieved from the NOAA Paleoclimatology database (https://www.ncdc.noaa.gov/data-access/paleoclimatology-data/datasets). It was derived from 2,222 tree-ring chronologies from sites in Asia, New Zealand, and North and South America. This Niño3.4 index describes prior winter conditions and covers the interval from 1301-2005. A correlation analysis was performed to determine its suitability for reconstruction modelling. The PNA index is a proxy of October-April atmospheric pressures and spans the interval from 1658-2009. The PDO index was developed from tree-ring chronologies collected at sites in coastal Pacific North America extending from Alaska to northern California. It extends from 1599-1983 and targets mean spring PDO (March- May) conditions. Rigerous prescreening of the ENSO, PNA and PDO indices indicated they shared a correlated variability to instrumental streamflow records from the study area.

3.4.6 Model development strategy

An iterative nesting method was used to develop the streamflow reconstructions. This approach involved organizing the tree-ring data over a common period and iteratively removing shorter series to allow for extension of the reconstruction back (as well as forward) in time. Residual chronologies in years *t*, *t+1* and *t+2* that showed significant correlation with streamflow were entered into the predictor pool, so that the tree-ring information in subsequent years could inform on streamflow conditions in a given year (Cook and Kairiūkštis, 1990). Cross-validation was performed using a

traditional split period approach to independently verify the tree-ring based streamflow estimates. The nests were then scaled so each had the same mean and variance as the most replicated nest (hereafter referred to as N1), after which the relevant sections of each were spliced together to derive the full-length reconstruction. Forward nests were similarly treated (hereafter referred to as F). Multiple linear regression, using a forward stepwise procedure, was used to estimate summer streamflow from the set of candidate tree-ring predictors in each nest.

Separate calibration and validation analyses were performed on each nested series to allow for assessment of temporal changes in reconstruction quality. The strength of the regression models was reported using an adjusted R^2, which provides a measure of the model explanatory power. Regression residuals were tested for autocorrelation using the Durbin-Watson test and the mean variance inflation factor (VIF) was calculated to identify multicollinearity among predictors. For the verification period, the reduction of error (RE) statistic was used to provide a measure of model skill. RE has a possible range of $-\infty$ to 1. An RE of 1 indicates perfect prediction for the validation period, and can be achieved only if the model residuals are zero. As a rule of thumb, a positive RE is accepted as evidence of some prediction skill (Fritts, 1976). The root-mean-square error (RMSE) was used as a measure of the uncertainty in the predicted values over the validation period. The Pearson correlation coefficient (r^2) for the validation period was also used to evaluate reconstruction performance. To derive the final reconstruction, all other nested series were scaled to N1, and the RMSE value recalculated for each nest.

The statistical properties of the reconstructions and instrumental summer streamflow records were compared to determine whether there were any significant

differences over the instrumental era, and also to assess the capacity of the model to approximate the statistical characteristics of the gauged data. Box plots were used to compare distributions of the instrumental and reconstructed series over common periods of time, and of the long-term reconstructions. In addition, a previous reconstruction of summer streamflow for the Skeena River (Starheim et al., 2013a) was compared to the LSR reconstruction and assessed using a sliding 40-year correlation analysis.

3.4.7 Analysis of the reconstruction

The summer streamflow reconstructions were evaluated at annual, decadal and multidecadal time scales. Taking advantage of the annual resolution afforded by the tree rings, the most extreme single-year low flow events in the reconstruction were identified. Compression of reconstructed values towards the mean, an unavoidable effect of regression, biases direct comparison of gauged and reconstructed streamflow values. Therefore, the thresholds were based on reconstructed values. The first ten lowest reconstructed individual years for each streamflow model over the shared common period of the instrumental data were identified and ranked in magnitude to determine a low flow threshold (Table 1; length of record). Years were classified as having low flow if they were below the threshold values determined for each streamflow reconstruction. A 40-year moving sum of the individual low flow years was compared graphically to visualize distinct low streamflow patterns over the length of each reconstruction.

At the decadal scale, the duration and severity of low and high flow periods were quantified by smoothing the reconstruction using a 10-year spline for event analysis. A low or high flow decadal episode was defined as an unbroken interval within the smoothed series above or below its mean, respectively. Within the decadal episodes, the

most severe low or high flow year (as z-scores) of the smoothed series was identified as exceeding $\leq 10^{th}$ percentile and $\geq 90^{th}$ percentile over the entire reconstructed period, respectively. The top ten lowest and highest years were rank ordered by magnitude, and compared with the severe events in the gauged record. The event analysis was needed to place gauged events important for water resource management in the context of the past, and to identify if severe events were confined to a single basin or widespread across the basins.

For multidecadal variability the reconstructions were smoothed with a 20-year spline. The smoothed streamflow reconstructions were compared to a January-September reconstruction of Gulf of Alaska (GOA) coastal surface air temperatures (SATs) over the common period (Wiles et al., 2014). The GOA reconstruction z-scores were smoothed using the same 20-year spline. A correlation analysis was performed to determine the strength of the relationships to the streamflow reconstructions. In addition, a recent April 1 SWE reconstruction for the Stikine basin (1789-2011) was utilized for comparisons with the summer streamflow in the Stikine basin (Welsh et al., 2019). The SWE reconstruction was similarly smoothed and long-term relationships assessed using a 40-year moving correlation.

3.5 Results

3.5.1 Hydroclimate relationships

Correlation was used to summarize the relationships between summer streamflow and monthly climate records. Results of the Seascorr analyses indicate a negative association between mean temperatures in May through August of the current year and, independently, positive with winter precipitation (see Supplemental Information 3.7,

Figure S3.1). The streamflow data also exhibited temporally-stable, significant positive linear correlations with April 1 SWE (Table 3.4), and an apparent weaker April 1 SWE association with the STK summer streamflow data compared to the LSR and NSR data. Results of the Seascorr analyses also indicate that summer streamflow is sensitive to fluctuations in the ocean and atmosphere over the North Pacific Ocean. The temporally-stable, negative correlations at monthly or seasonal intervals for the PDO, Niño 3.4 and PNA are listed in Table 4. Generally, the highest correlations with summer streamflow were during the winter and/or spring months.

Table 3.4: Hydroclimate correlations and their temporal stability.

Streamflow data (July-August)	SWE[a]	p[b]	PDO[c]	Month[d]	p[b]	Nino3.4[e]	Month[d]	p[b]	PNA[f]	Month[d]	p[b]
LSR	0.60**	0.833	-0.42**	DEC-May	0.914	-0.54**	Mar-May	0.542	-0.40**	Jan-Jun	0.591
NSR	0.61**	0.898	-0.52**	May	0.827	-0.48**	Mar-May	0.810	-0.32*	Feb-Apr	0.765
STK	0.30*	0.193	-0.26*	Apr-Jun	0.954	-0.46**	Mar-May	0.643	-0.34*	Jan-Mar	0.685

[a] Correlations of streamflow with April 1 SWE; significance at $p < 0.05$ (*) or $p < 0.01$ (**).
[b] p-value for a test of the null hypothesis that the population sample correlations in the preceding column for the first and second halves of the test period are the sample (split-correlations not listed).
[c] Correlations of streamflow with PDO; significance at $p < 0.05$ (*) or $p < 0.01$ (**).
[d] Month(s) corresponding to the preceding column of correlations; all upper case letters represent months from the year preceding growth.
[e] Correlations of streamflow with Nino3.4; significance at $p < 0.05$ (*) or $p < 0.01$ (**).
[f] Correlations of streamflow with PNA; significance at $p < 0.05$ (*) or $p < 0.01$ (**).

3.5.2 Tree-ring chronologies and diagnostic climate relationships

Twenty site-specific ring-width chronologies were developed from a total of 756 radial series from 405 trees, with chronology lengths ranging from 512 to 204 years (Table 3.5). Series intercorrelation values, a measure of the strength of the signal common to all sampled trees, range from 0.500 to 0.686 (Table 3.5). Mean sensitivity is a measure that describes the interannual changes in ring width (Fritts, 1976) and, in this

instance, the values range from 0.156 to 0.284 (Table 3.5). These values indicate strong synchronicity within the ring-width chronologies developed for this study. A total of three site-specific maximum latewood density chronologies were developed from 56 radial series from 54 trees, with chronology lengths ranging from 338 to 241 years (Table 3.5). Series intercorrelation values range from 0.465 to 0.645 and mean sensitivity values range from 0.081 to 0.042, substantially lower than the ring-width values.

Table 3.5: Tree-ring chronology statistics.

ID	Period (AD years)	Series, trees	Interseries correlation	Mean sensitivity	RBAR[a]	r_1[b]	Year[c] EPS >0.80
Tree ring width chronologies							
TC	1773-2014	40, 20	0.658	0.204	0.474	-0.006	1775
EL	1689-2013	40, 20	0.548	0.178	0.299	-0.003	1708
DP	1802-2015	40, 20	0.614	0.174	0.380	0.000	1808
GP	1757-2015	90, 47	0.558	0.160	0.301	0.001	1789
TL	1809-2013	41, 20	0.619	0.173	0.437	0.003	1819
IT	1725-2016	39, 20	0.607	0.237	0.383	0.002	1770
B2	1501-2013	32, 16	0.647	0.229	0.421	0.016	1624
MR	1696-2013	38, 19	0.644	0.218	0.416	0.004	1746
OP	1664-2016	43, 22	0.691	0.284	0.470	-0.004	1686
SG	1633-2004	44, 22	0.570	0.215	0.321	0.003	1705
CM	1646-2004	39, 20	0.686	0.261	0.480	-0.001	1660
CS	1616-2004	33, 20	0.615	0.203	0.386	-0.001	1739
ER	1576-2004	28, 22	0.610	0.244	0.372	0.000	1646
HN	1652-2015	36, 19	0.607	0.207	0.382	0.001	1687
ME	1646-2015	40, 20	0.583	0.190	0.250	0.000	1782
TP	1630-2014	39, 20	0.685	0.271	0.458	0.001	1672
HB	1670-2002	40, 20	0.597	0.156	0.363	-0.001	1713
NM	1706-2012	30, 17	0.515	0.173	0.324	-0.003	1810
BB	1754-2006	18, 14	0.500	0.205	0.296	-0.006	1862
GG	1711-2002	46, 27	0.570	0.171	0.309	0.001	1739
Tree ring density chronologies							
B2d	1675-2013	18, 17	0.467	0.081	0.217	0.003	1775
ELd	1702-2013	19, 17	0.477	0.043	0.231	0.000	1835
TCd	1773-2014	19, 20	0.645	0.042	0.413	0.002	1780

[a]Mean correlation coefficient among the tree-ring series
[b]First order autocorrelation coefficient after autoregressive modeling
[c] Year chronologies were truncated based on the EPS calculation

To assess any temporal variability in the strength of the common radial growth signal, running series of average correlations (RBAR) were calculated for each chronology.

RBAR is the mean correlation coefficient for all possible pairings among tree-ring series in a chronology, computed for a specified common time interval (Cook and Kairiūkštis, 1990). For this study, a 50-year window with an overlap of 25 years between adjacent windows was employed. RBAR values ranged from r = 0.217 to 0.584. First-order autocorrelation was removed during detrending (r_1 values in Table 3.5). Chronologies were truncated according to the EPS calculation.

The results of the correlation analyses with summer streamflow and April 1 SWE data are presented in Table 3.6. Five chronologies (i.e., MR, ME, HB, NM and ELd) were omitted from further analysis, as they did not meet the minimum requirements (chronology information not presented). All the white spruce chronologies were positively correlated with April 1 SWE over the calibration period, an association that can be attributed to moisture sensitivity in white spruce (Welsh et al., 2019). The April 1 SWE from the Telegraph Creek SWE station showed the highest correlations with the chronologies, with TC site correlated to both the Telegraph Creek and Ningunsaw Lake April 1 SWE data. Strong negative correlations were found between the mountain hemlock and SWE data, an association related to the impact of late-lying snowpacks on the radial growth of mountain hemlock trees (e.g., Laroque and Smith, 1999; Gedalof and Smith, 2001; Coulthard et al., 2016). Most site were consistently correlated with SWE records from Mount Cronin, with GG and OP site correlated to both the Mount Cronin and Ningunsaw Lake April 1 SWE data.

Significant negative correlations to summer streamflow were observed for all the mountain hemlock chronologies during the year of tree-ring growth (Table 3.6). Together, these results suggest that winters with above average SWE are associated with

years of both increased melt-season discharge and depressed tree ring growth (Starheim et al., 2013a). In general, the strongest correlations were found with the LSR summer streamflow records.

Table 3.6: Significant ($p<0.05$) correlation coefficients of gauged Jul-Aug river runoff with the tree-ring index chronologies. Correlations in bold are significant at $p<0.01$.

Site ID[a]	LSR	*p*-value[b]	NSR	*p*-value[b]	STK	*p*-value[b]	SWE[c]
Tree ring width chronologies							
TC					0.33	0.247	**0.42**[1,2]
EL	-0.29	0.930					**0.61**[1]
GP	**-0.34**	0.195	-0.27	0.669	-0.25	0.235	**0.47**[1]
TL	**-0.33**	0.319					**0.49**[1]
IT	**-0.35**	0.834					**-0.45**[3]
B2	**-0.42**	0.952	-0.30	0.572			**-0.51**[3]
SG	**-0.47**	0.788					**-0.32**[3]
CM	**-0.49**	0.194	-0.39	0.257			**-0.60**[3]
CS	**-0.33**	0.055					**-0.46**[3]
ER	**-0.40**	0.107	-0.31	0.414			**-0.60**[3]
HN	-0.30	0.453	-0.28	0.903			**-0.38**[3]
TP	**-0.48**	0.846	-0.42	0.965			**-0.58**[3]
GG	-0.29	0.316					**-0.40**[3,2]
OP	**-0.52**	0.597	**-0.44**	0.696	-0.28	0.800	**-0.50**[3,2]
BB	**0.36**	0.259	**0.41**	0.085			
DP *t+1*	0.25	0.160					--
TC *t+2*	-0.28	0.361					--
TP *t+2*					0.30	0.129	--
Tree ring density chronologies							
B2d	-0.37	0.509	-0.30	0.572			**-0.51**[3]
TCd			0.32	0.444	0.31	0.733	**0.50**[2,1]
B2d *t+2*					0.31	0.234	--

[a] See Table 3 for site names and locations.
[b] *p*-value for a test of the null hypothesis that the population sample correlations in the preceding column for the first and second halves of the test period are the same (split-correlations not listed).
[c] Highest correlation coefficients are listed and superscript numbers indicate with what station(s); [1]Telegraph Creek; [2]Ningunsaw Lake; [3]Mount Cronin.

The relationship between the summer streamflow records and white spruce chronologies demonstrated mixed correlation responses. Both TC chronologies (ring-width and density; see TCd, Table 3.6) demonstrated a positive correlation to summer

streamflow and corroborates a previously described sensitivity to winter precipitation (Welsh et al., 2019). The remaining white spruce chronologies describe a negative correlation with summer streamflow, which could describe a temperature-induced moisture response. Positive growth responses to current-year summer temperatures were described by Welsh et al. (2019) and combined with increased SWE levels, reflect a distinct positive response to increased soil moisture availability. Therefore, the physiological link between these chronologies and streamflow are distinctly related to melt-season temperature conditions. These relationships indicate that a summer with above (below) average temperatures is indicative of both decreased (increased) melt-season discharge and increased (decreased) ring growth.

The positive growth response of the Douglas-fir chronology (BB site) to summer flow observed for LSR and NSR was expected. Prior research on growth-climate relationships of Douglas-fir in the Pacific Northwest has demonstrated the importance of spring/summer moisture availability (i.e., rainfall) on growth (Brubaker et al., 1992; Little et al., 1995; Watson and Luckman, 2002; Pederson et al., 2006).

Residual white spruce and mountain hemlock chronologies showing significant associations with summer streamflow at lags *t+1* and *t+2* were also included in model development (Table 3.6). These lags possibly reflect a delay in response due to the inertia in tree biology or hydrology. Therefore, additional hydroclimate information for year *t* is contained in the tree-ring data in successive years and was included in the predictor pool. Collectively, these results demonstrate that tree-ring data from the study area contains strong hydroclimatologic signals.

3.5.3 Reconstruction model

To improve the prediction strength of the streamflow reconstructions, tree-ring derived paleoreconstructions of PDO, ENSO (Niño 3.4) and PNA shown to be correlated with summer streamflow (see Supplemental Information 3.7, Table S3.1) were considered in the model predictor pool. Regression and cross-validation statistics for the iterative nesting method are summarized in Table 3.7. N1 with a calibration R^2 of 0.58, 0.43 and 0.42 (for LSR, NSR and STK, respectively) explains the greatest amount of streamflow variance in the full record. The calibration R^2 for LSR between 1819-2002 are comparable to the predictive skill reported by Starheim et al. (2013a) with a significant improvement in skill during N1 (1862-1983) period. Overall, calibration R^2 values decrease as the length of the record increases. This appears to occur as the predictive pool decreases, suggesting the more recent nests contain tree-ring chronologies that are more important to the overall skill of the reconstruction. Analysis of the residual estimates using the Durbin-Watson (D-W) statistic showed no significant first-order autocorrelation and the VIF suggested no multicollinearity issues among the model predictors in each nest.

The N1 reconstruction and gauged summer streamflow data are compared over the calibration period in Figure 3.3. For comparison purposes, the most replicated "tree-ring only" predictive model was also included in Figure 3.3 (see Table 3.7; shaded row for model statistics). The N1 reconstruction captures the year-to-year variability of the gauged summer streamflow data with acceptable accuracy. The magnitudes of the low and high flow years were more closely estimated using N1 models (that include paleoreconstructions): no major discrepancies between the gauged and reconstructed

records occur during those years. Overall, a visual inspection of the calibration time plots shows that the magnitudes of high flow years were slightly underestimated compared to low flow years in both models.

Table 3.7: Nested regression model statistics. Tree-ring only model shaded in grey.

Model	A/R[a]	Nest year	R^2	D-W[b]	VIF[c]	Equation
A) LSR						
N1	20/4	1862-1983	0.58	1.78	1.16	-7.171 + 4.465 (DP_{t+1}) + 2.854 (BB) – 1.045 (PDO) – 0.284 (PNA)
N2	19/2	1819-1861	0.41	1.98	1.00	-3.889 + 4.103 (DP_{t+1}) – 1.043 (PDO)
N3	17/2	1789-1818	0.38	1.59	1.00	6.775 – 4.588 (TC_{t+2}) – 2.008 (GP)
N4	9/2	1687-1788	0.29	1.93	1.62	1.698 – 0.625 (PDO) – 1.568 (OP)
N5	1/1	1599-1686	0.23	2.04	1.00	0.148 – 1.074 (PDO)
F1	19/3	1984-2002	0.42	1.63	1.24	2.796 – 2.505 (GP) – 1.832 (OP) + 1.592 (BB)
F2	4/2	2003-2015	0.31	1.95	1.25	4.012 – 1.804 (GP) – 2.230 (OP)
F3	2/1	2016	0.27	1.96	1.00	2.585 – 2.586 (OP)
B) NSR						
N1	11/3	1862-2004	0.43	1.76	1.04	1.087 – 3.204 (GP) – 0.283 (ENSO) + 2.206 (BB)
N2	10/3	1789-1861	0.42	1.65	1.03	-5.691 – 4.224 (GP) – 0.263 (ENSO) + 9.968 (TCd)
N3	5/2	1672-1788	0.26	1.55	1.06	2.044 – 1.981 (TP) – 0.218 (ENSO)
N4	4/2	1660-1671	0.23	1.50	1.04	1.597 – 1.527 (CM) – 0.234 (ENSO)
N5	2/2	1624-1659	0.23	1.51	1.01	1.918 – 0.258 (B2) – 1.822 (ENSO)
N6	1/1	1301-1623	0.14	1.74	1.00	0.086 – 0.283 (ENSO)
F1	9/3	2005	0.44	1.45	1.04	-0.780 – 2.069 (TP) + 2.929 (BB) – 0.214 (ENSO)
F2	8/2	2006	0.36	1.21	1.00	-0.370 – 2.487 (TP) + 2.932 (BB)
F3	7/2	2007-2013	0.26	2.09	1.11	-8.970 – 2.238 (TP) + 11.236 (TCd)
F4	1/1	2013-2016	0.18	1.97	1.13	2.157 – 2.191 (OP)
C) STK						
N1	7/4	1789-2005	0.42	2.17	1.11	-4.838 + 2.303 (TC) – 4.288 (GP) + 6.811 ($B2d_{t+2}$) – 0.163 (ENSO)
N2	5/3	1775-1788	0.25	1.88	1.05	-5.859 + 2.142 (TC) + 5.446 ($B2d_{t+2}$) – 1.706 (OP)
N3	4/2	1773-1774	0.15	1.83	1.04	-6.206 + 6.214 ($B2d_{t+2}$) – 0.230 (ENSO)
N4	2/2	1670-1772	0.15	1.93	1.09	-1.860 + 1.930 (TP_{t+2}) - 0.253 (ENSO)
F1	6/3	2004-2012	0.38	2.09	1.11	-5.681 + 2.882 (TC) -3.916 (GP) + 6.732 ($B2d_{t+2}$)

[a] A/R represents available predictors/retained predictors.
[b] Durban-Watson statistic.
[c] Variance inflation factor.

The full summer streamflow reconstructions and validation metrics for LSR, NSR and STK are presented in Figure 3.4. The reconstructions span the interval 1599-2016 for LSR, 1301-2016 for NSR, and 1670-2012 for STK. Validation r^2 values are greater than zero for all nests, and are similar for the late and early validation periods for each streamflow reconstruction. Overall, validation r^2 values are >0.40 from 1789-2016 for

LSR, 1624-2016 for NSR, and 1775-2012 for STK streamflow reconstruction. RE values are positive for all nests and demonstrate good predictive skill, but are lower for the earlier validation period in the STK reconstruction.

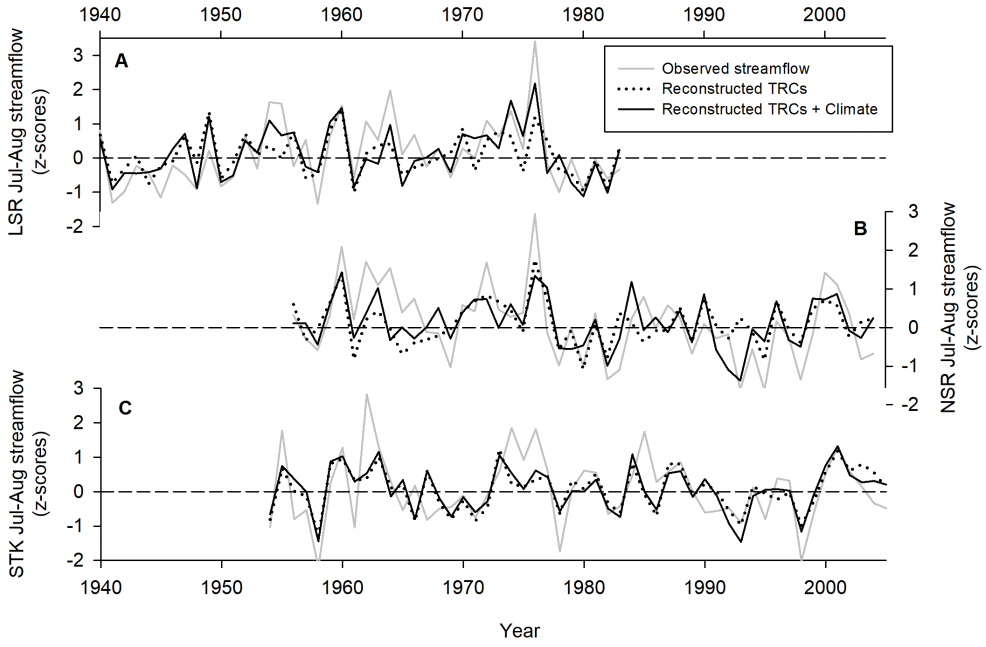

Figure 3.3: Time plot of Jul-Aug streamflow over the calibration periods for models using tree-ring chronologies (TRCs) and the most replicated nested iterative model (ie., N1) using paleoreconstructions of climate indices for the: A) Skeena River (LSR; 1940-1983 calibration period), B) Nass River (NSR; 1956-2004 calibration period) and, C) Stikine River (STK; 1954-2005 calibration period).

The results of comparative statistics between the gauged and reconstruction periods were expected. The standard deviation is lower in the reconstruction than in the gauged data for the same period, reflecting the fact that not all the variance in summer flow is explained in the regression model. The mean flow values are generally similar between the gauged and reconstructed records, a finding that is expected when linear least squares is used for reconstruction. Reconstruction bias towards higher median values, as well as the typical compression of variance by the reconstruction process, is evident in box plots (Figure 3.5). Because the statistics of the reconstructions are biased relative to those of

the instrumental time series, placement of the hydroclimate statistics of the short instrumental period in a long-term context is restricted to comparisons of reconstructed data.

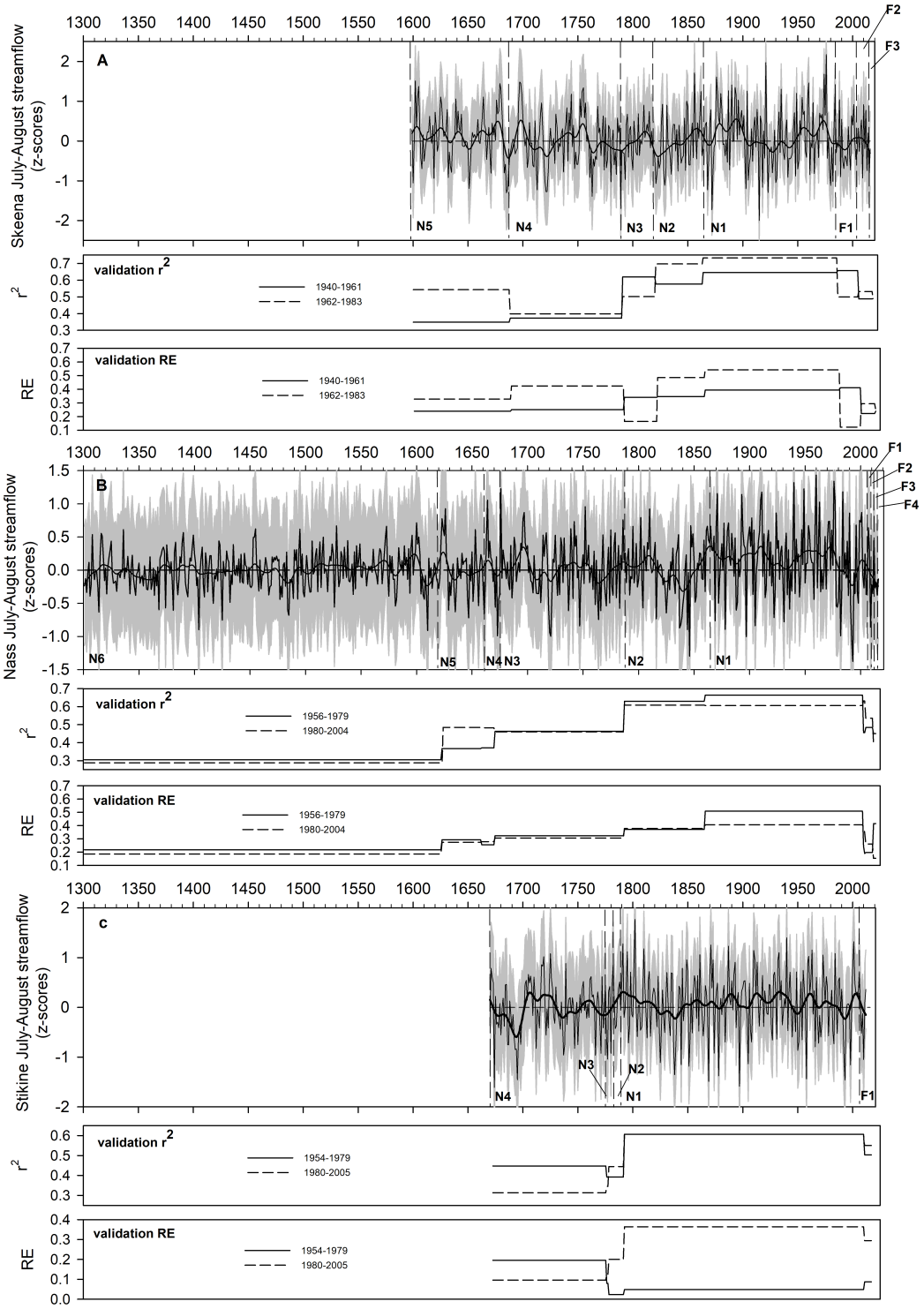

Figure 3.4: Jul-Aug streamflow reconstruction and assessment metrics for the A) Skeena River, B) Nass River, and C) Stikine River. Errors are derived from the RMSE values after rescaling to N1.

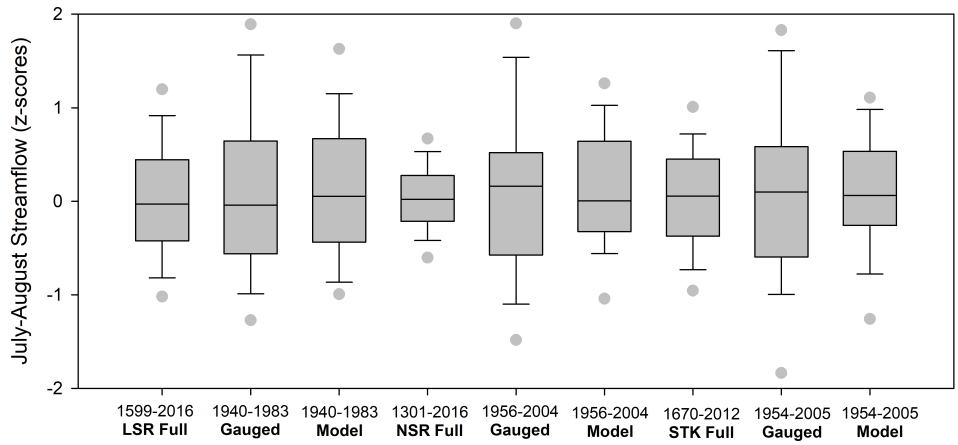

Figure 3.5: Box plots of Jul-Aug streamflow for the full reconstruction and calibration periods for each river. Plots show median (bold horizontal line), 10th and 90th percentiles (whiskers), 25th and 75th percentiles (boxes), and 5th and 95th percentiles (outliers).

Figure 3.6 compares the LSR reconstruction with the Starheim et al. (2013a) LSR reconstruction using a sliding 40-year correlation. The reconstructions are well correlated except during two obvious periods: in the late-1700s and late-1800s. Overall, the reconstructions complement each other. The LSR reconstruction extends the streamflow record 61 years into the past, and updates the reconstruction to 2016. The LSR reconstruction captured the year-to-year variability of the gauged data with higher accuracy ($r^2 = 0.74$; $p < 0.01$) compared to the Starheim et al. (2013a) reconstruction ($r^2 = 0.66$; $p < 0.01$) over the shared common period (1940-2009).

3.5.4 Model analysis

The LSR reconstruction was significantly correlated with NSR ($r^2 = 0.52$, $p < 0.01$) and to a lesser extent, with the STK reconstruction ($r^2 = 0.28$, $p < 0.01$). Similarly, a significant interannual relationship was found between the NSR and STK reconstruction ($r^2 = 0.49$, $p < 0.01$). A similar correlation pattern was found between the gauged data (all correlations at $p < 0.01$; data not shown).

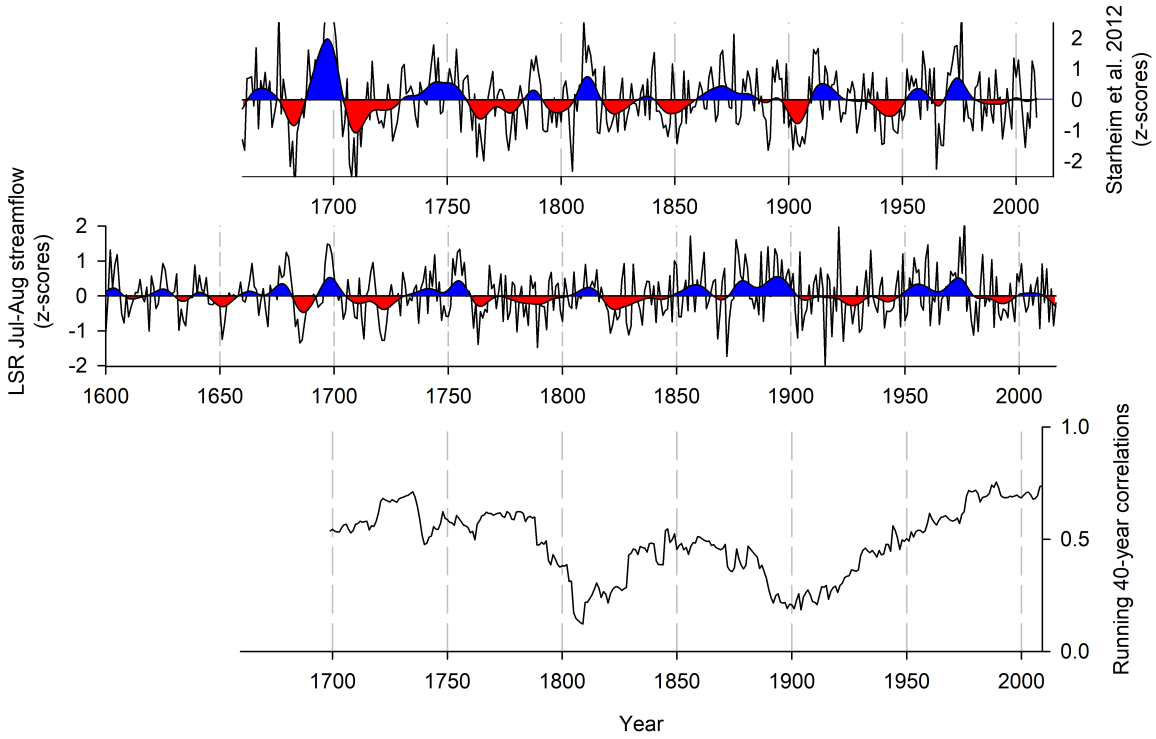

Figure 3.6: Comparisons of the Skeena River (LSR) Jul-Aug streamflow reconstruction (1599-2016) with the Starheim et al. (2013a) reconstruction (1660-2009). Smoothed function is a 20-year spline. Low flow episodes, or smoothed series below mean, shaded red. High flow episodes, or smoothed series above mean, shaded blue. Lower panel shows sliding 40-year correlation values between the two Skeena River reconstructions.

The identification of single-year extremes yielded 51 low flow years in the LSR reconstruction, 66 low flow years in the NSR reconstruction, and 48 low flow years in the STK reconstruction (Figure 3.7). The occurrence of extreme single-year events clustered during the 1820s-1840s and 1900s-1950s in the LSR (Figure 3.7A). Brief episodes of extreme single-year events occurred in the 1680s, 1720s, 1780s, 1980s and starting in 2009. Compared to other centuries, the occurrence of single-year extreme events has increased since the 20th century in the LSR. The NSR and STK reconstructions had similar clusters in the occurrence of extreme single-year events during the 1750s-1780s, mid-1800s, and late-1800s to-early 1900s (Figures 3.7B and C). An increase in extreme

single-year events also occurred during the 1630s-1660s in the NSR and during the 1680s-1690s in the STK. The STK shows a distinct cluster in extreme low flows starting in the mid-20th century. It also appears that the extreme low flow clusters in the LSR are generally asynchronous over time with the NSR and STK (Figure 3.7; 40-year sum).

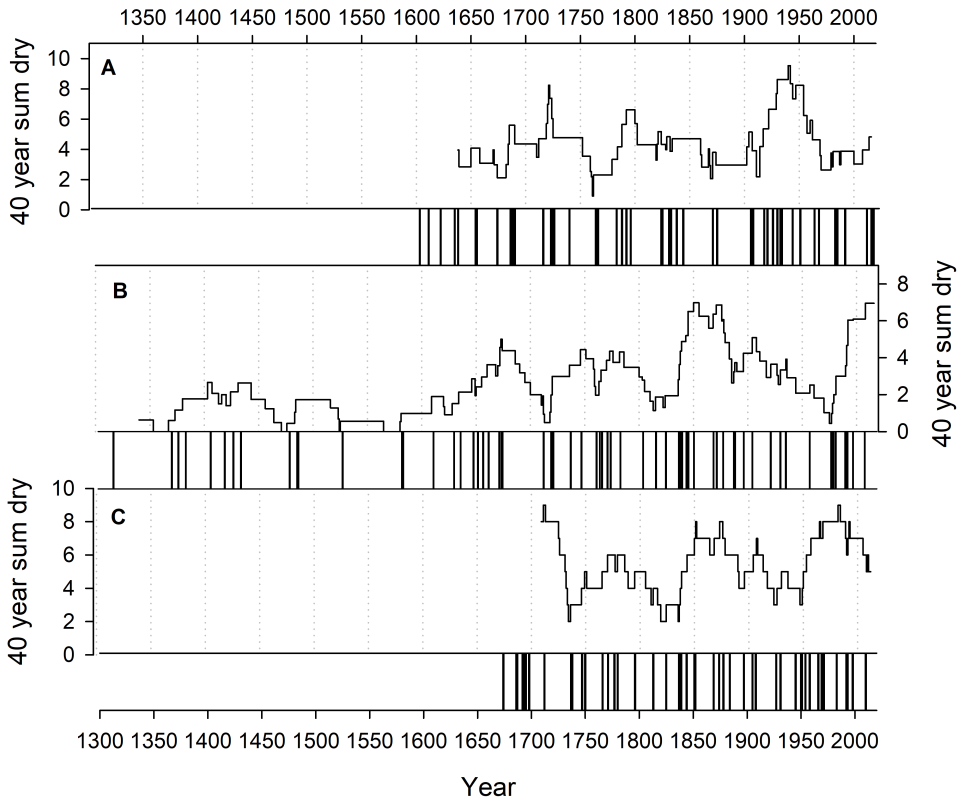

Figure 3.7: Line graphs shows the frequency of low flow years in 40-yr moving windows for the A) Skeena River, B) Nass River, and C) Stikine River. Extreme single-year low flow events are represented in the bar plots below each corresponding line plot.

A comparison of the duration and severity of the lowest and highest episodes in the 10-year smoothed streamflow reconstructions, to the most severe periods in the smoothed gauged streamflow data, indicates that many low and high episodes occurred prior to the gauged record (Table 3.8). However, the magnitude of the 2016 low flow period in the gauged record was the most severe event compared to any reconstructed periods in the

LSR and NSR (2016 was not include in STK analysis). Prior to the 2016-gauged extreme, there were a number of pre-gauged periods in the LSR of greater magnitude (i.e., 1686, 1722 and 1763). No period in the NSR reconstruction surpassed the magnitude of the extreme values in the gauged record, which could be explained by the greater degree of reconstruction compression (refer to Figure 3.5). This pattern was also observed for all high flow events across each basin. In the STK reconstruction, the severity of the gauged low flow events was not nearly as extreme as a reconstructed low flow period in the 17th century (i.e., 1684-1699).

Each streamflow reconstruction contains both basin-specific and regional (i.e., shared) low and high flow periods (Table 3.8). The late-1980s to late-1990s low flow episode identified in the gauged data and a prolonged early- to mid-1800s low flow episode appeared to be the only events shared across each basin. The 2016 extreme low flow period identified the gauged record was ranked among the top 10 lowest in the LSR reconstruction. The timing of the 1950s to late-1970s high flow period identified in the gauged record was apparent in both the LSR and NSR reconstruction, but was intermittent in the STK. The STK gauged record identified a longer high flow period that occurred in 1970s to the end of the 1980s that is demonstrated in the reconstruction, further describing an asynchronous pattern across the basins.

Table 3.8: Ending year, magnitude and duration of decadal-scale (10-yr smoothed reconstruction) dry (A) and wet (B) episodes ranked by magnitude. Bold values indicate observations during the instrumental period.

	LSR (1599 – 2016)				NSR (1301 – 2016)				STK (1670 – 2012)			
	End year	Max. magnitude[a] (year)	Years of episode[b]	Years below low flow threshold[c]	End year	Max. magnitude[a] (year)	Duration of episode[b]	Years below flow low threshold[c]	End year	Max. magnitude[a] (year)	Duration of episode[b]	Years below low flow threshold[c]
	A)											
	1693	-0.91 (1686)	12	7	**1996**	**-0.58 (1993)**	**8**	**5**	1699	-0.85 (1695)	16	11
	1727	-0.80 (1722)	9	5	1847	-0.51 (1839)	13	9	**1998**	**-0.53 (1993)**	**9**	**5**
	1767	-0.70 (1763)	8	5	1724	-0.47 (1721)	7	5	1842	-0.50 (1838)	9	4
	1836	-0.64 (1822)	19	5	1620	-0.35 (1609)	17	6	1740	-0.36 (1736)	10	5
	1656	-0.56 (1651)	11	4	1829	-0.32 (1825)	14	5	1829	-0.34 (1825)	8	3
	1637	-0.51 (1634)	7	3	1675	-0.32 (1673)	7	4	1682	-0.31 (1677)	10	4
	1983	**-0.48 (1980)**	**6**	2	1489	-0.31 (1485)	14	5	**1971**	**-0.29 (1969)**	**6**	**1**
	1932	-0.45 (1928)	10	5	1766	-0.30 (1764)	17	6	**2011**	**-0.27 (2009)**	**5**	**1**
	2016	**-0.43 (2016)**	**4**	**1**	**1983**	**-0.28 (1981)**	**5**	**3**	1752	-0.26 (1748)	8	0
	1997	**-0.43 (1993)**	**9**	**3**	1638	-0.25 (1634)	10	7	1780	-0.18 (1771)	16	0
Gauged	2016	-3.18 (2016)	4	3	2016	-1.62 (2016)	8	3	1999	-0.49 (1993)	10	3
	1951	-0.68 (1944)	12	3	1998	-0.84 (1994)	10	3	1971	-0.47 (1968)	6	2
	1998	-0.66 (1993)	11	1	1984	-0.54 (1981)	6	0	1959	-0.44 (1957)	6	1

	End year	Max. magnitude[a] (year)	Years of episode[b]	Years above high flow threshold[c]	End year	Max. magnitude[a] (year)	Duration of episode[b]	Years above high flow threshold[c]	End year	Max. magnitude[a] (year)	Duration of episode[b]	Years above high flow threshold[c]
	B)											
	1702	1.01 (1698)	9	5	1920	0.63 (1910)	30	12	**2006**	**0.57 (2002)**	**8**	**5**
	1977	**0.96 (1974)**	**10**	**6**	1628	0.56 (1624)	8	5	1944	0.55 (1912)	36	7
	1759	0.95 (1755)	9	5	1702	0.55 (1697)	16	6	**1965**	**0.54 (1962)**	**12**	**4**
	1883	0.85 (1878)	9	6	**1978**	**0.54 (1975)**	**41**	**22**	1710	0.51 (1706)	10	4
	1681	0.80 (1679)	9	5	1886	0.48 (1864)	33	12	1730	0.48 (1718)	16	5
	1606	0.61(1604)	6	3	**2007**	**0.40 (2000)**	**11**	**3**	1804	0.44 (1791)	24	5
	1900	0.65 (1896)	13	8	1603	0.40 (1600)	19	5	1894	0.38 (1889)	13	3
	1960	**0.51 (1955)**	**12**	**3**	1669	0.39 (1665)	7	3	1875	0.38 (1872)	7	1
	1630	0.44 (1626)	9	0	1815	0.35 (1809)	22	3	**1978**	**0.35 (1975)**	**7**	**0**
	1645	0.36 (1641)	8	0	1745	0.27 (1742)	8	0	**1989**	**0.19 (1987)**	**6**	**0**
Gauged	1978	1.03 (1975)	27	7	1978	1.15 (1962)	22	6	1989	0.91 (1975)	18	4
	2002	0.26 (2000)	4	0	2002	0.31 (2001)	4	0	1965	0.80 (1962)	6	2
	1987	0.23 (1985)	4	0	1988	0.21 (1987)	4	0	2008	0.34 (2002)	9	0

[a] Ranked by maximum deviation of smoothed series. [b] Length is the number of years where smoothed series exceeds or drops below the mean. [c] Years exceeding the extreme threshold for dry and wet (ie., 10^{th} and 90^{th} percentile, respectively) of smoothed series.

3.5.5 Multidecadal comparisons with other climate indices

Figure 3.8A compares the streamflow reconstructions with the Wiles et al. (2014) GOA coastal SATs over the common periods. Overall, the GOA air temperatures correlate strongest with the LSR reconstruction (r = -0.36; $p < 0.01$). The STK reconstruction and the GOA air temperatures show a positive correlation (r = 0.23; $p <$ 0.01). This relationship is particularly apparent during 20-year high flow periods that coincide with warmer temperatures; for instance, between 1717-1730, 1781-1804, 1869-1875, 1909-1944, 1957-1964, and 1975-1978. Figure 8B shows the April 1 SWE reconstruction for the Stikine River basin (Welsh et al., 2019) and 40-year moving correlations between the SWE and STK reconstructions (in red). Two periods between 1840-1880 and 1990-2011 were negatively correlated. The instrumented gauge records of April 1 SWE and summer streamflow also describe a negative correlation following 1990s, more specifically between two main periods: 1990-1995 and 1999-2004 (data not shown). Aside from those, the correlations show a stable positive association with April 1 SWE over the remainder of the streamflow record. These results help to validate the reliability of the reconstructions, and corroborates a north-south "see-saw" pattern in hydroclimate for the study area (Welsh et al., 2019).

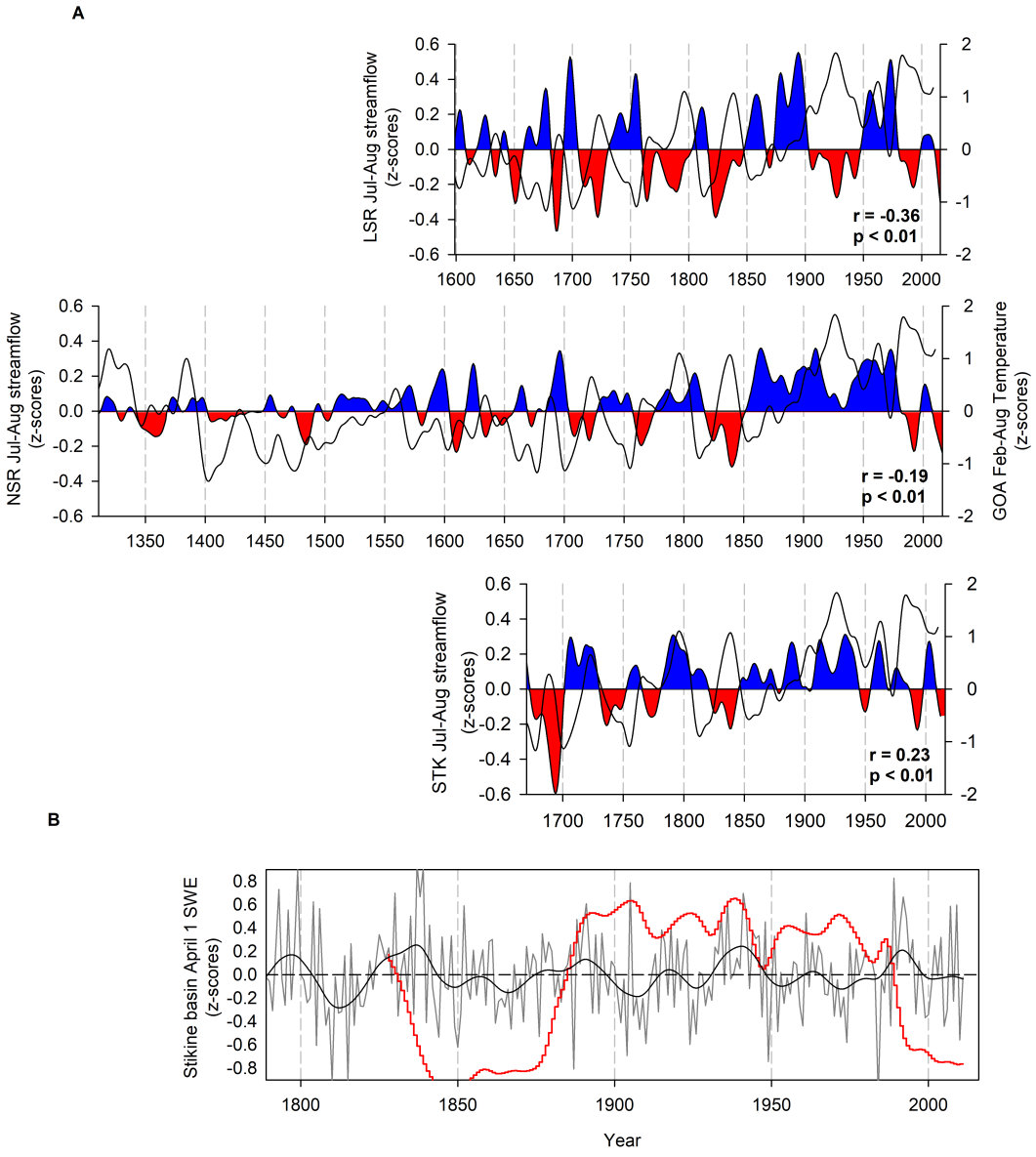

Figure 3.8: A) Jul-Aug streamflow reconstructions for the Skeena (LSR), Nass (NSR), and Stikine (STK) compared to the Wiles et al. (2014) reconstruction of Jan-Sep Gulf of Alaska (GOA; smoothed back line) surface air temperatures over the common period. Smoothed function is a 20-year spline for both series. Low flow episodes, or smoothed series below mean, shaded red. High flow episodes, or smoothed series above mean, shaded blue. B) April 1 SWE reconstruction (dark grey line; mm) for the period 1789-2011. The black line is a 20-year spine of the reconstructed values. The red line represents 40-year moving correlations between the SWE and STK reconstructions.

3.6 Discussion

3.6.1 Correlation analyses and reconstruction skill

A major goal of this study was to demonstrate the validity of tree-ring reconstructions of summer streamflow combined with hemispheric climate signals for snow-dominated basins in northern BC. The study provided reconstructions of July-August (summer) streamflow for three large rivers serving important ecological and socio-economic values that experienced detrimental low flows in recent decades. For most of the replicated nests, the models accounted for a high level of annual variance in the instrumental records from 42 to 58%. The amount of variance explained varied through time as predictor chronologies decreased into the past. However, verification statistics (RE and r^2; Figure 3.4) demonstrated good predictive skill over the length of the records. The datasets and analyses presented in this research extend modern streamflow observations across northern BC to bridge a critical gap in the regional network of proxy-hydroclimate records.

The LSR, NSR, and STK summer streamflow reconstructions were based on tree species with sensitivities to regional-scale SWE and hemispheric variability (i.e., PDO, ENSO and PNA). Correlation analyses indicate that runoff is primarily driven by snowmelt (Figure 3.2 and S3.1), and that the selected tree-ring predictors and hemispheric reconstructions operate as a suitable proxy (Table 3.6 and S3.1). The sensitivity of the gauged summer streamflow data to April 1 SWE and winter precipitation (particularly, LSR and NSR) supports the interpretation that the hydrologic regimes of these rivers are largely snow-dominated. The weaker correlations observed between April 1 SWE and summer streamflow for STK could reflect a greater influence

of summer rainfall or late-summer glacier melt contributions. Summer precipitation and glacier melt were not captured in the model, and may explain some of the underestimated high flow periods when compared to the gauged flows. The Douglas-fir chronology (i.e., rainfall signal) selected in some of the iterative nests in the LSR and NSR reconstruction (e.g., N1 and tree-ring only nest) may suggest the need to incorporate more summer precipitation-sensitive proxies are necessary to improve summer streamflow model estimations for this region.

The gauged summer streamflow is also influenced by spring and summer temperature fluctuations, which can influence the timing of melt, and reduce flows in the summer (in the absence of changes in precipitation) (Barnett et al., 2005). The model residuals are correlated with mean spring and summer temperatures (r^2 values range from -0.29 to -0.53 May-July, p <0.01), similar to (but weaker than) the instrumented gauged data. The reconstructions presented in this research are primarily "tuned" to SWE-driven runoff variations and may not fully capture any temperature-driven summer streamflow variability (i.e., evaporation). This finding likely contributes to some of the general underestimation of the severity of the lowest gauged flows as seen in Table 3.8.

As is typical in tree-ring based hydroclimatic reconstructions, the models do not capture the full range of instrumental streamflow variability (Figure 3.3 and 3.5). The compression of variance by the reconstruction process is unavoidable. As a result, the reconstruction estimates of extreme events are considered conservative (i.e., reconstructed high flows were likely higher and low flows were likely lower). The vertical compression of the reconstructed series and expansion of the error bars in the earliest part of the reconstruction also reflect a weakened signal (Figure 3.4). For

example, the climate signal before 1623 in the NSR reconstruction, in particular, is weak not only because the lack of available predictors, but because the ENSO predictor has a relatively weak signal for summer streamflow (Table 3.7; $R^2 = 0.14$).

The Starheim et al. (2013a) reconstruction correlated well with the new LSR reconstruction aside from two periods in culminating the late-1700s and late-1800s as identified by a 40-year sliding correlation analysis (Figure 3.6). A closer examination of these periods show a longer dry and wet periods during the late-1700s and late-1800s, respectively, identified in the LSR reconstruction. Above-average summer streamflow in the late-1800s in a headwater tributary of the Skeena River was previously documented by Gottesfeld and Gottesfeld (1990) and corresponds to a prolonged period of positive glacier mass balance and enhanced end-of-winter SWE in the Canadian Rocky Mountains and southern Coast Mountains (Watson and Luckman, 2004; Larocque and Smith, 2005). In addition, the timing and length of the late-1700s dry period corresponds well with the documented cold and dry conditions that prevailed through much of the 18th century (Wolfe et al., 2005). Although independent evidence corroborates these earlier events, there is a general lack of relevant high-resolution records in the area.

This research contributes to a growing number of successful dendrohydrological studies from "non-traditional" environments. Previously, cooler and wetter settings in northern Canada were not considered to have high dendroclimatological potential (Watson and Luckman, 2006). Significantly, the LSR reconstruction utilized updated multi-species, tree-ring chronologies (extending the previous reconstruction >60 years) and captured the year-to-year variability of the gauged data with improved accuracy.

It is also important to highlight that this research established the use of hemispheric circulation reconstructions as proxies for summer streamflow variability, capitalizing on the influence these patterns have on snow accumulation and subsequent melt conditions in northern BC. Similarly, other research has also demonstrated the value in using both tree-ring chronologies and SSTs for improving reconstructions. For instance, Anderson et al. (2012) improved reconstructions of SWE obtained using tree-chronologies of a major tributary of the Upper Colorado River basin, by considering the Southern Oscillation and PDO Index as additional predictors using stepwise linear regression. More recently, Patskoski et al. (2015) used a similar hybrid approach that used tree-ring chronologies and SSTs to reconstruct annual streamflow in the southern United States. Their approach resulted in improved streamflow estimates for eight selected watersheds, particularly with regard to high flow estimates. This study also demonstrates the improved skill of utilizing both relevant hemispheric circulation records and tree-rings for reducing uncertainties in streamflow estimates.

3.6.2 Interbasin comparisons

A second goal of the research was to compare multi-century reconstructions of summer streamflow across the three major basins in northern BC and investigate linkages to North Pacific climate variability. Single-year, low-flow extremes totaled 51 in the LSR reconstruction, 66 in the NSR reconstruction, and 48 in the STK reconstruction. The distribution of these events showed a distinct asynchronous clustering pattern, particularly between the LSR and STK reconstruction (Figure 3.7). In addition, the multi-decadal patterns of summer streamflow were significantly correlated (p <0.01) with other temperature reconstructions (i.e., Wiles et al., 2014; GOA air temperature) (Figure 3.8),

but showed opposing relationships. In particular, summer streamflow variability in the Stikine River basin generally varied positively with GOA SATs over the past ~300 years, whereas the LSR reconstruction showed inverse relationships (and weaker inverse relationships in the NSR reconstruction). These results support previous findings of a north-south "see-saw" pattern of hydroclimate variability in western Canada and coastal Alaska (Moore and McKendry, 1996; Rodenhuis et al., 2009; Trenberth, 2011). The positive relationship with winter precipitation (i.e., Welsh et al., 2019; Stikine April 1 SWE) and summer streamflow in the STK is consistent with these relationships.

These findings suggest the persistence of more complex interrelationships of moisture availability and transport within the land-atmosphere-ocean system in this region than has been reported. Previously, El Niño (positive ENSO Index) and positive phases of the PDO were associated with above-average winter temperatures and below-average precipitation in western Canada, while La Niña (negative ENSO Index) and negative phases of the PDO were associated with below-average temperatures and above-average precipitation (Eaton and Moore, 2010). PDO and ENSO conditions, as described above, have been linked to snowpack accumulation and streamflow timing and magnitude in catchments located throughout southern BC and US Pacific Northwest (Mantua et al., 1997; Wang et al., 2006; Fleming et al., 2007). However, changes in synoptic-scale circulation involving the Aleutian Low have been shown to affect winter precipitation differently across western Canada and Alaska. A stronger Aleutian Low is associated with enhanced northward flow of relatively warm, moist air masses into Alaska, causing increased wintertime precipitation along the southern Alaska coast (Rodionov et al., 2007). Many northerly BC snow courses and coastal Alaskan weather

stations experienced significant increases in winter precipitation in concert with a state shift in 1976/1977 from a weak to a strong Aleutian Low (Trenberth and Hurrell, 1994; Mantua et al., 1997; L'Heureux et al., 2004). For instance, Mantua et al. (1997) demonstrate that wintertime precipitation (December through February) was positively correlated with PDO in the same season along the coast of the GOA, and reported a tendency of coastal Alaska to experience enhanced cyclonic activity by a deepening of the Aleutian Low that increased the flow of warm, moist air under positive PDO conditions in contrast to other areas in BC and Washington state. Over the past two centuries snowpack dynamics in the Stikine River basin also describe a distinct in-phase relationship with PDO patterns that differs from those established in southern BC (Welsh et al., 2019). Similarly, a 1200-year seasonally- to annually-resolved ice core record of snow accumulation in the Alaska Range found a near doubling of precipitation since ~1840 CE synchronous with an increase in absolute humidity, warming SSTs and the long-term strengthening of the Aleutian Low (Winski et al., 2017). This study contributes to growing evidence demonstrating a specific regional phenomena (a deepening Aleutian Low) that occurs in conjunction with warming, resulting in a dramatic increase in regional precipitation (and vice versa).

It is recognized that the reconstructions underestimate the magnitudes of historical low summer flow events. As a result, comparisons with instrumental data are interpreted with caution. The combined information from the reconstructions indicates that although the instrumental gauged period used for current water supply planning contains some of the most extreme low flows over the last several centuries, it likely does not include the full range of natural variability inherent in the system. The magnitude of the 2016 low

flow event is rare over the long-term context. A prolonged hydrologic drought along the coast, the Skeena, Nass and Stikine region has impacted municipalities, agriculture, industry and fish stocks since 2016 (BC Provincial Government, 2016 Information Bulletins). The conditions have worsened in recent years, and in 2018 provincial drought response levels for the region were listed as "*extremely dry*", a drought level associated with insufficient water supply to meet community and ecosystem needs. The early-1990s was also a period of water scarcity in the region, and the summer streamflow reconstructions suggest that these conditions could have been equaled or exceeded in prior centuries. In particular, the duration of decadal-scale low flow periods in the LSR reconstruction identifies three periods that exceeded the magnitude of the early-1990s instrumental period (e.g., end periods 1693, 1727, and 1767), whereas the STK reconstruction identifies one prolonged period (e.g., end period 1699). The length of the low flow period identified in the 1600s was longer, and likely drier, compared to the early-1990s condition in the gauged record. It is also apparent that, severe pre-gauged low flows periods ($\leq 10^{th}$ percentile threshold) were generally more persistent.

Development of the long reconstructions also enabled the high flow periods in the gauged record to be put in the perspective of the past several centuries. Similar to the low flow periods, the magnitude of the most severe high flow period in the smoothed gauged data was rarely exceeded. The only period that came close to exceeding the prolonged 1970s high flow event was in the LSR reconstruction in late-1600s (e.g., end year 1702) following the aforementioned low flow period. This high flow period was also identified in the NSR reconstruction. Summer streamflow in the early 2000s were high and was exceeded by most pre-gauged high flow periods. However, it is possible that some of the

reconstructed high flows are over-represented. For example, the STK and NSR reconstruction have high flow magnitudes that exceed the magnitudes of the same period in the instrumental record. Such apparent discrepancies can be explained partly by the influence of La Niña events (i.e., introduced by the ENSO predictor) on high flows in the streamflow estimates. In particular, there was a relatively strong La Niña episode that lasted from mid-1998 through early 2001 that coincides with a period of overestimation in the high flow magnitudes in the STK and NSR reconstructions.

As previously discussed, the hydrology of the study area is dominated by snow accumulation and melt processes. Nevertheless, while gauged streamflow in the large, nival basins are well correlated with April 1 SWE, there are numerous occurrences of anomalously large (small) streamflow levels in below (above)- or near-normal SWE years (Curry and Zwiers, 2018). The STK reconstruction demonstrates this in Figure 8B. During the early-1990s, below-average summer streamflow coincided with a prolonged period of above-average regional spring maximum temperatures (data not shown). At the same time, SWE levels in the Stikine basin were above-average resulting in a negative correlation. The correspondence likely reflects the combined impact of several processes. For instance, an earlier freshet due to warmer air temperatures the previous spring, and therefore earlier exhaustion of the seasonal snowpack and lesser opportunity for mid-to-late summer snowmelt runoff generation. That is, the normal seasonal recession to summer base-flow occurs earlier, giving lower-than-average summer flows. Conversely, during 1999-2004, above-average summer streamflow (and below-average SWE) coincided with a prolonged period of above-average spring and summer precipitation in the Stikine basin (data not shown). The outcome suggests higher rainfall contributions to

mid-to-late summer flows compared to snowmelt runoff. Similarly, conditions during the mid-to-late 1800s also demonstrate a negative correlation associated with reduced winter SWE and increasing summer runoff. These conditions correspond to a time of decreasing winter mass-balance (Wood et al., 2011), below-average June-July air temperatures (Pitman and Smith, 2013) and increasing summer runoff (Starheim et al., 2013a) in the Coast Mountains, supporting the finding of reduced winter snow accumulation.

Understanding broader temporal and spatial patterns in streamflow in northern BC can help water managers better plan for future water demand. By first demonstrating that tree-ring and hemispheric climate records capture much of the variance in summer (July-August) streamflow records, and then placing the contemporary record of streamflow in a long-term context, managers now have more information to better plan for periods of low or high variability in flow. Past variability in summer streamflow indicates that the magnitude of the 2016 drought condition is a rare event over a multi-century context and that at lower frequencies (i.e., decadal droughts), low flow conditions were longer (and possibly exceeded) in prior centuries. Therefore, the instrumental record does not adequately represent the historic range of variability present in the reconstructions, and water supply systems may not be prepared to meet demand under more extreme and persistent conditions. Maintaining high expectations for future availability of summer streamflow could have catastrophic consequences if, for example, a prolonged period of severe drought is encountered. Finally, this research identifies basin-specific variability in summer streamflow associated with moisture transport and atmospheric-ocean circulation. The results demonstrate a characteristic north-south “see-saw” pattern of streamflow variability previously identified by Welsh et al. (2019) and others. This study

has attempted to refine and expand the existing understanding of temporal and spatial patterns of streamflow variability and its climate drivers in northern BC. The contribution of a new network of tree-ring chronologies also allows the potential for a valuable expansion of future paleo-climate research in the region.

3.7 Supplemental Information

3.7.1 Relationship between seasonal climate and gauged summer streamflow

Figure S3.1 displays correlations between summer streamflow (Jul-Aug) and historical regionalized climate records (Terrace, Smithers and Dease Lake weather stations). These correlation tests were calculated using the program Seascorr, which summarizes the strength of monthly and seasonally aggregated climate data and assesses significance of correlation by a Monte Carlo method (Meko et al., 2011). I tested monthly and 3-, 6-, and 12-month seasonal correlations between the streamflow data and climate data over a 14-month period beginning in July of the previous year and ending in August of the current year. Partial correlations calculated by Seascorr were then used to identify any influence of seasonal precipitation on the streamflow data independent of the temperature influence. The highest correlations indicate a negative association between mean temperatures in May through August of the current year and, independently, with mainly winter precipitation. The correlations with precipitation increase with increasing length of the average period, at least through 6-months for Skeena and Nass rivers; maximum correlation is reached for the 6-month period ending with June. August temperatures in the previous year were also negatively correlated with the summer streamflow data.

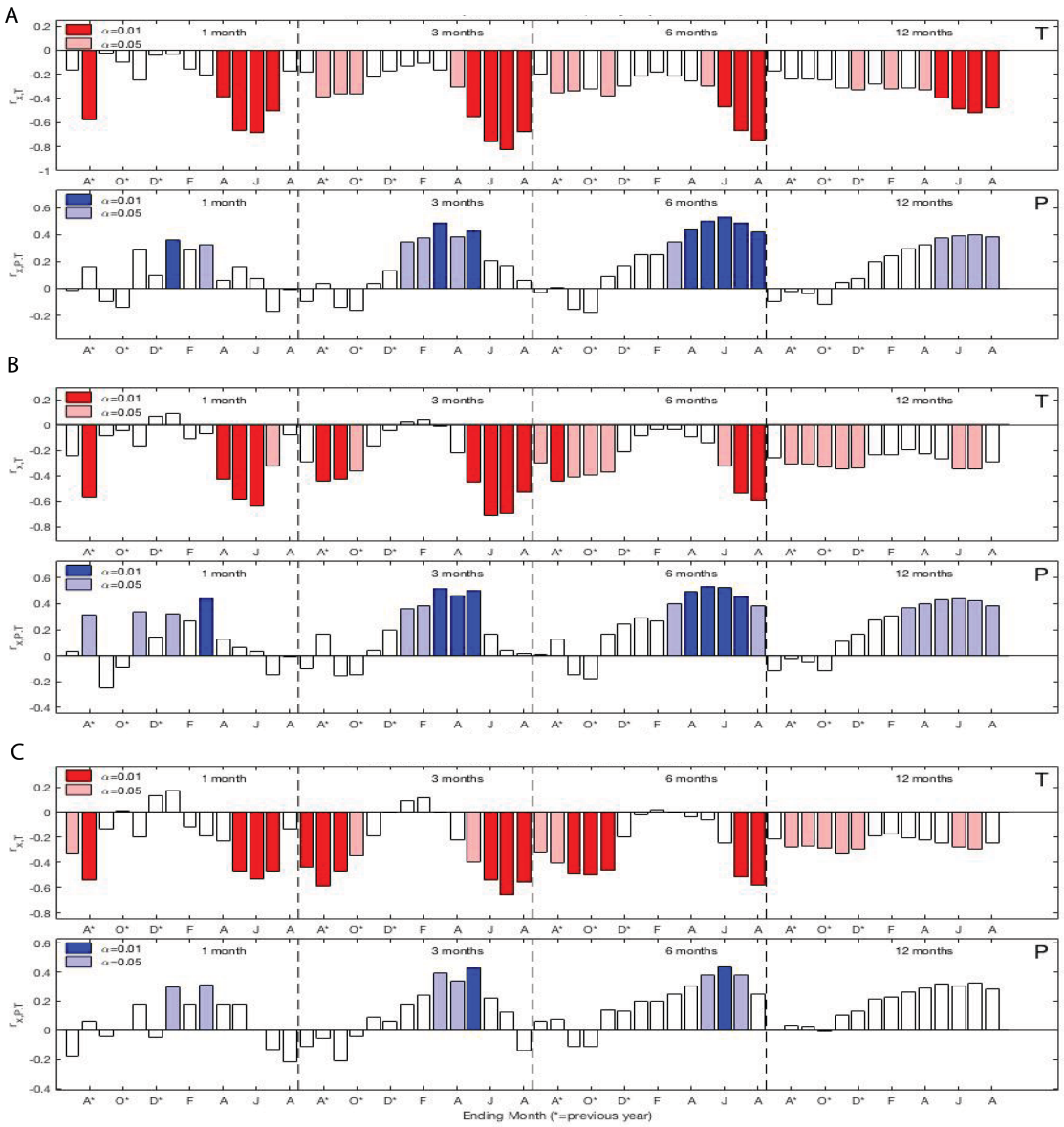

Figure S3.1: Monthly and seasonal correlations between A) Skeena, B) Nass, and C) Stikine river July-August streamflow and mean temperature, over 1-, 3-, 6-, and 12-month sliding windows beginning in the previous July through current August (top; red bars), and; monthly and seasonal partial correlations between flows and precipitation, controlling for the influence of mean temperature (bottom; blue bars). All calculations made using Seascorr.

3.7.2 Proxy-based Pacific Ocean climate indices

Table S3.1 lists correlations between the gauged Jul-Aug streamflow records for the Skeena (LSR), Nass (NSR) and Stikine (STK) rivers and long-term, proxy-based climate indices of PDO, PNA and ENSO. The proxy records were assessed for their use in the predictor pool for the reconstruction model approach.

Table S3.1: Significant ($p<0.05$) correlation coefficients of gauged Jul-Aug river runoff with selected proxy reconstructions of Pacific climate variability. Correlations in bold are significant at $p<0.01$.

Index reconstruction	LSR	NSR	STK
PDO[a]	**-0.48**		
PNA[b]	-0.31		
ENSO Nino 3.4[c]	-0.31	**-0.38**	-0.29

[a] Gedalof & Smith, 2001; UVTRL archives.
[b] Starheim et al., 2013a; UVTRL archives.
[c] Li et al., 2013; NOAA Paleoclimatology program

Chapter 4: Long-term variability of Skeena River steelhead trout (*Oncorhynchus mykiss*) abundance linked to ocean-atmospheric climate patterns: a dendrochronological evaluation

4.1 Abstract

Long-term records of salmonid population abundance and survival trends can help guide management and conservation action with information about the biophysical factors affecting them. Steelhead trout (*Oncorhynchus mykiss*) are an important part of the ecosystem, economy, and culture of the Pacific Northwest. However, steelhead populations appear to have declined throughout much of their southern range, and there are specific concerns about the viability of populations to the north. These concerns underscore the need to develop long-term perspectives of steelhead-climate relationships. The research capitalizes on the influence of large-scale ocean and atmospheric forcings on both tree growth and steelhead escapement to generate a long-term history of abundance for summer-run steelhead in the lower Skeena River. The tree-ring record explained 51% of the annual variance in the enumerated escapement data (with a *r* value of 0.73) and the model was used to reconstruct steelhead abundance from AD 1813-2005. The model described alternating intervals of persistently above-average and below-average steelhead abundance that corresponds to oceanic Pacific Decadal Oscillation-like influences. Notable high-abundance periods occurred between 1838-1848 and 1926-1942, both periods previously unidentified (i.e., prior to the enumerated record). Single, low-abundance years could describe links to "warm-warm" ENSO-PDO years associated with in-river low flow periods, partitioning the effects of survival in marine and freshwater habitats. The reconstruction provides a better understanding of the long-term

role of climate variability on steelhead abundance, providing new insights to guide appropriate management and conservation actions.

4.2 Introduction

Steelhead trout (*Oncorhynchus mykiss*), the anadromous form of rainbow trout, are found in all major coastal river systems in British Columbia (BC). Steelhead abundance has become of increasing concern to fisheries managers because the status of many populations in BC require increased emphasis on conservation (Slaney et al., 1996). Threats to these and other Pacific salmon populations are well known and associated with the conflict between industrial-scale human activity and wild resources (Montgomery, 2004). Unsustainable levels of harvest, genetic introgression of hatchery stocks, degradation or loss of freshwater habitat, and changes in ocean conditions, have led to an uncertain future for many of these fisheries. As concern mounts over the future of these populations, the necessity to improve our understanding of these interactions is heightened.

Widespread changes in Pacific salmon abundance are known to be closely tied to low-frequency climate shifts associated with the Aleutian Low (AL) pressure centre, and sea surface temperatures (SSTs) (Beamish and Bouillon, 1993; Beamish et al., 1997; Mantua et al., 1997; Starheim et al., 2013b; Mood et al., *unpublished*). Dramatic changes in an array of marine and terrestrial ecological variables in western North America coincided with oscillations between "cool" and "warm" phases that began around 1925, 1947, 1977, and 1998 in the North Pacific Ocean; the last two reversals correspond to documented shifts in salmon production regimes (Mantua et al., 1997; Mantua, 2015). However, not all species of salmon and not all regions were affected equally (Beamish et

al., 2009). Mantua et al. (1997) described positive biophysical relationships between Alaskan pink and sockeye abundance and the Pacific Decadal Oscillation (PDO), but found converse biophysical relationships between those stocks to the south (i.e.,Washington, Oregon, and California). Studies suggest that future responses by BC Pacific salmon north of 50-55°N will be different than by those in the south of this latitude, based on persistently observed historical oscillations in productivity between northern and southern populations (Beamish et al., 2009). These complex climate impacts have encouraged research intended to better understand the biophysical conditions that may affect the growth and survival of salmonid species in the Pacific Northwest (e.g., Grantham et al., 2012; Starheim et al., 2013b; Mantua, 2015; Kendall et al., 2017).

Much less is known about steelhead-climate relationships, due in part to the complex life history of steelhead, which makes estimating abundance, productivity, and survival metrics difficult (Kendall et al., 2017). Research has shown that marine survival of Pacific Northwest steelhead trout has varied greatly over time and that the environmental conditions during the first marine year (i.e., as smolts) are a strong determinant to survival rates (Kendall et al., 2017). In addition, steelhead populations appear to have declined since the 1980s throughout much of the southern part of their range (Busby et al., 1996), and there are specific concerns about the viability of populations in various other regions to the north (*Thompson and Chilcotin Steelhead Trout Emergency Assessment*, COSEWIC 2018). With persistent pressures on Pacific salmonids by humans, the increasing threat of climate change, and continued calls for recovery, monitoring population abundance and survival trends over space and time is essential for identifying the factors affecting population dynamics to guide appropriate

management and conservation actions (Burke et al., 2013). Unfortunately, the short duration of both climate and steelhead abundance records largely restricts our understanding to the past century.

Proxy salmon abundance histories developed from tree-ring data provide an opportunity to extend these limited records to multi-century timescales. For example, Drake and Naiman (2007) used the relationship between Pacific salmon and nutrient-limited riparian tree-ring growth to reconstruct the abundance of stream-spawning salmon over the past 150 to 350 years in the Pacific Northwest (including three mid-order rivers in southeastern Alaska). The reconstructions provided evidence that salmon populations are not only cyclical at large scales (as ocean conditions change), but also show patterns at much smaller scales (by stocks). More recently, Starheim et al. (2013b) used regional networks of climate-sensitive tree-ring chronologies to reconstruct multi-century long regional abundance histories for populations of sockeye, chinook, chum, and pink salmon in west central BC (1400-2009 AD). The authors identified a number of previously unrecorded population collapses and characterized the long-term influence of large-scale climate and ocean oscillations on Pacific salmon population trends in the area.

This study combines tree ring-width and maximum latewood density records to offer long-term insight on climate-induced trends in early-run (summer) steelhead trout abundance in the Skeena River. The research targets relationships between tree rings, trout abundance, and large-scale climate oscillations generated from the Pacific Ocean as a means to reconstruct population trends. The research capitalizes on the influence of large-scale ocean and atmospheric forcings on the radial growth of trees and steelhead

escapement to generate a long-term history of abundance for summer steelhead in the lower Skeena River.

4.3 Study Area

This study focuses on the early-run (summer) steelhead trout populations returning to natal tributaries in the Skeena River basin. Steelhead returning to overwinter in this region migrate through Chatham Sound and up the Skeena River at Telegraph Passage (Figure 4.1). Compared to other large salmonid-bearing basins in North America, the Skeena River watershed remains relatively pristine. While there are historical, ongoing and proposed land use changes (such as timber harvest, road systems and mining), human population densities are relatively low and dispersed, there are no major dams, and little history of hatchery propagation of steelhead (Gottesfeld and Rabnett, 2008).

The Skeena River basin is the second largest basin in BC with an approximate area of 54,400 km^2. From its headwaters in the northern interior Nechako Plateau and Skeena Mountains, the Skeena River flows 570 km southwest through the Hazelton Ranges and into the Coast Mountains via a broad glacial valley extending from Kitwanga to the Dixon Entrance (Figure 4.1). Major subbasin tributaries include the Sustut, Babine, Bulkely, Kitwanga, Zymoetz, Lakelse and Kitsumkalum rivers.

Climate in the Skeena River basin varies with relative proximity to the Pacific Ocean and the BC Coast Mountain ranges. The western flank of the study area is distinguished by abundant precipitation (average 2,590 mm per year), cool summers and mild winters. Precipitation reaches a maximum in the fall and early winter, when it is associated with intense cyclonic storms from the North Pacific that can cause severe and sudden flooding, particularly in the form of rain-on-snow events. The degree and extent

of the moderating coastal influence diminishes quickly with elevation and in an easterly direction. The interior portion of the study area has a cooler and drier boreal climate.

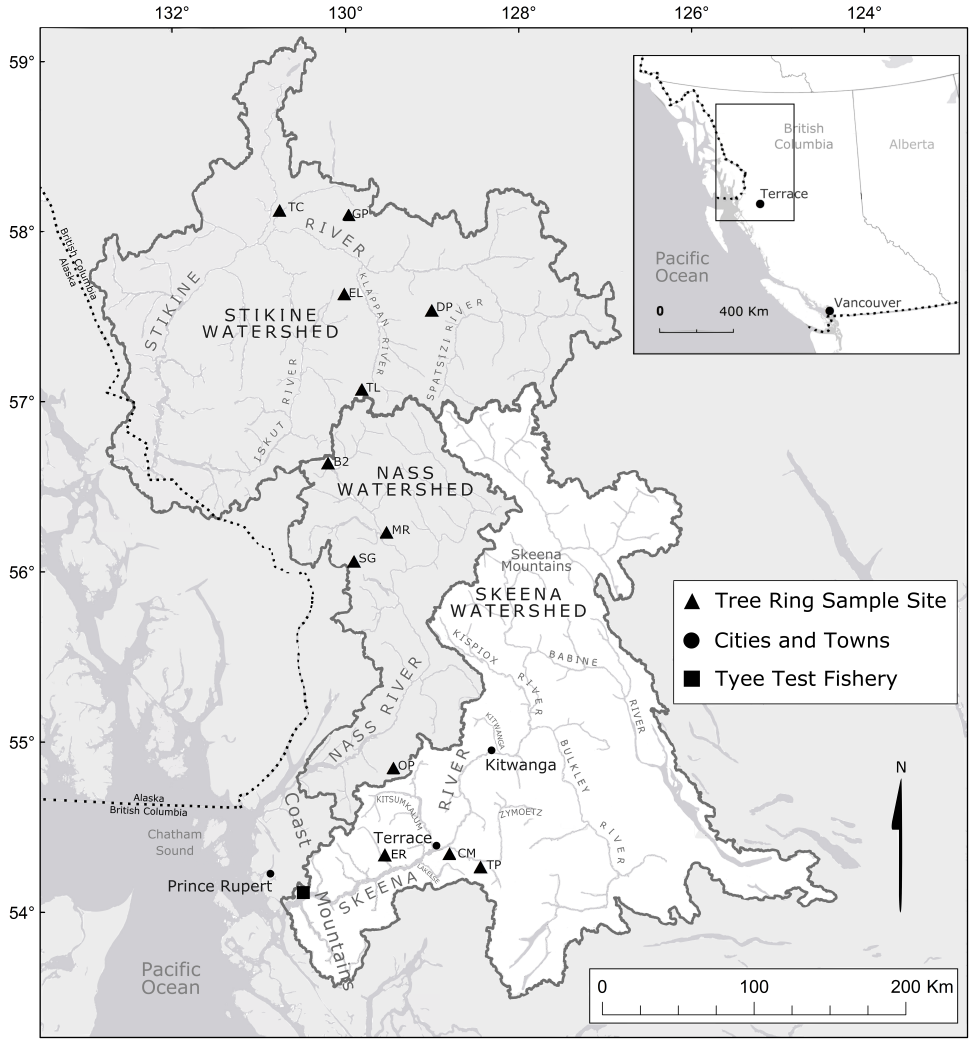

Figure 4.1: Location of the Skeena River watershed showing tree-ring sites and the Tyee Test Fishery. Tree-ring sites located in the Nass and Stikine river watersheds were included in the study.

4.4 Research Background

4.4.1 Steelhead trout life-histories

Steelhead display perhaps the most diverse life-history of any Pacific salmonid species (Thorpe, 1998; Quinn, 2005). Some individuals are resident in freshwater their whole lives (i.e., resident rainbow trout), while others migrate to the ocean and back following an anadromous life-history pattern (McPhee et al., 2007). In addition, some steelhead may be iteroparous (i.e., kelts), with the possibility of repeated spawning migrations. Moore et al. (2014) used scale analysis to demonstrate that 7.6% of the Skeena and Nass steelhead sampled performed multiple spawning migrations, and up to a maximum of four spawning migrations per lifetime. This complex array of life-history variation is possibly a compensating tactic for life in stochastic environments (Fleming and Reynolds, 2004).

In the lower Skeena River juvenile steelhead may spend up to five years in freshwater, although most spend two to four years in tributary streams before smolting (Whately et al., 1977; Grieve and Webb, 1999). Furthermore, adults vary in the number of years they spend in the ocean before migrating back to spawn, from two (Moore et al., 2014) to four years (Grieve and Webb, 1999). Summer-run steelhead trout enter the Skeena River between June and October and spawn from mid-May to late June of the following year (Beacham et al., 2012). Steelhead population declines have been linked with poor survival of smolts entering the ocean environment (Kendall et al., 2017). Steelhead are thought to be more pelagic than salmon, leaving the nearshore water over the continental shelf soon after entering salt water in the spring (Burgner et al., 1992). Steelhead make extensive seasonal migrations across broad areas of the North Pacific

Ocean, moving to the north and west in the spring through summer (concentrating on the Gulf of Alaska), and to the south and east, across the entire subarctic area (north of 38°N) from the North American coastline to at least 150°E, including portions of the Sea of Okhotsk and Bering Sea, from autumn through winter (Burgner et al., 1992; Atcheson et al., 2012). As a consequence of this wide-ranging distribution, steelhead are potentially affected by varying ocean-atmospheric factors and their survival may be an indicator of changing marine conditions, such as shifts in SST, water column stability, nutrients and zooplankton and phytoplankton productivity (Kendall et al., 2017).

4.4.2 Commercial fisheries impacts on steelhead abundance

Since the 1970s the bycatch and related mortalities of steelhead in the multi-species, mixed-stock commercial net fisheries of the Skeena River has been an ongoing issue of concern (Andrews and McSheffrey, 1976). Summer-run Skeena steelhead stocks co-migrate with much more abundant Skeena sockeye and pink stocks along their adult migration route back to overwinter and spawn in natal tributaries the following spring. As a result, the commercial fishery intercepts a variable number of steelhead trout (ranging from ~1000 to 17,000 fish caught, depending on the year) as bycatch (J.O. Thomas and Associates, 2010). Estimated steelhead abundance from escapements (hereafter, abundance), as indicated by annual estimates from the Fisheries and Oceans Canada (DFO) Tyee test fishery[1] are plotted in Figure 4.2. The data are compared to the annual commercial catch reports (1963-2018) in Area 3 (Chatham Sound area) and 4 (adjacent to

[1] Estimated abundance from escapements is computed using a cumulative average catch-per-unit effort index multiplied by an expansion factor based on the assumption that test gill-net catchability for steelhead is ~0.41% (Spence et al., *unpublished*).

the mouth of the Skeena River) gillnet and seine fisheries. During the mid-1980s, relatively large catches of steelhead were reported for Area 3 and 4 (Figure 2). By the early 1990s, fishery managers introduced a number of changes to commercial Skeena net fisheries (i.e., more selective fishing gear, revival tanks, and mandatory release) to limit the impacts on steelhead and less abundant non-target species, while still optimizing harvest on the target species. These changes, combined with the heightened awareness of the need for active steelhead conservation led to a major restructuring plan for Pacific fisheries (Wood, 2002). Since 2001 there has been a downward trend in steelhead bycatch in this fishery, likely due to imposed reductions in net fisheries opportunities during July and August when the majority of steelhead are present.

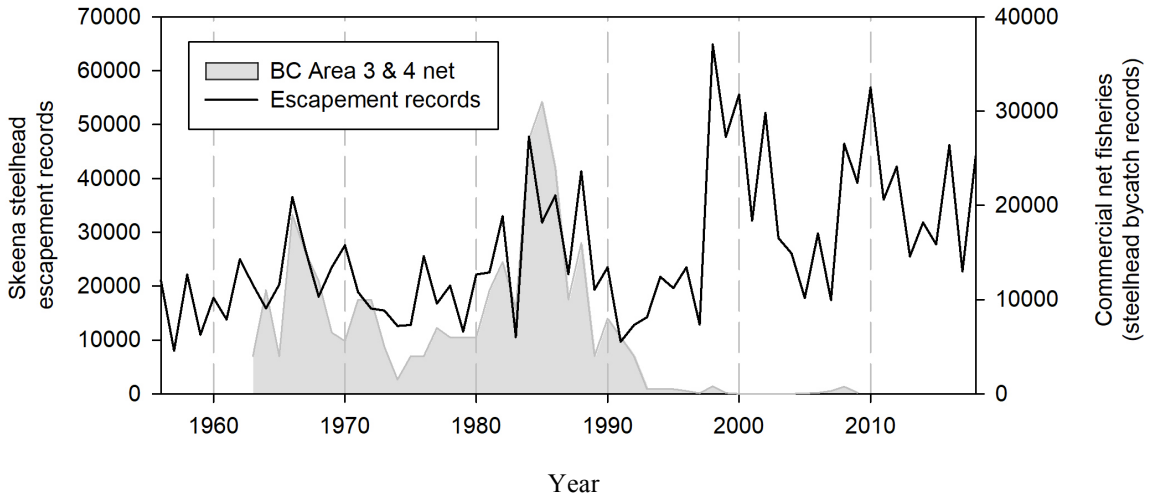

Figure 4.2: Annual reported catch in northern British Columbia (Area 3 and 4) gillnet and seine fisheries, compared to estimated escapement of Skeena summer steelhead from the Tyee Test Fishery (1956-2018).

4.4.3 Tree-rings as paleo-proxies of large-scale climate

Climate-sensitive trees provide the opportunity to extend climate records that accompany shifts in large-scale ocean and atmospheric forcings (i.e., D'Arrgio et al.,

2001; Gedalof and Smith 2001). The PDO is a major driver of climate variability in BC, and has been a major research focus for the past two decades (e.g., Mantua et al., 1997; McCabe et al., 2004; Whitfield et al., 2010). The PDO is a climate index based upon patterns of variation in SSTs that shift between two dominant patterns in the North Pacific Ocean, and has been linked to changes in ocean productivity (Mantua et al., 1997). The warm-phase PDO pattern is associated with warmer-than-normal SSTs, unusually high surface temperatures and variable precipitation patterns that depend on the direction of cyclonic storm activity during a stronger Aleutian Low (AL) pressure center (e.g., Welsh et al., 2019). Specifically, the PDO results in a documented multidecadal north-south "see-saw" pattern in winter/spring precipitation anomalies (e.g., Moore and McKendry 1996; Mantua et al., 1997; Rodenhuis et al., 2009; Welsh et al., 2019). During a warm-phase PDO pattern northern parts of BC and Alaska receive above-average precipitation in the form of winter storm activity along the Gulf of Alaska (GOA), whereas more southern and interior sections of the province experience low precipitation anomalies (Bailey et al., 2015), and the reverse pattern during a cool-phase PDO. Phase shifts of the PDO persist for ~20-40 years. El Niño (La Niña) events tend to occur during warm (cool)-phase PDO patterns and produce warmer (cooler) winter, spring and summer conditions (Stahl et al., 2006), and shift at interannual timescales. The PNA pattern is strongly influenced by the El Niño Southern Oscillation (ENSO) phenomenon and position of the AL. The positive phase of the PNA pattern tends to be associated with Pacific warm (e.g., El Niño and strong AL) episodes, and the negative phase tends to be associated with Pacific cool episodes (e.g., La Niña and weak AL), with little impact on surface temperatures in the summer months (Whitfield et al., 2010).

High-elevation trees respond to changes in regional hydroclimate and are associated with low-frequency climate oscillations in Pacific North America (e.g., Gedalof and Smith 2001; Starheim et al., 2013a; Coulthard et al., 2016; Welsh et al., 2019). Warm climatic conditions promote earlier bud and needle maturation and lengthen the period of active photosynthesis, thereby enhancing annual ring growth (Peterson and Peterson, 2001). In snowpack-sensitive species, shallow snowpack totals result in larger-than-average annual rings in high-elevation mountain hemlock (*Tsuga mertensiana* (Bong.) Carrière) due to a prolonged growing season, with smaller-than-normal rings demonstrated during deep winter snowpack seasons when late-lying snowpacks limit radial growth (Peterson and Peterson, 1994; Larocque and Smith, 1999; Gedalof and Smith, 2001; Starheim et al., 2013a). In contrast, an inverse relationship to seasonal snowpacks has been observed in the radial growth of white spruce (*Picea glauca*), whereby they respond positively to soil moisture availability during the growing season as a result of deeper-than-normal seasonal snowpacks (Welsh et al., 2019). It is important to note that this positive growth-soil moisture relationship was linked to the warm-phase pattern of the PDO accompanied by incoming winter storms in northern BC. The link between annual growth and surface climate preserved in long tree-ring records has enabled the reconstruction of a number of low-frequency hemispheric climate phenomena in North America (e.g., Biondi et al., 2001; D'Arrigo et al., 2001; Gedalof and Smith, 2001; MacDonald and Case, 2005; D'Arrigo et al., 2005; Trouet and Taylor, 2009).

4.5 Data and Methods

4.5.1 Tree-ring width and density chronology development

Tree-ring records were developed from mountain hemlock and white spruce increment core samples collected at 12 sites (Table 4.1; Figure 4.1). Sites within the Skeena River basin and in two adjacent basins share the same headwater location (i.e., Stikine and Nass river basin). Sampling involved extracting two 5.2-mm increment cores from 20 trees at each site whenever possible. Sample preparation, crossdating and chronology construction followed standard dendrochronological methods (Stokes and Smiley, 1968; Cook and Kairiukstis, 1990). Annual tree ring-widths were measured to the nearest 0.001mm using a Velmex "TA" System in conjunction with J2X software (version 5.0). Calendar dates were assigned to the ring-width series and verified with the COFECHA 3.0 crossdating program (Holmes, 1983; Grissino-Mayer, 2001). COFECHA uses segmented cross correlation techniques to detect measurement and crossdating errors. For this study, the time series were partitioned into 50-year segments with 25-year lags, with the significance determined at a 99% critical level at a correlation of 0.320.

Each crossdated series was standardized using ARSTAN (Cook and Holmes, 1984) to produce site-specific master chronologies. Standardization involved fitting an estimated growth function to the ring-width series and computing ring width indices by dividing width measurements by the expected value of the growth curve. For this study, long-term trends unrelated to climate were removed by fitting a cubic smoothing spline with a 50% frequency response cutoff at a wavelength of 67% of the series length to each series. Series from individual cores were combined into single standardized master chronologies at each site using a bi-weight robust mean (Mosteller and Tukey, 1977).

Adequacy of sample size is based on the expressed population signal (EPS) statistic (Wigley et al., 1984). Standard chronologies were truncated where EPS values fell below the standard value of 0.85, with only one decade of this time permitted to drop to an EPS value of 0.80.

Maximum latewood density records were developed from 12-mm core samples collected at one mountain hemlock and two white spruce sites. Each 12 mm core was prepared for densitometric analysis by first gluing it flush to the surface of a 2.5 cm-wide fibreboard block. A 2-mm thick wood lath was then cut (pith to bark) with a Waltech high precision twin-bladed saw to reveal the radial surface of the core (Haygreen and Bowyer, 1996). Resins were extracted from the laths using an acetone Soxhlet apparatus (Jensen, 2007). Each sample was then x-rayed using the University of Victoria Tree-Ring Laboratory (UVTRL) ITRAX MultiScanner densitometer (Cox Analytical Systems, see http://www.coxsys.se). Measurements were made at 0.05-mm increments for 125 µs, with the densitometer maintained at 30 kV and 40 mA. The digital x-ray images were analyzed using ITRAX Windendro® version (2008) to provide ring width and maximum density values.

The maximum latewood density series were crossdated by identifying characteristic annual ring patterns using corresponding ring-width measurements. Series crossdating was verified using COFECHA 3.0 (Holmes, 1983; Grissino-Mayer, 2001) and annually resolved maximum latewood density chronologies were produced. The crossdated site series were standardized with ARSTAN (Cook and Holmes, 1984) to produce species-specific master chronologies. A cubic smoothing spline with a 50% frequency response

cutoff at a wavelength of 67% of the series length was applied to each series to remove non-climatic impacts. Adequacy of sample size was determined by the EPS statistic.

Table 4.1: Tree-ring records and sampling locations.

Name	ID	Species[a]	Data[b]	Collection year	Zone	Easting UTM	Northing UTM	Elevation (m asl)
Tumeka Lake	TL	Sw	TRW	2014	09V	0463783	6341715	1179
Telegraph Creek	TC	Sw	TRW; MXD	2014	09V	0404699	6457089	720
Ealue Lake	EL	Sw	TRW	2014	09V	0449555	6403935	930
Danihue Pass	DP	Sw	TRW	2015	09V	0507624	6395571	1241
Gnat Pass	GP	Sw	TRW	1983[c]; 2011[d]; 2015	09V	0450205	6456084	1240
Bell 2	B2	Hm	TRW; MXD	2011[d]; 2014	09V	0443525	6292381	1143
Mount Richie	MR	Hm	TRW	2014	09V	0484022	6248506	1088
Surprise Glacier	SG	Hm	TRW	2005[d]	09V	0463396	6228516	808
Copper Mountain	CM	Hm	TRW	2005[e]	09U	0534539	6039285	887
Extew River	ER	Hm	TRW	2005[e]	09U	0492441	6037306	875
Trapper Mountain	TP	Hm	TRW	2015	09U	0555377	6031437	1256
Oscar Peak	OP	Hm	TRW	2016	09U	0495162	6093986	1306

[a] White spruce (Sw); Mountain hemlock (Hm)
[b] Ring-width (TRW); maximum latewood density (MXD)
[c] Crossdated tree-ring series from International Tree Ring Data Bank (ID: NOAA-tree-4426; Schweingruber, 1983)
[d] Crossdated tree-ring series from the University of Victoria Tree-Ring Laboratory (UVTRL) archives
[e] Crossdated tree-ring series from Starheim et al. (2013a)

4.5.2 Steelhead escapement and climate data

Annual steelhead escapement estimates were obtained from the Fisheries and Oceans Canada (DFO), Tyee test fishery. The DFO gillnet test fishery in the lower Skeena River has operated since 1956 and is used to evaluate the magnitude of salmon and steelhead trout returns after their passage through the commercial fisheries (Areas 3 & 4). Net set times vary according to tide height, timing of freshet, water clarity and temperature. This escapement record is considered to be the best indicator of timing and abundance for summer run steelhead returns to natal tributaries in the Skeena River basin (Walters et al., 2008).

Monthly mean atmospheric teleconnection index (ATI) records for the PDO (1900-2018) and the PNA (1950-2018) pattern were obtained from the Joint Institute for the Study of the Atmosphere and Ocean website (JISAO, 2016). Monthly Extended Reconstructed SST (ERSST version 4) in the Niño 3.4 region (1950-2018) were used to measure the variability linked to the El Niño-Southern Oscillation (ENSO) and were retrieved from the National Centre for Atmospheric Research (NOAA, 2016) database.

4.5.3 Model development and analysis

Multiple linear regression was used to estimate steelhead escapement abundance from the set of candidate tree-ring predictors. Standardized chronologies were entered in years *t* to *t-7*, so that the tree-ring information in previous years could inform on the climate conditions linked to steelhead abundance in a given year (Cook and Kairiūkštis, 1990). A reconstruction model was constructed using a forward stepwise procedure with a cross-validation stopping rule (Wilks, 1995). Cross-validation was performed using a traditional split period approach to independently validate the tree-ring based steelhead abundance estimates.

The strength of the regression models for the calibration period was reported using an adjusted R^2 to provide a measure of the model explanatory power. The *F* ratio of the regression model was computed as a goodness-of-fit-test and the standard error (SE) as a measure of uncertainty in the predicted values over the calibration period. Regression residuals were tested for autocorrelation using the Durbin-Watson test and the mean variance inflation factor (VIF) was calculated to identify multicollinearity among predictors. For the verification period the reduction of error (RE) statistic was used to provide a measure of skill of the model. RE has a possible range of $-\infty$ to 1. An RE of 1

indicates perfect prediction for the validation period, and can be achieved only if the model residuals are zero. As a rule of thumb, a positive RE is accepted as evidence of some prediction skill (Fritts, 1976). The root-mean-square error (RMSE) of cross-validation residuals was used to measure of the uncertainty in the predicted values over the validation period and was compared to the SE as a measure of uncertainty in the regression estimates. The best model calibrated over the full common data period was used to reconstruct historical steelhead escapement variability over the length of the shortest predictor dataset.

Extreme low steelhead abundance years were defined based on a bottom tenth percentile threshold, calculated over the full reconstruction record. The magnitude of the low abundance years were quantified as departures from the mean of the steelhead record calculated over the reconstructed and instrumental shared period, and compared. The steelhead abundance reconstruction was then compared with PDO paleoreconstructions (Gedalof and Smith, 2001) and Gulf of Alaska surface air temperature (Wiles et al., 2014) over the common data period to investigate large-scale climatological influences on the variability of steelhead abundance. A correlation analysis was preformed to test the strength of association between the paleo-climate records and the steelhead reconstruction.

4.5.4 Spectral and wavelet analysis

A multi-taper method (MTM) spectral analysis (Mann and Lees, 1996) was performed on the steelhead escapement reconstruction to evaluate dominant frequencies of variability in the time series. MTM offers the appeal of being nonparametric and does not prescribe an *a priori* model for the process generating the time series. The MTM uses

orthogonal windows (or tapers) to obtain independent estimates of the power spectrum and averages them to yield a more stable spectral estimate compared to other single-taper methods. It is particularly well suited for short and noisy time series, in that it has the ability to detect small amplitude oscillations without the necessity of filtering the signal and allows for an *F* test to be used to determine the significance level of the different frequency components. The MTM spectral analysis was implemented using the MTM-SSA Toolkit with robust background estimation (Ghil et al., 2002). Following the suggestion of Mann and Park (1993), where climate records consist of a few hundred observations, three tapers and a bandwidth parameter p=2 were employed. As a complement to the MTM method, a wavelet analysis was used to highlight the evolution of significant frequencies of variability in the steelhead reconstruction over time (Torrence and Compo, 1998; Grinsted et al., 2004). The transformation was computed using the Morlet wavelet with a wavelet power of significance tested at a 90% confidence level against a red-noise background. The wavelet transformations were implemented in R package biwavelet (Gouhier et al., 2016).

4.6 Results

4.6.1 Tree-ring chronologies and diagnostic climate relationships

Fourteen site-specific chronologies were developed from a total of 551 radial series from 305 trees, with chronology lengths ranging from 512 to 204 years (Table 4.2). Series intercorrelation values, a measure of the strength of the signal common to all sampled trees, range from 0.467 to 0.686 (Table 4.2). Mean sensitivity is a measure that describes the interannual changes in ring width (Fritts, 1976) and, in this instance, the values range from 0.160 to 0.284 (Table 4.2). These values indicate strong synchronicity

within the ring-width chronologies developed for this study. Mean sensitivity of the density measurements was substantially lower than the ring-width values.

To assess any temporal variability in the strength of the common radial growth signal, running series of average correlations (RBAR) were calculated for each chronology. RBAR is the mean correlation coefficient for all possible pairings among tree-ring series in a chronology, computed for a specified common time interval (Cook and Kairiūkštis, 1990). For this study, a 50-year window with an overlap of 25 years between adjacent windows was employed. RBAR values ranged from $r = 0.234$ to 0.457. Chronologies were truncated according to the EPS calculation.

Table 4.2: Tree-ring chronology statistics.

ID	Period (AD years)	Series, trees	Interseries correlation	Mean sensitivity	RBAR[a]	Year[b] EPS >0.80
TC	1773-2014	40, 20	0.658	0.204	0.457	1775
EL	1689-2013	40, 20	0.548	0.178	0.293	1751
DP	1802-2015	40, 20	0.614	0.174	0.345	1808
GP	1757-2015	90, 47	0.558	0.160	0.250	1795
TL	1809-2013	41, 20	0.619	0.173	0.366	1825
TCd	1773-2014	19, 20	0.645	0.042	0.402	1788
B2	1501-2013	32, 16	0.647	0.229	0.336	1634
MR	1696-2013	38, 19	0.644	0.218	0.379	1754
OP	1664-2016	43, 22	0.691	0.284	0.455	1686
SG	1633-2004	44, 22	0.570	0.215	0.284	1705
CM	1646-2004	39, 20	0.686	0.261	0.411	1692
ER	1576-2004	28, 22	0.610	0.244	0.320	1657
TP	1630-2014	39, 20	0.685	0.271	0.426	1675
B2d	1675-2013	18, 17	0.467	0.081	0.192	1816

[a] RBAR: Mean correlation coefficient among the tree-ring series
[b] Year chronologies were truncated based on the EPS calculation

The results of the correlation analyses with the ATI data are presented in Table 4.3. Significant correlations were detected between the lagged steelhead escapement records and the seasonalized ENSO and PDO indices. No significant correlations were detected with the PNA index. Strong correlations were observed during spring (Mar-May) five

years prior to the steelhead escapement records for both ENSO and PDO, with the PDO demonstrating the strongest relationships overall.

Significant correlations were detected between all the mountain hemlock site-chronologies and the ENSO and PDO indices. Fewer, and generally weaker, significant correlations were observed with the white spruce chronologies. The chronologies also appear to be more strongly and consistently correlated with the ATIs during the spring season (Mar-May), reflecting the tendency of these species to record complex, composite climate signals related to snowpack conditions (Peterson and Peterson, 2001; Welsh et al., 2019). Correlations between the tree-ring chronologies and the steelhead records are presented in Table 4.4. The correlations were stronger with the predictor tree-ring chronologies at a lag of five years, consistent with the observed relationships with the ATI records. However, TCd and SG had higher correlations at no lag (negative correlation) and one-year lag (positive correlation), respectively.

Table 4.3: Correlation values for end-of-season steelhead escapement and tree-ring records to seasonalized climate oscillation indices. DJF = December (of the previous year), January, and February; MAM = March, April, and May; JJA = June, July, and August; A = Annual. Lag-8 and PNA was excluded from the table as no significant correlations were documented with the steelhead escapement record. Bold values indicate correlations with $p < 0.01$.

Steelhead Escapement			*Tree-ring Records*													
				White Spruce						Mountain Hemlock						
				TC	EL	DP	GP	TL	TCd	B2	MR	OP	SG	CM	ER	TP	B2d
ENSO	Value	Season	Interval														
lag-5	0.29	MAM	DJF									0.26					
	0.25	JJA	MAM		0.26							**0.33**					
	0.26	A	JJA	0.29	**0.36**	**0.32**	0.28	0.27	**0.33**	**0.37**	**0.35**	0.30	0.30		0.32	0.28	**0.33**
lag-6	0.27	MAM	SON	0.28	0.25	0.26			0.31	**0.32**	0.27	0.26			0.27		0.29
	0.25	A	A		0.30				0.28	**0.36**	0.27	**0.39**		0.27	0.31	0.29	**0.33**
lag-7	0.26	MAM															
	0.27	A															
PDO	Value	Season	Interval														
lag-1	0.25	DJF	DJF							**0.30**	**0.28**	**0.43**	**0.32**	**0.34**	**0.29**	**0.31**	**0.29**
lag-2	0.26	MAM	MAM		**0.30**		0.25			**0.28**	0.24	**0.40**	**0.36**	**0.33**	**0.28**	**0.27**	0.23
lag-3	0.25	MAM	JJA		0.21	0.22				**0.26**	0.21	**0.36**	**0.33**	0.21	0.23	0.22	0.25
lag-4	**0.32**	**MAM**	SON							0.22		**0.27**					
lag-5	0.26	DJF	A		0.25					**0.32**	0.26	**0.43**	**0.36**	**0.32**	**0.30**	**0.28**	**0.27**
	0.40	**MAM**															
	0.38	**JJA**															
	0.35	**A**															
lag-6	0.26	DJF															
	0.35	**MAM**															
	0.29	**A**															

Table 4.4: Correlation values between end-of-season steelhead escapement (*t* to *t*-7) and tree-ring records. Bold values indicate correlations with $p < 0.01$.

Record	lag-0	lag-1	lag-2	lag-3	lag-4	lag-5	lag-6	lag-7
TC				0.31	**0.35**	**0.44**	0.30	0.29
EL				**0.37**	**0.36**	**0.48**	0.31	0.27
DP		0.28		**0.35**		**0.45**	0.28	**0.33**
GP				0.29		**0.36**		
TL		**0.41**		**0.32**		**0.41**		0.29
TCd	**-0.44**					**0.33**		0.27
B2					**0.33**	**0.50**	**0.37**	**0.40**
MR				0.29	0.32	**0.38**		0.29
OP					0.28	0.29		
SG	0.33	**0.54**	0.32	0.34	0.33	**0.39**		
CM					0.34	0.30		
ER								
TP		0.26		0.28	0.28	0.30		
B2d						**0.33**		

4.6.2 Steelhead escapement model estimation

The significant relationships detected between ATIs, tree-ring growth and the steelhead escapement record advocate for the use of climate-sensitive tree-ring measurements to construct records of long-term steelhead abundance. Three predictor tree-ring chronologies were selected for reconstruction, Surprise Glacier (SG), Danihue Pass (DP) and Telegraph Creek (TCd) at time *t-1, t-5*, and *t* respectively. The model equation is:

$$\text{Steelhead}_t = 104098.8 + 30069.4\ (\text{SG}_{t-1}) + 39992.5\ (\text{DP}_{t-5}) - 148355.5\ (\text{TCd}_t)$$

The reconstruction spans the interval from 1813-2004 and explains 51% of the variance in the steelhead escapement data. Regression and cross-validation statistics are summarized in Table 4.5. Analysis of the residual estimates using the Durbin-Watson (D-W) statistic showed no significant first-order autocorrelation. The VIF suggested no multicollinearity among the model predictors and the *F*-ratio indicates a statistically

significant regression equation. The RE values of the cross-validation statistics indicate that the reconstruction has considerable predictive skill. The R^2 and r of the observed and split period estimates also attest to good model skill.

The reconstructed estimates and steelhead escapement record was compared over the calibration period (1956-2005) in Figure 4.3A. The reconstruction data capture the year-to-year variability of the escapement data with acceptable accuracy. The magnitudes of the lowest instrumental SWE years were accurately estimated: no major discrepancies between the instrumental and reconstructed records occur during those years. A visual inspection of the calibration time plot shows that the magnitudes of peak abundance years were slightly underestimated. The full reconstruction for summer run Skeena steelhead is presented in Figure 4.3B.

Table 4.5: Regression statistics of the tree-ring based steelhead escapement reconstruction for the calibration period 1955-2004. Cross-validation statistics in bold.

Calibration							**Split period cross-validation**			
R^2	Adjusted R^2	D-W[a]	VIF[b]	SE	F ratio		**RE**	**RMSE[c]**	r[d]	R^2_v[e]
0.54	0.51	1.81	1.1	8884.21	18.05	**1956-1979**	**0.33**	**10062.80**	**0.54**	**0.30**
						1980-2005	**0.44**	**13405.14**	**0.71**	**0.51**

[a]Durban-Watson statistic
[b]Variance inflation factor
[c]Root mean square error
[d]Pearson correlation of observed and cross-validation estimates
[e]R^2 of observed and cross-validation estimates

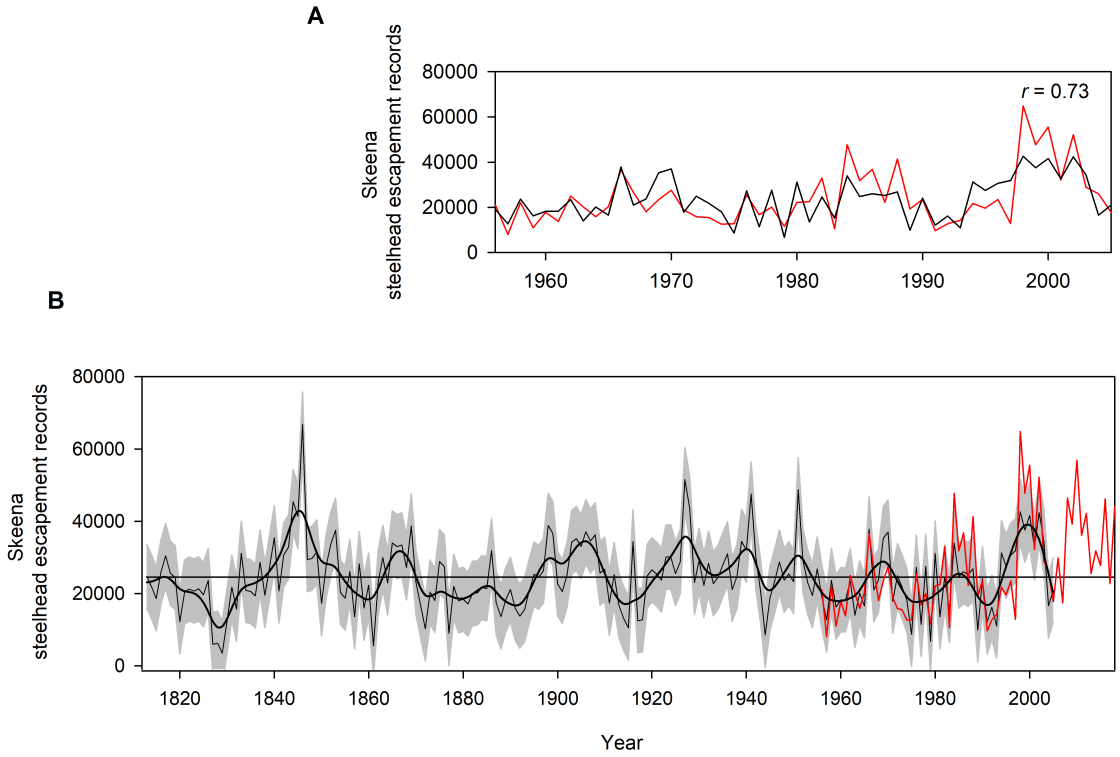

Figure 4.3: A) Time plot of estimated escapement of Skeena summer-run steelhead (red line) and reconstructed (black line) for the calibration period (1955-2005). B) The full steelhead escapement reconstruction (dark grey line) for the period 1813-2005. The black line is a 10-year cubic smoothing spline of the reconstructed values, the red line is the enumerated escapement records, and grey area is the ± 1 root-mean-square error uncertainty estimates from the verification period. The horizontal line represents the calibration mean.

4.6.3 Analysis of the reconstruction

The timing and magnitude of low steelhead abundance years over the length of the reconstruction and instrumental period are presented in Figure 4.3B and listed in Table 4.6. A total of 19 extreme low abundance years occurred over the duration of the reconstruction (1813-2005) based on the bottom tenth percentile threshold (cutoff <12,884). Twelve of these extreme low years occurred prior to the recorded escapement data (i.e., prior to 1956). The most severe mean departures in the reconstruction record occurred in 1829, 1861, 1827, 1828, and 1979. Three out of the six low-abundance years observed during the enumerated steelhead record were captured in the reconstruction

(Table 4.6). There were several extreme low-abundance years identified in the reconstruction that were not identified in the enumerated steelhead data. Only a small difference was required to meet the threshold cutoff in the enumerated steelhead data (cutoff <11,704; data not shown). Conversely, 1959 and 1983 were identified in the enumerated steelhead data as extreme low-abundance years but were not in the reconstructed dataset. These were negative departure years in the reconstruction but did not surpass the required threshold level (data not shown).

Table 4.6: Timing and magnitude of the reconstructed (A) and enumerated abundance records (B) of Skeena summer-run steelhead escapement data. Low escapement numbers within the enumerated record are in bold. Low escapement years were identified by calculating the bottom 10th percentile departures from the 1956-2005 reconstructed and actual record means.

	Year	Departure
A)	1829	-21,049
	1861	-19,003
	1827	-18,621
	1828	-18,290
	1979	**-17,838**
	1944	-16,874
	1975	**-15,874**
	1877	-15,584
	1989	**-14,698**
	1872	-14,301
	1915	-14,058
	1993	**-13,554**
	1977	**-13,144**
	1991	**-12,429**
	1820	-12,359
	1917	-12,088
	1830	-12,069
	1957	**-11,868**
	1918	-11,840
B)	1957	-18,540
	1991	-16,879
	1983	-16,039
	1959	-15,603
	1979	-14,971

Figure 4.4 compares the steelhead abundance reconstruction with the Wiles et al. (2014) GOA coastal surface air temperature (Feb-Aug) and the Gedalof and Smith (2001) spring PDO (Mar-May) reconstructions. Correlations analyses reveal a positive association between the steelhead reconstruction and the long-term GOA air temperature ($r = 0.45$; $p = 0.01$) and PDO ($r = 0.30$; $p = 0.01$) lagged at five years prior to escapement. This lagged effect is consistent with the correlation analysis described in Table 4.3 (e.g., strongest correlations with spring PDO at lag-5). Since the 1900s, there has been an apparent increase in correspondence between the records compared to the 1800s (Figure 4). A prolonged period of high abundance occurred between 1926-1942, that corresponds to warmer-than-normal temperature in the GOA_{t-5} and warm phase of the PDO_{t-5}. Another prolonged period occurred between 1838-1848 (prior to the enumerated record) and corresponds to warmer conditions in the paleorecords. A number of cooler-than-normal periods were identified that corresponded to low steelhead abundance in the reconstruction, but were shorter in persistence compared to responses observed during warmer conditions.

4.6.4 Spectral and wavelet analysis

The results of the MTM spectral analysis indicated a significant ($p \leq 0.05$) multidecadal component of variability (~25 yrs), as well as significant ($p \leq 0.05$) variability at interannual time scales (~2 yrs) in the steelhead abundance reconstruction (Figure 4.5). High frequency variability in the 2 to 3 year range is commonly associated with ENSO (Ribera and Mann, 2003). Frequencies within multidecadal bands (ie., 20-70 yr) have been associated with ocean-atmospheric forcings, such as the PDO, where shifts in oscillation patterns (i.e., “warm” or “cool” phases) are marked by widespread shifts in

climates in the Pacific Basin and North America (Minobe, 2000). The wavelet results generally mirror those of the MTM analysis, with significant multidecadal intervals (~25-30 years) that persisted over the majority of the earlier part of the time series (specifically, 1813-1940). The wavelet power spectrum also revealed a marked quasidecadal band at ~15 years that persisted in the later part of the series between 1950 and 2000. The results of both the MTM and wavelet spectral analysis suggest that variability in steelhead escapement is influenced by multidecadal frequencies of variability associated with large-scale atmospheric teleconnections.

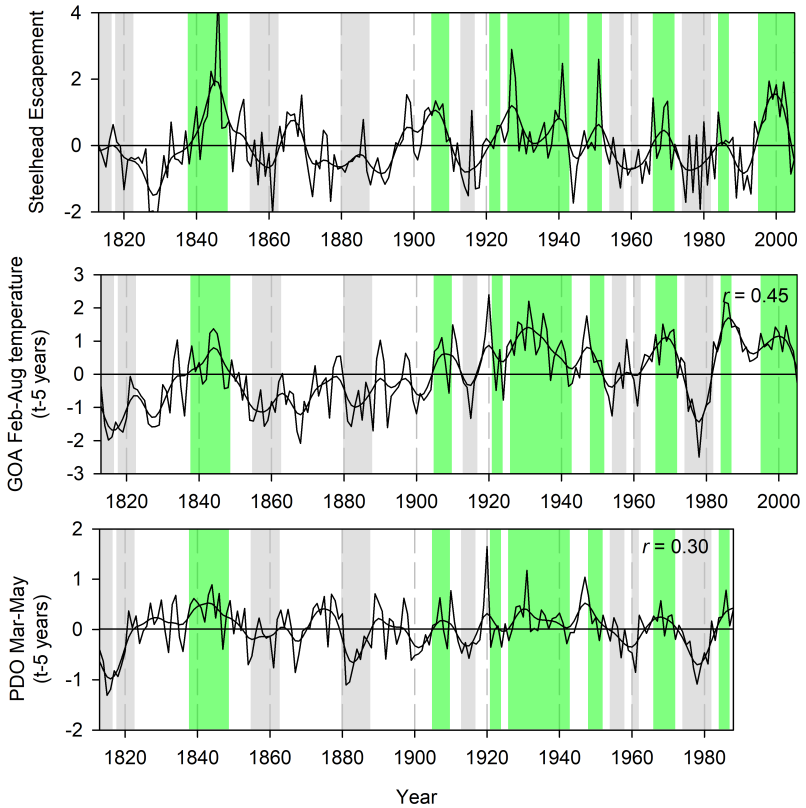

Figure 4.4: Comparisons between reconstructed steelhead records, Gulf of Alaska (GOA) Feb-Aug surface temperatures (Wiles et al., 2014) and Mar-May Pacific Decadal Oscillation (PDO) index (Gedalof and Smith, 2001). Both GOA and PDO data were lagged at t-5 years. The data were smoothed using a 10-year spline. Grey shaded areas highlight intervals typically exhibiting low steelhead numbers, low GOA_{t-5} temperatures, and cool PDO_{t-5} periods, whereas green shaded areas highlight the opposite relationship.

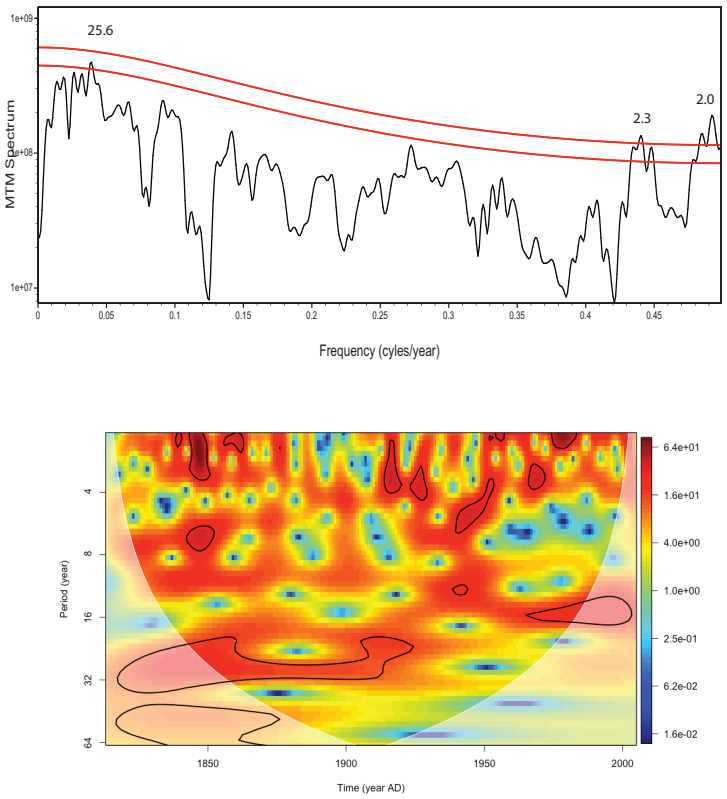

Figure 4.5: Above: Multitaper method (MTM) spectral analysis of the Skeena steelhead escapement tree-ring reconstruction for 1813-2005. Red curves represent the 95% and 99% confidence levels (bottom to top). Significant ($p \leq 0.05$) power exists at the frequencies that are labeled. Below: wavelet power spectrum for the steelhead reconstruction. The lighter shade was used to show the cone of influence where edge effects might be important. Legend indicates wavelet power in colours.

4.7 Discussion

4.7.1 Reconstruction of summer steelhead abundance

The primary objective of the research was to develop a long-term record of summer-run steelhead abundance for the Skeena River using snowpack sensitive tree-ring chronologies. The tree-ring model accounted for 51% of the annual variance in the enumerated escapement data (with a *r* value of 0.73) and the model was used to reconstruct steelhead abundance from AD 1813-2005. The model describes alternating

intervals of persistently above-average and below-average steelhead abundance throughout the 192-year long record. Notable high-abundance periods occurred between 1926-1942 and 1838-1848, both periods previously unknown (i.e., prior to the enumerated record) (Figure 4.3B). The timing and magnitude of single-year, low-abundance in the reconstruction shows good agreement with the enumerated data (Table 4.6), but could suggest some overall bias in the reconstructed data (i.e., via variance compression) contributing to the tabulated differences in low-abundance years by the threshold cutoff.

It is important to address the possible impacts of bycatch-related artifacts on abundance variability and model skill. Any level of harvest will, of course, impede stock rebuilding once abundance has declined to a very low level. However, bycatch mortality is unlikely to be the principal cause of abundance fluctuations in the data. This interpretation is supported by the strong statistical relationships between the steelhead escapement data and reconstruction to low frequency climate variability generated from the Pacific Ocean. Commercial net fisheries for salmon may capture adult steelhead as bycatch during their marine and lower river migrations and impose some level of mortality whose magnitude varies year-by-year. For the Thompson and Chilcotin steelhead aggregates, bycatch mortality is believed to be currently in the range of 0-25% and has generally been below sustainable harvest levels (Bison, 2016). Figure 4.2 shows that bycatch records from the Skeena River salmon fishery and steelhead escapement data correspond to each other, particularly during the 1963-1995 period ($r = 0.74$, $p < 0.01$). This relationship further supports the notion that the steelhead data used for model

reconstruction had little impact on interannual fluctuations in population productivity and, as such, introduced minimal human-related artifacts into the reconstruction.

4.7.2 Climate connections to the steelhead abundance reconstruction

Correlation analyses of steelhead abundance and the ATIs were strongest for the PDO, extending from one to six year lags with varying significant seasonal groupings (Table 4.3). The predictors entered into the model provide insights into the specific climate-related effects on steelhead abundance. First, the mountain hemlock SG tree-ring predictor at a *t-1* lag showed the highest statistically significant relationship with the escapement data. The site chronology was highly correlated with the seasonalized PDO index (excluding fall; Table 4.3) suggesting a link between marine conditions and adult survival trends the year before migration. Combined with the distinct low-frequency modes of variability identified using MTM and wavelet analyses, this finding indicates a clear PDO-like influence on the steelhead abundance prior to the 1940s (Figure 4.5). The variable presence or absence of this relationship suggests that steelhead teleconnections to the PDO strengthen and weaken over long timescales, possibly reflecting the strength and position of the AL (Litzow et al., 2018) or perhaps the growing influence of anthropogenic global warming. Moreover, Figure 4.4 demonstrates the link between warmer GOA temperatures, the warm PDO phase and connections to steelhead abundance. Support for this interpretation comes from known links between warmer ocean climate and the increased productivity of several oceanographic trophic levels (Francis and Hare, 1997). Further, increased survivorship of groundfish following the 1977 climate shift to warmer conditions (Beamish et al., 1999) offers additional support for the argument that the critical ecosystem changes that improved the salmonid survival

after 1977 occurred primarily in the ocean, as groundfish have no freshwater life history phase (Smith, 2000).

The model predictors also describe smolt survival patterns in ocean environments. At this stage of development, nearshore marine conditions are critically important to smolt growth (Kendall et al., 2017). In the Skeena River, steelhead trout typically spend up to four years in the ocean as adults before migrating back to overwinter and spawn in natal streams (Whately et al., 1977). The strong correlations observed during spring (Mar-May) at a *t-5* lag between steelhead escapement and PDO demonstrate a possible link to smolt survival. The DP predictor also reflects a positive association with steelhead escapement variability at a *t-5* lag, along with summer/fall ENSO and spring PDO (Table 4.3 and 4.4). It is plausible that the DP_{t-5} predictor describes fluctuations in survival rates during early marine residence (as smolts) and not later pelagic life as adults. Warm ocean conditions (during a warm phase PDO periods and/or El Niño) allow phytoplankton and zooplankton, which the smolts feed, to expand their range northward. The expanded area and increased productivity of lower tropic levels results in a more stable smolt-to-adult population (Welch et al., 2000).

Freshwater discharge in snowmelt-driven rivers in northern BC shows a similar decadal-scale pattern of variability as oceanic-atmospheric climate (Mantua et al., 1997), and has been shown to impact the freshwater production of salmonids (e.g., Smith, 2000; Grantham et al., 2012; Ohlberger et al., 2018). However, the freshwater controls suggest a converse relationship to steelhead abundance compared to the above ocean associations. For instance, Smoker (1955) found a strong positive correlation between commercial catch of western Washington coho salmon and summer streamflow, and suggested that

lower return numbers were likely causes by reduced survival in freshwater rearing habitat due to low summer flow. A similar control of freshwater production of steelhead trout by summer low flows has also been reported (Grantham et al., 2012). The TC tree-ring density predictor showed the strongest correlation to summer (Jun-Aug) ENSO index and a negative correlation with steelhead abundance in the year of migration (Table 4.3 and 4.4). In addition, spectral analyses identified significant frequencies of variability at interannual timescales indicating ENSO-like influence on steelhead abundance (Figure 5). Although no significant correlation was found between the steelhead abundance data and ENSO, there was a correlation of notability (r = -0.18, p > 0.05; data not shown in Table 4.3). Strong and regionally consistent ENSO-streamflow teleconnection have been established for the Skeena River watershed, and indicate a negative association particularly during "warm-warm" ENSO-PDO years (e.g., Stiff et al., 2015). Interestingly, over 80% of the single, low escapement number in the reconstruction occurred during low flow periods identified using a previously reconstructed summer streamflow tree-ring model of the Skeena River (data not shown).

Partitioning the effects of survival in marine and freshwater habitat on the abundance of adult salmonids returning to their natal tributaries is problematic, since mortality is integrated over both habitats (Bradford, 1995). Potential mechanisms by which interannual variations in freshwater discharge could modulate steelhead adulthood are through the changes to the environmental condition of migration habitats. Steelhead enter freshwater many months before spawning, apparently compromising growth opportunities at sea to access overwintering and spawning grounds in conjunction with specific seasonal patterns of flow and temperature along the migratory route (Robards

and Quinn, 2002). Flow conditions are frequently cited as stimulating or controlling the rate of upstream migration by salmonids. Low flows (due to periods without significant rainfall or snowmelt input) have been linked to slower passage of salmon (Banks, 1969; Liscom et al., 1985), as well as a reduction in invertebrate abundance (a food source for fish) in riffle habitats (Dewson et al., 2007). The inclusion of a potential streamflow signal in the model could suggest that the interannual variability (although by a smaller measure as the oceanic links) in summer-run steelhead migration in the Skeena River are modulated by river discharge characteristics, in particular low flows during summer.

4.7.3 Comparisons with other proxy records

Starheim et al. (2013b) used regional networks of climate-sensitive tree-ring chronologies to reconstruct multi-century long regional abundance histories for populations of sockeye, chinook, chum, and pink salmon in west-central BC. High-frequency interannual fluctuations in six salmon populations were shown to reflect changes in SSTs and atmospheric pressures induced by ENSO. Lower-frequency interdecadal oscillations in North Pacific salmon abundance histories were shown to be associated with shifts in oceanic and climatic conditions as described by the PDO and PNA. In summarizing their research, Starheim et al. (2013b) presented tree-ring proxy models of salmon abundance that demonstrated the interannual influence of large-scale oceanic and atmospheric climate changes on Pacific salmon survival over the last 600 years. The steelhead abundance model presented in this study shows a similar strength of association with large-scale oceanic and atmospheric climate changes. In particular, the Bulkley River region (a major tributary of the Skeena River) chinook and sockeye proxy records show a synchronous trend in abundances over the same period as the steelhead

reconstruction. For instance, the high abundance periods that occurred between 1926-1942 and 1838-1848 in the steelhead reconstruction were also identified in the Pacific salmon tree-ring reconstructions. This finding further supports the Starheim et al. (2013b) suggestion that salmonid population trends in the North Pacific are distinct from other populations to the south of the study area (Hare et al., 1999; Wells et al., 2006; Starheim et al., 2013b; Mood et al., *unpublished*).

Chapter 5: Conclusion

5.1 Introduction

This dissertation presents four dendrohydrological reconstructions and one dendroecological reconstruction developed using networks of moisture- and energy-limited tree-ring data that are sensitive to annual snowpack fluctuations. The hydroclimate reconstructions include a 223-year record of annual April 1 SWE (Stikine River basin), a 417-, 716-, and 343-year record of summer streamflow (Jul-Aug) for the Skeena, Nass and Stikine rivers, respectively, and finally, a 193-year reconstruction of summer-run steelhead abundance (Skeena River). This research was developed to provide a long-term context for understanding recent snowpack declines, hydrologic extremes, and fluctuations in steelhead abundance to inform more comprehensive water management strategies.

5.2 Summary of Main Research Results

1. This research provides a robust record of April 1 SWE variability for the Stikine River basin based on moisture-limited white spruce tree-ring chronologies collected from mid- to high-elevation locations. Successful crossdating among the tree-ring chronologies and statistically proven, time-stable relationships with the SWE record demonstrated a physiological link between snowpack and moisture availability important for annual radial growth of white spruce in northern BC. These relationships were strong enough to form the basis for paleohydrological models of April 1 SWE. See Chapter 2.

2. The reconstruction of April 1 SWE in Chapter 2 indicates that there has been considerable variability in SWE levels over the past two centuries in the Stikine region. The finding of lower-than-normal (higher-than-normal) SWE during a PDO cool (warm) phase is in contrast to findings to the south of the study area. This in-phase relationship supports the notion that the Aleutian Low influences the path and strength of winter cyclonic activity along the Gulf of Alaska in a manner that is distinct for surrounding regions in BC. Connections between April 1 SWE and the PDO are particularly concerning since the PDO is currently understood to be in its cool state, and suggests this association may continue to exacerbate the recent trend of a diminishing snowpack in the Stikine region.

3. The reconstruction of Stikine basin April 1 SWE (43% explanatory power) demonstrated that SWE values recorded in 2016 were likely among the lowest experienced within the past ~200-years. See Chapter 2.

4. This research demonstrated the validity of combining moisture- and energy-limited, snow-sensitive tree-ring records (ring-width and maximum latewood density chronologies) with specific hemispheric climate signals for reconstructing summer streamflow in a "non-traditional" environment. Previously, cooler and wetter settings in northern Canada were not considered to have high dendroclimatological potential. The research established the use of a multi-species, multi-proxy approach to improve reconstruction skill. See Chapter 3.

5. Interbasin comparisons of single, low flow events showed a distinct asynchronous clustering pattern and opposing relationships with GOA surface temperature consistent with previous findings of a north-south "see-saw" pattern of hydroclimate variability in western Canada and coastal Alaska (e.g., Moore and McKendry, 1996; Rodenhuis et al., 2009; Trenberth, 2011). The research suggests a more complex interrelationship of moisture availability and transport in the region than previously understood and is likely related to synoptic-scale circulation involving the Aleutian Low. See Chapter 3.

6. Capitalizing on the influence of ocean-atmospheric forcings on both tree growth and steelhead escapement, a 192-year reconstruction of summer-run steelhead abundance for the Skeena River was developed. The reconstruction (51% explanatory power) described alternating intervals of persistently above-average and below-average steelhead abundance that corresponds to PDO-like influences. Single, low abundance years describe possible links to "warm-warm" ENSO-PDO years associated with in-river low flow periods, partitioning the effects of survival in marine and freshwater habitats. See Chapter 4.

5.3 Conclusion

Hydrological records in western Canada are seldom as long as a century, and so do not represent multi-century fluctuations due to climate variability. Moreover, management recommendations for water supply forecasting and water storage planning based on these restricted records may well be inaccurate. The results of this research underscore the critical need for long-term estimates of hydroclimate variability to assess

the magnitude of hydroclimatic change in recent decades. This is particularly important in northern BC where diminishing water security has intensified and has been recognized by the provincial government as a critical environmental management challenge (BC Ministry of Environment, 2018).

The reconstruction models developed for this dissertation suggest that: 1) tree-ring data from moisture- and energy-limited, snow-sensitive conifer trees are useful paleo-proxies for snow, and snow-influenced streamflow; 2) current summer streamflow conditions have been more severe compared to the past, but more persistent low flow periods were identified prior to the gauged record; 3) a clear north-south "see-saw" hydroclimate pattern connected to shifts in the PDO is evident in the region; and 4) alternating intervals of above-average and below-average steelhead abundance in the reconstructed record corresponds to long-term PDO-like influences. The streamflow models also incorporate tree-ring derived reconstructions of hemispheric climate variability (i.e., Gedalof and Smith, 2001 [PDO]; Starheim et al., 2013a [PNA]; and Li et al., 2013 [Niño3.4]), which demonstrates the influence these patterns have on snow accumulation and subsequent melt conditions in northern BC. To the author's knowledge these are the first paleohydrological reconstruction of their kind, and they provide the longest, most statistically robust, annually-resolved records of historical snow and summer streamflow in northern BC.

The hydroclimate of BC is complex because of its close proximity to the Pacific Ocean, mountainous terrain, and large latitudinal expanse (Schnorbus et al., 2014). The varied hydrologic response to climate variability in BC is a key aspect of effective water management, and may well be critical to adapting to anticipated changes in streamflow

expected under future climate changes. Both snowpack and streamflow appear to be associated with ocean-atmospheric climate variability over multiple centuries, but demonstrates a distinct north-south, inverse teleconnection pattern with winter precipitation. This finding has substantial implications for water resource planning protocols. Understanding and anticipating basin-scale hydroclimate variability – and also the consequences of failing to do so – is key to managing water resources. This research demonstrates that hydroclimate variability in northern BC is complex and, because of this, has the potential to be especially challenging for climate-based water supply forecasting, storage planning, and ecosystem management. It is important to note that, while climate oscillation like the PDO and ENSO play a major part in snow and snow-influenced processes, this does not preclude the role of global climate warming in exacerbating recent declines.

The snowpack and streamflow reconstructions developed for this research can be used by water managers to: 1) extend the lengths of datasets used for forecasting and assessing low and high flow probabilities, in order to adapt before extreme events occur; and, 2) incorporate basin-specific responses to climate variability and change into hydrologic planning, particularly regional contingency protocols that need to address the specific impacts of prolonged deficits on natural and managed systems. Finally, the steelhead abundance reconstruction for the Skeena River can be used by fishery managers to: 1) improve stock monitoring; and, 2) predict climate-related shifts on salmonid survival and distinguish them from other effects (i.e., net fisheries and land-use changes).

5.4 Future Research

This dissertation addressed key research gaps and provided a novel perspective on hydroclimate variability in northern BC. Snow accumulation and melt are important components of the hydrologic cycle in northern BC, supplying the majority of the annual flow (Eaton and Moore, 2010). The loss of winter snowpack can have profound consequences for the generation of hydroelectricity, human water supply, and aquatic ecosystems, all increasing the complexity for the management of water resources. As such, it is critical to continue hydroclimatic research and monitoring in this region. Below lists a number of future research recommendations:

1. There is excellent potential to spatially expand hydroclimate reconstructions in northern BC. This dissertation showed that combining moisture- and energy-limited, snow-sensitive tree-ring proxies from mid- to high-elevation conifers in "non-traditional" environments has hydrological potential. Efforts should focus on areas where snowmelt and snow-influenced streamflow are important for human water use, industry and stream ecology.

2. Based on the climate-growth analysis of the white spruce chronologies, there is evidence to suggest a weakening of the SWE relationship (but not statistically significant). It is possible that climate has changed over time enough that cambial growth responses have been affected. Phenological studies should be conducted to provide concrete evidence that white spruce can continue to serve as proxy for snow, and snow-influenced streamflow.

3. It is clear from this research that summer precipitation is an important component of the hydrology of the area, which was not targeted in the summer streamflow models. The mid- to high-elevation conifers used in this study are not an effective predictor of high-resolution summer precipitation (i.e., not a limiting factor). It is possible that lower elevation conifers and/or other aridity proxy archives (i.e., Palmer Drought Severity Index) could be included to optimize the summer streamflow reconstructions and expand the application of this modeling approach.

Bibliography

Anderson, S., Aziz, O., Toole, G., Grissino-Mayer, H., and A. Barnett, 2012. Using Pacific Ocean climatic variability to improve hydrologic reconstructions. Journal of Hydrology. 434-435, 69-77.

Andrews, T.R., and H.M. McSheffrey, 1976. Commercial interception of steelhead trout stocks in British Columbia: a preliminary review. British Columbia Marine Resources Branch, Fisheries Management Report.

Aravena, J. C., Morimoto, D., Watson, E., Youngbult, D., and B.H. Luckman, 2002. Glacier Gulch – TSME – ITRDB CANA390. NOAA Study Page: https://www.ncdc.noaa.gov/paleo/study/16497

Arendt, A., Walsh, J., and W. Harrison, 2009. Changes of glaciers and climate in Northwestern North America during the late twentieth century. American Meteorological Society. 22, 4117-4134.

Arnell, N.W. and C. Liu, 2001. Chapter 4: Hydrology and water resources. In: Climate Change 2001: Impacts and Adaptations. In: Contribution of Working Group II to the Third Assessment Report of the Intergovernmental Panel on Climate Change [J. McCarthy and O. Canziani (Eds.)]. Cambridge University Press, Cambridge, UK. pp 191.

Atcheson, M.E., Myers, K.W., Beauchamp, D.A., and N.J. Mantua, 2012. Bioenergetic response by steelhead to variation in diet, thermal habitat, and climate in the North Pacific Ocean. Transactions of the American Fisheries Society. 141, 1081–1096.

Axelson, J.N., Sauchyn, D.J., and J. Barichivich, 2009. New reconstructions of streamflow variability in the South Saskatchewan River Basin from a network of tree ring chronologies, Alberta, Canada. Water Resources Research. 45, W09422.

Bales, R.C., Molotch, N.P., Painter, T.H., Dettinger, M.D., Rice, R., and J. Dozier, 2006. Mountain hydrology of the western United States, Water Resources Research. 42, 1-13.

Bailey, H.L., Kaufman, D.S., Henderson, A.C.G., and M.J. Leng, 2015. Synoptic scae controls on the $\delta^{18}O$ in precipitation across the Beringia. Geophysical Research Letters. 42, 4608-4616.

Banks, J.W., 1969. A review of the literature on the upstream migration of adult salmonids. Journal of Fish Biology. 1, 85–136.

Barnett, T.P., Adam, J.C., and D.P. Lettenmaier, 2005. Potential impacts of a warming climate on water availability in snow-dominated regions. Nature. 438, 303-309.

Beacham, T.D., Wallace, C.G., Le, K.D., and M. Beere, 2012. Population structure and run timing of steelhead in the Skeena River, British Columbia. North American Journal of Fisheries Management. 32, 262–275.

Beamish, R.J. and D.R. Bouillon, 1993. Pacific salmon production trend in relation to climate. Canadian Journal of Fisheries and Aquatic Science. 50, 1002-1016.

Beamish, R.J., Neville, C.M., and A.J. Cass, 1997. Production of Fraser River sockeye salmon (*Oncorhynchus nerka*) in relation to decadal-scale changes in the climate and the ocean. Canadian Journal of Fisheries and Aquatic Sciences. 54, 543-554.

Beamish, R.J., Noakes, D.J., McFarlane, G.A., Klyashtorin, L., Ivanov, V.V., and V. Kurashov, 1999. The regime concept and natural trends in the production of Pacific salmon. Canadian Journal of Fish and Aquatic Science. 56, 516–526.

Beamish, R.J., Riddell, B.E., Lange, K.L., Farley Jr., E., Kang, S., Nagasawa, T., Radchenko, V., Temnykh, O., and S. Urawa, 2009. The effects of climate on Pacific salmon – A summary of published literature. North Pacific Anadromous Fish Commission (www. npafc.org).

Beriault, A.L., and D.J. Sauchyn, 2006. Tree-ring reconstructions of streamflow in the Churchill River Basin, northern Saskatchewan. Canadian Water Resources Journal. 31, 249-262.

British Columbia Ministry of Environment and Climate Change Strategy, 2018. British Columbia Drought Response Plan (https://www2.gov.bc.ca/gov/content/environment/air-land-water/water/drought-flooding-dikes-dams/drought-information).

British Columbia Ministry of Forest, Lands, and Natural Resource Operation, 2018. Government's Action Plan: Responding to wildfire and flood risks (https://www2.gov.bc.ca/gov/content/governments/organizational-structure/ministries-organizations/ministries/forests-lands-natural-resource-operations-and-rural-development).

Biondi, F., Gershunov, A., and D.R. Cayan, 2001. North Pacific decadal climate variability since AD 1661. Journal of Climate. 14, 5-10.

Bison, R.G., 2016. Estimation of steelhead escapement to the Nicola River watershed. BC Ministry of Environment, Fisheries Branch, Kamloops, BC.

Bonsal, B.R.,Wheaton, E.E., Chipanshi, A.C., Lin, C., Sauchyn, D.J., and L. Wen, 2011. Drought research in Canada: A review. Atmosphere-Ocean. 49, 303-319.

Box, G., and G. Jenkins, 1976. Time Series Analysis: Forecasting and Control, revised ed. Holden-Day, Oakland, CA.

Bradford, M.J., 1995. Comparative review of Pacific salmon survival rates. Canadian Journal of Fish and Aquatic Science. 52, 1327-1338.

Brubaker, L.B., Vega-Gonzalez, S., Ford, E.D., Ribic, C.A., Earle, C.J., and G. Segura, 1992. Old-growth Douglas-fir in western Washington. In: The response of western forests to air pollution. Springer-Verlag, New York, USA.

Burgner, R.L., Light, J.T., Margolis, L., Okazaki, T., Tautz, A., and S. Ito, 1992. Distribution and origins of steelhead trout (*Oncorhynchus mykiss*) in offshore waters of the North Pacific Ocean. International North Pacific Fisheries Commission, Vancouver, B.C., Canada.

Burke, B.J., Peterson, W.T., Beckman, B.R., Morgan, C., Daly, E.A., and M. Litz, 2013. Multivariate models of adult Pacific salmon returns. PLoS ONE. 8, e54134.

Busby, P.J., Wainwright, T.C., Bryant, E.J., Lierheimer, L.J., Waples, R.S., Waknitz, F.W., and I.V. Lagomarsino, 1996. Status review of West Coast steelhead from Washington, Idaho, Oregon, and California. NOAA Northwest Fisheries Science Center, Seattle, Wash.

Cayan, D.R., 1996. Interannual climate variability and snowpack in the western United States. Journal of Climate. 9, 928-948.

Cochrane, D., and G.H. Orcutt, 1949. Application of least squares regression to relationships containing auto-correlated error terms. Journal of the American Statistical Association. 44, 32–61.

Committee on the Status of Endangered Wildlife in Canada (COSEWIC), 2018. Steelhead Trout (*Oncorhynchus mykiss*), Thompson River and Chilcotin River populations in Canada, 2018: COSEWIC Technical summaries and supporting information for emergency assessments.

Cook, E.R., and R.L. Holmes, 1984. Program ARSTAN. Upgraded version 40. Available from ftp://ftp.cricyt.edu.ar/users/dendro.

Cook, E.R., and L.A. Kairiūkštis, 1990. Methods of Dendrochronology: Applications in the Environmental Sciences. Kluwer Academic Publishers. Norwell, MA, USA.

Coulthard, B., and D.J. Smith, 2016. A 477-year dendrohydrological assessment of drought severity for Tsable River, Vancouver Island, British Columbia, Canada. Hydrological Processes. 30, 1676-1690.

Coulthard, B., Smith, D.J., and D.M. Meko, 2016. Is worst-case scenario streamflow drought underestimated in British Columbia? A multi-century perspective for the south coast, derived from tree-rings. Journal of Hydrology. 534, 205-218.

Cropper, J.P., 1982. Climate reconstructions (1801 to 1938) inferred from tree-ring width chronologies of the North American Arctic. Arctic and Alpine Research. 14, 223-241.

Curry, C.L., and W. Zwiers, 2018. Examining controls on peak annual streamflow and floods in the Fraser River Basin of British Columbia. Hydrology and Earth System Sciences. 22, 2285-2309.

D'Arrigo, R., Villalba, R., and G. Wiles, 2001. Tree-ring estimates of Pacific decadal climate variability. Climate Dynamics. 18, 219-224.

D'Arrigo, R., Cook, E.R., Wilson, R.J., Allan, R., and M.E. Mann, 2005. On the variability of ENSO over the past six centuries. Geophysical Research Letters. 32, L03711.

Déry, S.J., Stahl, K., Moore, R.D., Whitfield, P.H., Menounos, B., and J.E. Burford, 2009. Detection of runoff timing changes in pluvial, nival, and glacial rivers of western Canada. Water Resources Research. 45, W04426.

Dettinger, M.D., and D.R. Cayan, 1995. Large-scale atmospheric forcing of recent trends towards early snowmelt runoff in California. Journal of Climate. 8, 606-623.

Dewson, Z.S., James, A.B.W., and R.G. Death, 2007. Invertebrate response to short-term water abstraction in small New Zealand streams. Freshwater Biology. 52, 357-369.

Drake, D.C. and R.J. Naiman, 2007. Reconstruction of Pacific salmon abundance from riparian tree-ring growth. Ecological Applications. 17, 1523-1542.

Eaton, B., and R.D. Moore, 2010. Regional hydrology. Chapter 4. In: Compendium of Forest Hydrology and Geomorphology in British Columbia (vol 1 of 2) [Pike, R.G., Bennett, K.E., Redding, T.E., Moore, R.D, Winker, R.D., and K.D. Baldon] BC Ministry of Forests and Range, Forest Science Program, Victoria, BC and FORREX Forum for Research and Extension in Natural Resources, Kamloops, BC Land Management Handbook: 66.

Edwards, T.W.D., Birks, S.J., Luckman, B.H., and G.M. MacDonald, 2008. Climatic and hydrologic variability during the past millennium in the eastern Rocky Mountains and northern Great Plains of western Canada. Quaternary Research, 70, 188–197.

Environment Canada, 2015. Historical Climate Data. Access online: http://climate.weather.gc.ca/

Fleming, I.A., and J.D. Reynolds, 2004. Salmonid breeding systems. In Evolution Illuminated: Salmon and Their Relatives (Hendry, A. P. and Stearns, S. C., eds), pp. 264–294. New York: Oxford University Press.

Fleming, S.W., and D.J. Sauchyn, 2013. Availability, volatility, stability, and teleconnectivity changes in prairie water supply from Canadian Rocky Mountain sources over the last millennium. Water Resources Research. 49, 64-74.

Fleming, S.W., Whitfield, P.H., Moore, R.D., and E.J. Quilty, 2007. Regime-dependent streamflow sensitivities to Pacific climate modes cross the Georgia-Puget transboundary ecoregion. Hydrological Processes. 21, 3264-3287.

Fleming, S.W., Hood, E., Dahlke, H.E., and S. O'Neel, 2016. Seasonal flows of international British Columbia-Alaska rivers: the nonlinear influence of ocean-atmosphere circulation patterns. Advances in Water Resources. 87, 42-55.

Francis, R.C., and S.R. Hare, 1997. Regime scale climate forcing of salmon populations in the Northeast Pacific — some new thoughts and findings. In Estuarine and ocean survival of Northeast Pacific salmon: Proceedings of the Workshop [R.L. Emmett and M.H. Schiewe] NOAA Tech. Memo. NMFSNWFSC-29. pp. 113–128.

Fritts, H.C., 1976. Tree Rings and Climate. The Blackburn Press. Caldwell, New Jersey.

Gedalof, Z., and D.J. Smith, 2001. Interdecadal climate variability and regime-scale shifts in Pacific North America. Geophysical Research Letters. 28, 1515-1518.

Gedalof, Z., Peterson, D.L., and N.J. Mantua, 2004. Columbia river flow and drought since 1950. Journal of the American Water Resources Association. 40, 1579-1592.

Ghil, M., Allen, M.R., Dettinger, M.D., Ide, K., Kondrashov, D., Mann, M.E., Robertson, A.W., Saunders, A., Tian, Y., and P. Yiou, 2002. Advanced spectral methods for climatic time series. Review of Geophysics. 40, 1-41.

Gobena, A.K., and T.Y. Gan, 2009. The role of Pacific climate on low frequency hydroclimatic variability and predictability in Southern Alberta, Canada. Journal of Hydrometeorology. 10, 1465-1478.

Gottesfeld, A.S., and L.M.J Gottesfeld, 1990. Floodplain dynamics of a wondering river, dendrochronology of the Morice River, British Columbia, Canada. Geomorphology. 3, 159-179.

Gottesfeld, A.S., and K.A. Rabnett, 2008. Skeena River Fish and Their Habitat. Oregon State University Press, Corvallis, Oregon, USA.

Gouhier, T.C., Grinsted, A., and V. Simko, 2016. R Package 'biwavelet': Conduct Univariate and Bivariate Wavelet Analyses (https://cran.r-project.org/web/packages/biwavelet/index.html).

Grantham, T.E., Newburn, D.A., McCarthy, M.A., and A.M. Merenlender, 2012. The role of streamflow and land use in limiting oversummer survival of juvenile steelhead in California streams. Transactions of the American Fisheries Society. 141, 585-598.

Grieve, G.D., and D. Webb, 1999. Lakelse River Steelhead: Summary of current data and status review, 1997. BioLith Scientific Consultants Inc.

Grinsted, A., Moore, J.C., and S. Jevrejeva, 2004. Application of the cross wavelet transform and wavelet coherence to geophysical time series. Nonlinear Processes in Geophysics. 11, 561-566.

Grissino-Mayer, H., 2001. Evaluating crossdating accuracy: a manual and tutorial for the computer program COFECHA. Tree-Ring Research. 57, 205-221.

Hare, S.R., Mantua, N.J., and R.C Francis, 1999. Inverse production regimes: Alaska and west coast Pacific salmon. Fisheries. 24, 6-14.

Hart, S.J., Smith, D.J., and J.J. Clague, 2010. A multi-species dendroclimatic reconstruction of Chilko River streamflow, British Columbia, Canada. Hydrological Processes. 24, 2752-2761.

Haygreen J.G., and J.L. Bowyer, 1996. Forest Products and Wood Science, 3rd ed. Iowa State University Press, Ames.

Holmes, R.L., 1983. Computer-assisted quality control in tree-ring dating and measurement. Tree-Ring Bulletin. 43, 69-78.

Huntington, T.G., 2006. Evidence for intensification of the global water cycle: review and synthesis. Journal of Hydrology. 319, 83-95.

J.O. Thomas and Associates Ltd, 2010. Steelhead bycatch and mortalities in the commercial Skeena net fisheries of British Columbia from observer data: 1989-2009. Prepared for: The Pacific Salmon Foundation and British Columbia Ministry of Environment, Skeena Region.

Jensen, W.B., 2007. The origin of the Soxhlet extractor. Chemical Education Today. 84, 1913-1914.

Jevrejeva, S., Moore, J.C., and A. Grinsted, 2003. Influence of the Arctic Oscillation and El Nino-Southern Oscillation (ENSO) on ice conditions in the Baltic Sea: the wavelet approach. Journal Geophysical Research. 108, 4677.

JISAO (Joint Institute for the Study of the Atmosphere and Ocean website), 2016. Climate Data Archive. http://jisao.washington.edu/data_sets.

Kendall, N.W, Marston, G.W., and M.M. Klungle, 2017. Declining patterns of Pacific Northwest steelhead trout (*Oncorhynchus mykiss*) adult abundance and smolt survival in the ocean. Canadian Journal of Fish and Aquatic Sciences. 74, 1275-1290.

King, G.M., 2009. Factors influencing the growth of white spruce (*Picea glauca*) in the Mackenzie Delta, NWT. B.Sc. Thesis. Carleton University, Ottawa, ON.

Kozlowski, T.T., Kramer, P.J., and S.G. Pallardy, 1991. The Physiological Ecology of Woody Plants. New York, NY: Academic Press.

L'Heureux, M.L., Mann, M.E., Cook, B.I., Gleason, B.E., and R.S. Vose, 2004. Atmospheric circulation influences on seasonal precipitation patterns in Alaska during the latter 20th century. Journal of Geophysical Research. 109, 1-17.

Larocque, C.P., and D.J. Smith, 1999. Tree-ring analysis of yellow cedar (*Chamaecyparis nootkatensis*) on Vancouver Island, British Columbia. Canadian Journal of Forest Research. 29, 115– 123.

Larocque, C.P., and D.J. Smith, 2005. 'Little Ice Age' proxy mass balance records reconstructed from tree rings in the Mt Waddington area, British Columbia Coast Mountains, Canada. The Holocene. 15, 748-757.

Larsen, C.P.S., and G.M. MacDonald, 1995. Relations between tree-ring widths, climate, and annual area burned in the boreal forest in Alberta. Canadian Journal of Forestry Research. 25, 1746-1755.

Li, J., Xie, S., Cook, E.R., Morales, M.S., Christie, D.A., Johnson, N.C., Chen, F., D'Arrigo, R., Fowler, A.M., Gou, X., and K. Fang, 2013, El Nino modulations over the pas seven centuries. Nature Climate Change. 3, 822-826.

Liscom, K., Stuehrenberg, L., and F. Ossiander, 1985. Radio-tracking studies of adult chinook salmon and steelhead to determine the effects of ''zero'' river flow during water storage at Little Goose Dam on the lower Snake River. Final report to the Bonneville Power Administration, Portland, Oregon.

Little, R.L., Peterson, D.L., Silsbee, D.G., Shainsky, L.J., and L.F. Bednar, 1995. Effects of climate on radial growth of Douglas-fir *Pseudotsuga menziesii* in the Siskiyou Mountains, Oregon. Canadian Journal of Forest Research. 25, 724-735.

Litzow, M.A., Ciannelli, L., Puerta, P., Wettstein, J.J, Rykaczewski, R.R., and M. Opiekun, 2018. Non-stationary climate-salmon relationships in the Gulf of Alaska. Proceedings of the Royal Society. 285, 20181855.

Ljung, G.M., and G.E.P. Box, 1978. On a measure of a lack of fit in time series models. Biometrika. 65, 297-303.

Loaiciga, H.A., Haston, L., and J. Michaelsen, 1993. Dendrochronology and long-term hydrologic phenomena. Reviews of Geophysics. 31, 151–171.

MacDonald, G.M., and R.A. Case, 2005. Variations in the Pacific Decadal Oscillation over the past millennium. Geophysical Research Letters. 32, L08703.

Mann, M.E., and J. Park, 1993. Spatial correlations of interdecadal variation in global surface temperatures. Geophysical Research Letters. 20, 1055-1058.

Mann, M.E., and J.M. Lees, 1996. Robust estimation of background noise and signal detection in climatic time series. Climate Change. 33, 409-445.

Mantua, N., 2015. Shifting patterns in Pacific climate, West Coast salmon survival rates, and increased volatility in ecosystem services. Proceedings of the National Academy of Sciences of the United States of America. 112, 10823-10824.

Mantua, J.N., Hare, S.R., Zhang, Y., Wallace, J.M. and R.C. Francis, 1997. A Pacific interdecadal climate oscillation with impacts on salmon production. Bulletin of the American Meteorological Society. 78, 1069-1079.

Margolis, E.Q., Meko, D., and R. Touchan, 2011. A tree-ring reconstruction of streamflow in the Santa Fe River, New Mexico. Journal of Hydrology. 397, 118–127.

Maxwell, S., Harley, G., Maxwell, J.T., Rayback, S.A., Pederson, N., Cook, E.R., Barclay, D.J., Li, W., and J.A. Rayburn, 2017. An interbasin comparison of tree-ring reconstructed streamflow in the eastern United States. Hydrological Processes. 31, 2381-2394.

McCabe, G.J., Palecki, M.A., and J.L. Betancourt, 2004. Pacific and Atlantic Ocean influences on multidecadal drought frequency in the United States. Proceedings of the National Academy of Sciences. 101, 4136-4141.

McGuire, A.D., Ruess, R.W., Clein, J.S., Lloyd, A.H., Yarie, J., and G.P. Juday, 2010. Vulnerability of white spruce tree growth in interior Alaska in response to climate variability: Dendrochronological, demographic, and experimental perspectives. Canadian Journal of Forest Research. 40, 1197–1209.

McPhee, M.V., Utter, F., Stanford, J.A., Kuzishchin, K.V., Savvaitova, K.A., Pavlov, D.S. and F.W. Allendorf, 2007. Population structure and partial anadromy in *Oncorhynchus mykiss* from Kamchatka: relevance for conservation strategies around the Pacific Rim. Ecology of Freshwater Fish. 16, 539–547.

Meko, D.M., 2006. Tree-ring inferences on water-level fluctuations of Lake Athabasca. Canadian Water Resources Journal. 31, 229-248.

Meko, D.M., and C.A. Woodhouse, 2011. Application of streamflow reconstruction to water resources management. In: Dendroclimatology: Progress and Prospects [Hughes, M.K., Swetnam, T.W., and H.F. Diaz] Volume 11. Springer, pg. 231-261.

Meko, D.M., Touchan, R., and K.J. Anchukaitis, 2011. Seascorr: A MATLAB program for identifying the seasonal climate signal in an annual tree-ring time series. Computers and Geosciences. 37, 1234-1241.

Meko, D., Woodhouse, C., and K. Morino, 2012. Dendrochronology and links to streamflow. Journal of Hydrology. 412-413, 200-209.

Michaelsen, J., 1987. Cross-validation in statistical climate forecast models. Journal of Climate and Applied Meteorology. 26, 1589-1600.

Minobe, S., 2000. Spatio-temporal structure of the pentadecadal variability over the North Pacific. Progress in Oceanography. 47, 381–408.

Montgomery, D., 2004. King of Fish: The Thousand-Year Run of Salmon. Basic Books, New York.

Mood, B.J., Welsh, C., and D.J. Smith, *unpublished manuscript*. Chinook and Coho salmon have experienced contrasting, cyclical abundance changes over the last 300 years in southwestern British Columbia, Canada.

Moore, R.D., 1996. Snowpack and runoff responses to climatic variability, southern Coast Mountains, British Columbia. Northwest Science. 70, 321-333.

Moore, R.D., and I.G. McKendry, 1996. Spring snowpack anomaly patterns and winter climatic variability, British Columbia, Canada. Water Resources Research. 32, 623-632.

Moore, R.D., Allen, D.M., and K. Stahl, 2007. Climate change and low flows: Influences of ground water and glaciers. Final report prepared for Climate Change Action Fund. Vancouver, BC: Natural Resources Canada.

Moore, R.D., Spittlehouse, D., Whitefield, P., and K. Stahl, 2010. Weather and climate. Chapter 3. In: Compendium of forest hydrology and geomorphology in British Columbia (vol 1 of 2) [Pike, R.G., Bennett, K.E., Redding, T.E., Moore, R.D, Winker, R.D., and K.D. Baldon] B.C. Ministry of Forests and Range, Forest Science Program, Victoria, B.C. and FORREX Forum for Research and Extension in Natural Resources, Kamloops, B.C. Land Management Handbook: 66.

Moore, J.W., Yeakel, J.D., Peard, D., Lough, J., and M. Beere, 2014. Life-history diversity and its importance to population stability and persistence of a migratory fish: steelhead in two large North American watersheds. Journal of Animal Ecology. 83, 1035-1046.

Mosteller, F., and J.W. Tukey, 1977. Data Analysis and Regression: a Second Course in Statistics. Pearson Publishing. New York, New York.

Mote, P.W., Parson, E.A., Hamlet, A.F., Keeton, W.S., Lettenmaier, D., Mantua, N., Miles, E.L., Peterson, D.W., Peterson, D.L., Slaughter, R., and A.K. Snover, 2003. Preparing for climatic change: the water, salmon, and forests of the Pacific Northwest. Climate Change. 61, 45–88.

Newcome, R. G., 1998. Interval estimation for the difference between independent proportions: Comparison of eleven methods. Statistics in Medicine. 17, 873–890.

Nijssen, B., O'Donnell, G.M., Hamlet, A.F., and D.P. Lettermaier, 2001. Hydrologic sensitivity of global rivers to climate changes. Climate Change. 50, 143-175.

O'Neel, S., Hood, E., Bidlack, A.L., Fleming, S.W., Mayumi, A., Arendt, A., Burgess, E., Sergeant, C.J., Beaudreau, A.H., Timm, K., Hayward, G.D., and S. Pyare, 2015. Icefield-to-ocean linkages across the northern Pacific coastal temperate rainforest ecosystem. Bioscience. 65, 499-512.

O'Neil, H.C., Prowse, T.D., Bonsal, B.R., and Y.B. Dibike, 2017. Spatial and temporal characteristics in streamflow-related hydroclimate variables over western Canada. Part 2: future projections. Hydrology Research. 48, 932-944.

Ohlberger, J., Ward, E.J., Schindler, D.E., and B. Lewis, 2018. Demographic changes in Chinook salmon across the Northeast Pacific Ocean. Fish and Fisheries. 19, 533-546.

Pacific Fisheries Resource Conservation Council, 2016. Priorities and Strategies for Canada's Wild Pacific Salmon and Steelhead. Advisory Report, ISBN: 11-897110-63-4.

Patskoski, J., Sankarasubramanian, A., and H. Wang, 2015. Reconstructed streamflow using SST and tree-ring chronologies over the southeastern United States. Journal of Hydrology. 527, 761-775.

Pederson, G.T., Gray, S.T., Fagre, D.B., and L.J. Graumlich, 2006. Long-duration drought variability and impacts on ecosystem services: A case study from Glacier National Park, Montana. Earth Interactions. 10, 2-28.

Peterson, D.W., and D.L. Peterson, 1994. Effects of climate on radial growth of subalpine conifers in the North Cascade Mountains. Canadian Journal of Forest Research. 24, 1921–1932.

Peterson, D.W., and D.L. Peterson, 2001. Mountain hemlock growth responds to climatic variability at annual and decadal time scales. Ecology. 82, 3330-3345.

Pisaric, M.F.J., 2001. Holocene environmental change at the subarctic alpine treeline in northern British Columbia and the southern Yukon Territory. PhD Thesis, Queen's University. Kingston, ON.

Pitman, K.J., and D.J. Smith, 2013. A dendroclimatic analysis of mountain hemlock (*Tsuga mertensiana*) ring-width and maximum density parameters, southern British Columbia Coast Mountains, Canada. Dendrochronologia. 31, 165-174.

Pojar, J., Klinka, K., and D. Meidinger, 1987. Biogeoclimatic ecosystem classification in British Columbia. Forest Ecology and Management. 22, 119-154.

Polge, H., 1966. Determination of wood density variation curves by densitometric exploration of x-rays of samples taken from live trees. Annals of Forest Science. 23, 1-206.

Porter, T.J., Pisaric, M.F.J., Kokelj, S.V., and P. deMontigny, 2013. A ring-width-based reconstruction of June-July minimum temperatures since AD 1245 from white spruce stands in the Mackenzie Delta region, northwestern Canada. Quaternary Research. 80, 167-179.

Quinn, T.P., 2005. The Behavior and Ecology of Pacific Salmon and Trout. University of Washington Press, Seattle, Washington, USA.

Ribera, P., and M.E. Mann, 2003. ENSO related variability in the Southern Hemisphere, 1948-200. Geophysical Research Letters. 30, 1006(1)-(4).

Robards, M.D., and T.P. Quinn, 2002. The migratory timing of adult summer-run steelhead in the Columbia River over six decades of environmental change. Transactions of the American Fisheries Society. 131, 523-536.

Rodenhuis, D., Bennett, K.E., Werner, A., Murdock, T.Q., and D. Bronaugh, 2009. Hydro-climatology and future climate impacts in British Columbia. Pacific Climate Impacts Consortium, University of Victoria, Victoria, BC.

Rodionov, S.N., Overland, J.E., and N.A. Bond, 2005. The Aleutian Low and winter climate conditions in the Bering Sea. Part I: Classification. Journal of Climate. 18, 160-177.

Rodionov, S.N., Bond, N.A., and J.E. Overland, 2007. The Aleutian Low, storm tracks, and winter climate variability in the Bering Sea. Deep-Sea Research. 54, 2560-2577.

Salzman, M., Weser, H., and R. Cherian, 2014. Robust response of Asian summer monsoon to anthropogenic aerosols in CMIP5 model. Journal of Geophysical Research. 119, 11321-11337.

Sauchyn, D., and S. Kulshreshtha, 2008. Prairies. In: From Impacts to Adaptation: Canada in Changing Climate 2007 [D.S. Lemmen, F.J. Wareen, J. Lacroix and E. Bush] Government of Canada, Ottawa, ON. pg. 276.

Sauchyn, D., Demuth, M., and A. Pietroniro, 2009. Upland watershed management and global change: Canada's Rocky Mountains and western plains. In: Managing water resources in a time of global change: mountains, valleys, and flood plains [Garrido, A., and A. Dinar] Routledge, New York, New York. pg. 32-49.

Schnorbus, M., Werner, A.T., K. Bennett, 2014. Impacts of climate change in three hydrologic regimes in British Columbia, Canada. Hydrological Processes. 28, 1170-1189.

Schweingruber, F. H., 1983. Gnat Pass Dease Lake - PCGL - ITRDB CANA086. NOAA Study Page: https://www.ncdc.noaa.gov/paleo/study/4426

Shapiro, S.S., and M.B. Wilks, 1965. An analysis of variance test for normality (complete samples). Biometrika. ¾, 591-611.

Slaney, T.L., Hyatt, K.D., Northcote, T.G., and R.J. Fielden, 1996. Status of anadromous salmon and trout in British Columbia and Yukon. Fisheries. 21, 20-35.

Smith, B.D., 2000. Trends in wild adult steelhead (*Oncorhynchus mykiss*) abundance for snowmelt-driven watershed of British Columbia in relation to freshwater discharge. Canadian Journal of Fish and Aquatic Science. 57, 285-297.

Smoker, W.A., 1955. Effects of stream flow on silver salmon production in western Washington. Doctoral dissertation. University of Washington, Seattle.

Snedecor, G.W. and W.G. Cochran, 1989. Statistical Methods. Ames: IA. Iowa State University Press.

Spencer, C.R., Facchin, A.R., Tautz, A.F., and R.S. Hooton, *unpublished*. A method of estimating the commercial catch escapement of steelhead trout (*Oncorhynchus mykiss*) at the mouth of the Skeena River. For the Pacific Stock Assessment Review Committee.

Stahl, K., Moore, D., and I.G. McKendry, 2006. The role of synoptic-scale circulation in the linkage between large-scale ocean-atmospheric indices and winter surface climate in British Columbia, Canada. International Journal of Climatology. 26, 541-560.

Starheim, C.C.A., Smith, D.J., and T.D. Prowse, 2013a. Dendrohydroclimate reconstructions of July–August runoff for two nival‐regime rivers in west central British Columbia. Hydrological Processes. 27, 405–420.

Starheim, C.C.A., Smith, D.J. and T.D. Prowse, 2013b. Multi-century reconstructions of Pacific salmon abundance from climate-sensitive tree rings in west central British Columbia. Ecohydrology. 6, 228-240.

Stewart, I.T., Cayan, D.R., and M.D. Dettinger, 2004. Changes in snowmelt runoff timing in western North America under a "business as usual" climate change scenario. Climatic Change. 62, 217-232.

Stewart, I.T., Cayan, D.R., and M.D. Dettinger, 2005. Changes toward earlier streamflow timing across Western North America. Journal of Climate. 18, 1136-1155.

Stiff, H.W., Hyatt, K.D., Hall, P., Finnegan, B., and D. Macintyre, 2015. Water temperature, river discharge, and adult Sockeye salmon migration observations in the Babine watershed, 1946- 2014. Canadian Manuscript Report of Fisheries and Aquatic Sciences. 3053, vi + 169.

Stocker, T.F., Dahe, Q., Plattner, G., and G.K. Plattner, 2013. Technical Summary. In: Climate Change 2013: The Physical Science Basis. Contribution of Working Group I to the Fifth Assessment Report of the Intergovernmental Panel on Climate Change [Stocker, T.F., D. Qin, G.-K. Plattner, M. Tignor, S.K. Allen, Boschung, J…and P.M. Midgley (eds.)]. Cambridge University Press, Cambridge, United Kingdom and New York, NY, USA. pg. 33-115.

Stokes, M.A., and T.L. Smiley, 1968. An Introduction to Tree-Ring Dating. The University of Chicago Press. Illinois, USA.

Szeicz, J.M., and G.M. MacDonald, 1996. A 930-year ring-width chronology from moisture-sensitive white spruce (*Picea glauca* Moench) in northwestern Canada. The Holocene. 6, 345-351.

Thorne, R., and M. Woo, 2011. Streamflow response to climatic variability in a complex mountainous environment: Fraser River Basin, British Columbia, Canada. Hydrological Processes. 25, 3076-3080.

Thorpe, J.E., 1998. Salmonid life-history evolution as a constraint on marine stock enhancement. Bulletin of Marine Science. 62, 465–475.

Torrence, C., and G. Compo, 1998. A practical guide to wavelet analysis. Bulletin of the American Meteorological Society. 79, 61-78.

Trenberth, K.E., 2011. Changes in precipitation with climate change. Climate Research. 47,123-138.

Trenberth, K.E., and J.W. Hurrell, 1994. Decadal atmosphere-ocean variations in the Pacific. Climate Dynamics. 9, 303-319.

Trouet, V., and A.H. Taylor, 2009. Multi-century variability in the Pacific North American circulation pattern reconstructed from tree rings. Climate Dynamics. 35, 953-963.

Vaganov, E., Hughes, M., Kirdyanov, A., Schweingruber, F., and P. Silkin, 1999. Influence of snowfall and melt timing on tree growth in subarctic Eurasia. Nature. 400, 149–151.

Walters, C.J., Lichatowich, J.A., Peterman, R.M., and J.D. Reynolds, 2008. Report of the Skeena Independent Science Review Panel. A report to the Canadian Department of Fisheries and Oceans and the British Columbia Ministry of Environment.

Wang, T.A., Whitfield, P.H., and A.J. Cannon, 2006. Influence of Pacific climate patterns on low-flows in British Columbia and Yukon, Canada. Canadian Water Resources Journal. 31, 25-40.

Watson, E., and B.H. Luckman, 2002. The dendroclimatic signal in Douglas-fir and ponderosa pine tree-ring chronologies from the southern Canadian Cordillera. Canadian Journal of Forest Research. 32, 1858-1874.

Watson, E., and B.H. Luckman, 2004. Tree-ring based reconstructions of precipitation for the southern Canadian Cordillera. Climatic Change. 65, 209-241.

Watson, E., and B.H. Luckman, 2006. Long hydroclimate records from tree-rings in western Canada: potential, problems, and prospects. Canadian Water Resources Association. 31, 205-228.

Welch, D.W., Ward, B.R., Smith, B.D., and J.P. Eveson, 2000. Temporal and spatial responses of British Columbia steelhead (*Oncorhynchus mykiss*) populations to ocean climate shifts. Fish and Ocenography. 9, 17-32.

Wells, B.K., Grimes, C.B., Field, J.C., and C.S. Reiss, 2006. Covariation between the average lengths of mature coho (*Oncorhynchus kisutch*) and Chinook (*O. tshawytscha*) and the ocean environment. Fisheries Oceanography. 15, 67-79.

Welsh C., Smith D.J., and B. Coulthard, 2019. Tree-ring records unveil long-term influence of the Pacific Decadal Oscillation on snowpack dynamics in the Stikine River Basin, northern British Columbia. Hydrological Processes. 33, 720-736.

Whatley, M.R., Chudyk, W.E., and M.C. Morris, 1977. Morice River steelhead trout: the 1976 and 1977 sport fishery and life history characteristics from angers' catches. B.C. Fish and Wildlife Branch, Smithers, B.C.

Whitfield, P.H., and E. Taylor, 1998. Apparent recent changes in hydrology and climate of coastal British Columbia. In: Mountains to Sea: Human Interactions with the Hydrologic Cycle. Proceedings of the 51st Canadian Water Resources Association Conference. pg. 22-29.

Whitfield, P.H., Moore, R.D., Fleming, S.W., and A. Zawadzki, 2010. Pacific Decadal Oscillation and the hydroclimatology of western Canada – review and prospects. Canadian Water Resources Journal. 35, 1-28.

Wigley, T.M.L., Briffa, K.R., and P.D. Jones, 1984. On the average value of correlated time series, with applications in dendroclimatology and hydrometeorology. Journal of Climate and Applied Meteorology. 23, 201-213.

Wiles, G.C., D'Arrigo, R.D., and G.C. Jacoby, 1998. Gulf of Alaska atmosphere-ocean variability over recent centuries inferred from coastal tree-ring records. Climate Change. 38, 159-205.

Wiles, G.C., D'Arrigo, D., Barclay, D., Wilson, R.S., Jarvis, S.K., Vargo, L., and D. Frank, 2014. Surface air temperature variability reconstructed with tree rings for the Gulf of Alaska over the past 1200 years. The Holocene. 24, 198-208.

Wilks, D., 1995. Statistical Methods in Atmospheric Sciences. Academic Press. Cambridge, Massachusetts, USA.

Winski, D., Osterberg, E., Ferris, D., Kreutz, K., Wake, C., Campbell, S., Hawley, R., Roy, S., Birkel, S., Introne, D., and M. Handley, 2017. Industrial-age doubling of snow accumulation in the Alaska Range linked to tropical ocean warming. Scientific Reports. 7, 17869.

Wolfe, B.B., Karst-Riddoch, T.L., Vardy, S.R., Falcone, M.D., Hall, R.I., and T.W.D. Edwards, 2005. Impacts of climate and river flooding on the hydro-ecology of a floodplain basin, Peace-Athabasca Delta, Canada since AD 1700. Quaternary Research. 64, 147–162.

Wood, C.C., 2002. Managing biodiversity in Pacific salmon: The evolution of the Skeena River sockeye fishery in British Columbia. Washington, DC: Global Environment Facility.

Wood, L.J., Smith, D.J., and M.N. Demuth, 2011. Extending the Place Glacier mass-balance record to AD 1585, using tree rings and wood density. Quaternary Research. 76, 305-313.

Wood, L.J., and D.J. Smith, 2013. Climate and glacier mass balance trends from 1780 to present in the Columbia Mountains, British Columbia, Canada. Holocene. 23, 739-748.

Wood, L.J., and D.J. Smith, 2015. Intra-annual dendroclimatic reconstruction for northern British Columbia, Canada, using wood properties. Trees. 29, 461-474.

Woodhouse, C.A., 2003. A 431-yr reconstruction of Western Colorado snowpack from tree rings. Journal of Climate. 16, 1551-1561.

Woodhouse, C.A., and J.J. Lukas, 2006. Drought, tree rings and water resource management in Colorado. Canadian Water Resources Journal. 31, 297-310.

Youngblut, D. K., and B.H. Luckman, 2013. Evaluating the temperature sensitivity of radial growth patterns from whitebark pine in the western Canadian Cordillera. Dendrochronologia. 31, 16–28.

Zhang, X., Harvey, K.D., Hogg, W.D., and T.R. Yuzyk, 2001. Trends in Canadian streamflow. Water Resources Research. 37, 4490-4512.